SURFACE EFFECTS ON THE ULTRAFAST ELECTRONIC RELAXATION OF SOME SEMICONDUCTOR AND METALLIC NANOPARTICLES

A Dissertation
Presented to
The Academic Faculty

by

Qusai A. Darugar

In Partial Fulfillment
of the Requirements for the Degree
Doctor of Philosophy in the
School of Chemistry and Biochemistry

Georgia Institute of Technology

August 2006

SURFACE EFFECTS ON THE ULTRAFAST ELECTRONIC RELAXATION OF SOME SEMICONDUCTOR AND METALLIC NANOPARTICLES

Approved by:

Dr. Mostafa A. El-Sayed, Advisor
School of Chemistry and Biochemistry
Georgia Institute of Technology

Dr. Zhong Lin Wang
School of Materials Science and Engineering
Georgia Institute of Technology

Dr. Andrew Lyon
School of Chemistry and Biochemistry
Georgia Institute of Technology

Dr. Z. John Zhang
School of Chemistry and Biochemistry
Georgia Institute of Technology

Dr. Thomas Orlando
School of Chemistry and Biochemistry
Georgia Institute of Technology

Date Approved: June, 23 2006

This work is dedicated to those who believed in me. To my mother Zaitoon Darugar and my father Aunali Darugar, who gave me the opportunity to come to the US and believing in me and in my goals. To my loving wife Zainab whose patience, love and support have made my long time dream come true. To my son Mohammed, so he can be and dream what he desires.

ACKNOWLEDGEMENTS

It has been a blessing to work in a challenging but supportive environment such as the Laser Dynamics Laboratory (LDL) at Georgia Tech. I can not thank Professor Mostafa El-Sayed enough for both his scientific and personal guidance. Professor El-Sayed always made me think independently and offered help in every possible way when needed. His dedication towards research, encouragement and support is unmatched and I have been grateful to be a part of his research group. I would also like to thank Drs. Mona Mohamed and Jung whan Yoo for their initial help with material synthesis and discussion through the years. Additionally, I had a great opportunity to work and collaborate with Drs. Wei Qian, Stephan Link, Christy Landes and Alexander Schill.I would also like to thank Mr. Christopher Tabor for carefully reading this thesis and providing helpful feedback and Mr. Wenyu Huang for all his help throughout the years both in and out of the research lab.

I would like to thank my dear sister Alifiya Dossaji and my brother-in-law Abid Dossaji for all their help since the first day I arrived in the US. I can not thank them enough for their support throughout my undergraduate and graduate studies.

I would like to thank my brothers Hamza and Huzefa for their financial support during my undergraduate studies.

Finally, I would like to thank my loving wife Zainab for her support through this challenging journey. She has always wanted the best things for me and I can vouch that I can not ask for anything better then to have her by my side.

TABLE OF CONTENTS

LIST OF TABLES

LIST OF FIGURES

FIGURE PAGE

LIST OF EQUATIONS

EQUATION PAGE

Summary

My research has focused on understanding the surface effects on the optical and electronic properties of some metallic and semiconductor nanomaterials. When the particle sizes are on the nanometer length scale, a large fraction of atoms in the particles are on the surface. The bonding of the surface atoms being unsaturated could cause trapping and introduce defects that interact with the excited electrons. The effect of the surface on the optical and electronic properties of some semiconductor and metallic nanoparticles is investigated. When the size and shape of nanomaterials change, both the electron density of the excited electrons on the surface and the electronic structure change. Therefore, it becomes important to understand how these changes affect the electronic motion in the particles in order to exploit their full potential in a variety of applications.

A very critical part of the research presented in this thesis has been the nanomaterial synthesis. Chapter two discusses different methods used to make some metallic and semiconductor nanoparticles of different sizes and shapes. Learning different techniques is found to be very important in designing new synthetic methods to make desired materials. Making CdSe nanorods 40 nm in length and having the diameter smaller than the Bohr radius (quantum confinement limit) has important accomplishments of the present work.

The synthesis of copper nanoparticles of different sizes ranging from 10 nm to 60 nm in diameter is also described. This was the first synthesis to achieve isolated copper nanoparticles in this size range using photochemical methods. It was necessary to have control over the size in order to study size dependent ultrafast electron relaxation dynamics.

Synthesis of high quality, monodispersed CdS nanoparticles is also described. The quantum yield for CdS nanoparticles was found to be very good without passivation by a higher band gap material. Optical gain was observed in this material in solution at room temperature.

Chapter three examines the effect of changing the size and shape of CdSe nanoparticles on the rate of thermalization of hot electrons. It was believed that electron relaxation in semiconductor nanoparticles would be very long due to quantum confinement, leading to the phonon bottle neck effect. This was not found to be the case experimentally and was thought to be due to the fact that electrons relax from upper states by giving off energy to the holes. We also found that electron thermalization gets slower when the size of spherical particles is increased or when the shape is changed into rod. Using femtosecond transient spectroscopy, chapter three also shows that electron coupling to the surface state is a viable mechanism for promoting rapid relaxation rates in practical type particles synthesized by bottom up method in colloidal solutions. This mechanism

shows that upper state electrons relax faster than electrons in lower excited state due to a higher density of electrons.

Chapter four shows that the probability of electrons to become trapped increases with increasing excitation energy by monitoring the steady state fluorescence. This indicates that electron trapping is more efficient from upper excited states. It is shown that by passivating the particles with ZnS, one can minimize surface traps and hence increase fluorescence quantum yield. The effect of shape on the fluorescence lifetime is also investigated and there is shown to be a sharp change in the lifetime when the particle's aspect ratio becomes larger than 1.35. These results are in agreement with the previous theoretical calculations that energy state crossover at this aspect ratio making the transition allowed along the z-axis.

Chapter five discusses the effect of electron-surface phonon coupling on the relaxation dynamics copper nanoparticles of different sizes. For the first time, the size dependence of electron-surface phonon relaxation in such a system was observed. Fluorescence was also observed and shown to be 10^5 times stronger than that observed in bulk copper. Smaller particles gave weaker fluorescence quantum yield which was attributed to more surface defects due to a larger surface to volume ratio.

Chapter six examines the observation of optical gain in high quality CdS nanoparticles in solution. These particles were used as synthesized without size selective precipitation or surface passivation. Using CdS nanoparticles can potentially be very useful for making lasers in the blue region. This allows a penetration under water where there is a transmission window. Also, solution suspended particles provide an added advantage for high powered laser in which heat dissipation can be accomplished more effectively.

In chapter 7, the ultrafast rise time of the 1S state is shown to be dependent on the concentration of CdSe nanoparticles. First, Förster type energy transfer was thought to be the reason for such dependence, but the calculated distance was much too large (500A) for such a process to occur. The presence of a small amount of aggregates may show such dynamics. A number of experiments were carried out to show that aggregation indeed can cause a faster rise time of the 1S state. The cause of aggregation is still under investigation.

Chapter eight looks into the nature of the electron quenching site and the origin of bi-exponential decay for the fluorescence lifetime. Steady state fluorescence intensity and fluorescence lifetime are monitored under different perturbations and sample quality. The origin and the type of trap sites responsible for the bi-exponential are explained and quenching mechanisms are proposed.

CHAPTER I

INTRODUCTION

Research Goals

The goal of the research presented in this thesis is to obtain a better understanding of the chemical and physical aspects of materials, both metallic and semiconductor, in the nano-size regime. These materials have shown great promise in a variety of applications such as high density data storage (1-4), LED's (5-8), medical diagnostics (9-11), and in making high pumped power Lasers (12-15). Many of these applications were realized using theoretical calculations, but the reality is far from an idealistic situation. Therefore, properties of these nanomaterials need to be determined experimentally. Theoretical determination of the effects of surface quality and passivation and particle size and shape on the optical and electronic properties may not always reflect the experimental results. The ultimate motivation for research in this field is to gain further experimental understanding of properties of nanomaterials so that their full potential can be realized.

Synthetic techniques for a variety of metallic and semiconductor nanoparticles will be initially presented that have been used in order to obtain the desired samples needed to answer specific questions. Subsequently, work done to study the effect of surface quality, particle size and particle shape on the absorption,

emission and electronic relaxation in semiconductor nanocrystals will be presented.

The effect of changing the aspect ratio of cadmium selenide (CdSe) particles on the optical properties will be presented together with the steady state and fluorescence lifetime measurements as a result of changing surface passivation. Ultimately, the effect of size on the electronic relaxation for both semiconductor and metallic nanoparticles will be discussed. For metallic nanoparticles, two different sizes, namely 12 nm and 30 nm, are studied. It is important to use copper nanoparticles of two different sizes in order to experimentally determine the contribution of surface-phonons in the electron relaxation. Some fundamental theoretical and experimental properties of semiconductor nanoparticles that are helpful in understanding the work presented herein will follow.

Effect of size on quantum confinement

In bulk semiconductor materials, the electron and hole are bound together by a screened coulomb interaction to form a Mott-Wannier exciton (16). The Bohr radius of the exciton is given by equation 1.1:

$$a_{\mathbf{B}} = \frac{\hbar^2 \varepsilon}{e^2 \mu} \qquad (1.1)$$

Where ε is the dielectric constant and μ is the reduced effective mass of the electron and hole.

A strong confinement regime exists in the small nanocrystals when the radius of the nanocrystals is much smaller than the exciton Bohr radius. It leads to an increased spacing between energy levels as the size of the nanocrystals is decreased. As a result, the energy levels become discrete and transitions are only allowed between levels with the same quantum numbers (21). The band gap state is then given by equation 1.2 (17-21).

$$\Delta E = E_g + \frac{\pi^2 \hbar^2}{2\mu} \cdot \frac{1}{a^2} - \frac{1.786\ e^2}{\varepsilon} \cdot \frac{1}{a} \qquad (1.2)$$

Where E_g is the bulk band gap energy and a is the radius of the nanocrystals.

In CdSe semiconductor quantum dots, because of this quantum confinement, the optical properties can be tuned through most of the visible spectrum by changing

the size of the particles as shown in figure 1-1. Murray and Bawendi (22) were first to show a chemical route for preparing high quality semiconductor nanoparticles by adding precursor molecules to a hot surfactant solution.

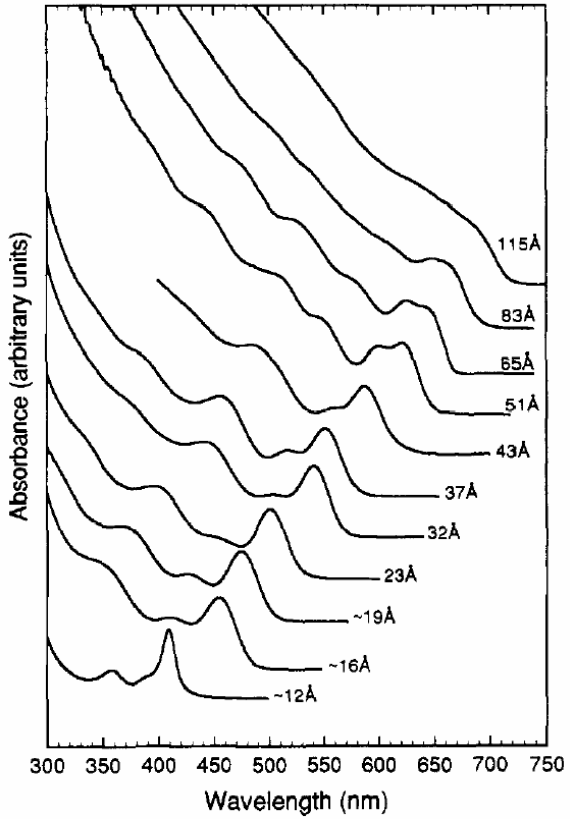

Figure 1-1: Room temperature optical absorption spectra of CdSe nanocrystallites dispersed in hexane ranging in size from 12 to 115A, from ref. 22.

Detailed experimental results are given in chapter II including modifications by Peng et al (23-24) where they introduced the use of CdO as a replacement for more expensive and very toxic dimethylcadmium.

The advantages of Murray's method are:

1- Very narrow size distribution (nearly monodispersed).

2- Large quantities of the material can be obtained.

3- Soluble in most non-polar solvents such as toluene, hexane, chloroform, etc.

4- The capping material Tri-octylphosphine oxise (TOPO) can be easily replaced with other capping materials such as pyridine, mercaptoacetic acid, ZnS(TOPO), oleic acid, etc.

5- Cost effective since CdO was successfully used.

6- Ability to control size of the nanocrystals.

7- This method can be modified to grow different shapes of the particles such as rods, tripods and tetrapods.

The structure of the lowest exciton state was studied experimentally using Photoluminescence Excitation (PLE) and Fluorescence Line Narrowing (FLN) techniques (25-28). Band gap fluorescence is the result of lowest excited state electron-hole pair recombination. Figure 1-2 shows emission spectra of different size CdSe nanoparticles spanning over most of the visible region of the spectrum.

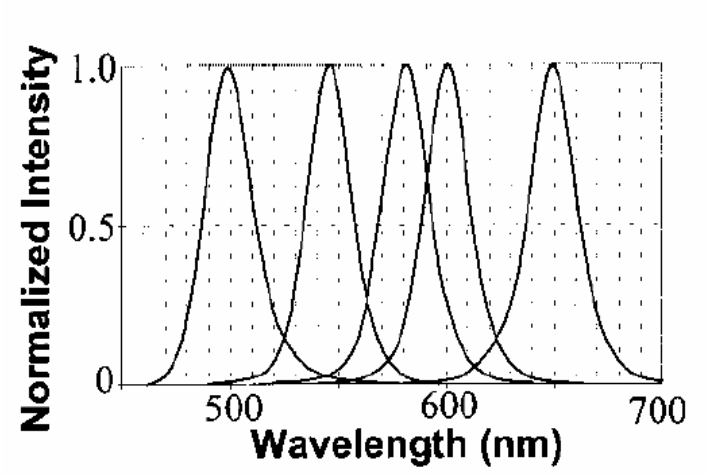

Figure1-2: Emission spectra of different-sized CdSe nanocrystals, from ref. 29. Sizes of the nanoparticles from left to right are 2.0, 3.2, 4.0, 4.5 and 6.5 nm in diameter.

It is found that the global emission peaks show an increasing red shift from the first excitonic absorption peak (band gap absorption) (30). When the excitation energy is much higher than the energy of the absorption threshold observed in an ensemble quantum dot sample, a large fraction of the quantum dots are excited. This results in a Gaussian type emission band that is red shifted and explained in terms of a global stokes shift due to inhomogeneous size distribution. Because of its volume dominance, larger CdSe nanoparticles absorb most of the incident photons resulting in a red shifted emission peak (30).

Semiconductor nanocrystals synthesized using the pyrolysis technique are normally passivated with TOPO and have quantum yields of roughly 2-10% indicating other non-radiative relaxation pathways due to large surface defects such as missing atoms (selenium vacancies), oxidized atoms, surface capping

and oxygen complexes (31-35). These defects can lead to a large density of surface states with energies below the band gap state that can quench the charge carrier and hence the fluorescence.

Hines et al (36) provided a very important modification to minimize surface state defects by passivating the CdSe nanoparticles with an inorganic material of wider band gap, ZnS. It is suggested that by confining the charge carriers within the nanoparticles minimizes the possibility of coupling to the surface states is minimized. This could result in a large increase in the luminescence quantum yield.

Figure 1-3 shows a dramatic size dependent fluorescence from ZnS passivated CdSe nanoparticles. The size ranges from 2.3 nm (Blue emission) to 5.5 nm (Red emission).

Figure 1- 3 High quantum yield, size tunable fluorescence from CdSe/ZnS nanoparticles.. Photo by Felice Frankel from Bawendi group web-page. URL: http://web.mit.edu/chemistry/nanocluster/home.html

Carrier dynamics in semiconductor nanoparticles

Quantum confinement of electronic motion in semiconductor nanoparticles leads to quantization of its band continua of the bulk. The relaxation between the resulting quantized levels by electron-phonon coupling was expected to be slow due to the small phonon frequencies. However, experimentally this was not found to be true.

In a semiconductor nanocrystal, quantum confinement leads to quantization of its energy levels (37). The conduction band is replaced by quantized energy levels, similar to the molecular case. Unlike the large molecular case however, semiconductors do not have large vibration quanta. As a result, the electronic energy separations become much larger than the phonon quanta. It was then

expected that semiconductor nanoparticles could show a “phonon bottleneck” in the thermalization process of their excited electrons (35-39). However, the relaxation of excited electrons in semiconductor nanoparticles is found to be very rapid (in the subpico-to picosecond time scale), just as fast as the relaxation in large molecules.

In order to explain the rapid thermalization of excited electrons in semiconductor nanoparticles, several mechanisms have appeared in the literature. The coupling between the electron and hole is proposed by Efros et al. (40) to transfer electronic excitation energy to hole excitation. The density of the hole states allows it to accept any amount of energy that the electron gives off in its thermalization process with no problem of energy mismatch. An illustration of a linear Auger type mechanism proposed by Efros is shown in figure 1-4 below.

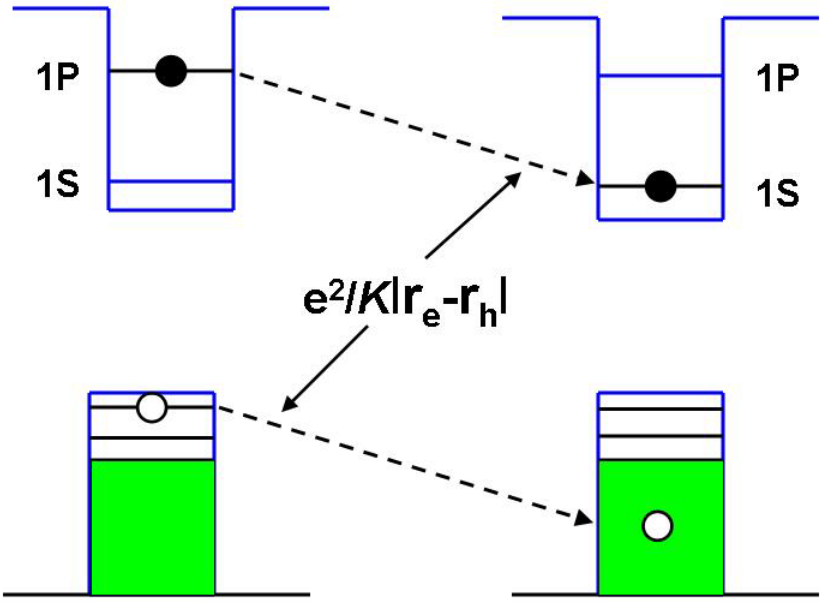

Figure 1-4: Diagram of the Linear Auger type mechanism in a semiconductor nanocrystal. An electron from 1P state relaxes to 1S state giving off its energy to a hole.

Another possible mechanism includes a nonlinear Auger process involving multiple electron-hole pair excitation that leads to electron-hole pair recombination where the energy released is used to ionize other excited electrons as shown in figure 1-5 (41). In our studies, we have examined different mechanisms by changing the size and shape of CdSe nanoparticles and studying the effect on the electron thermalization (27).

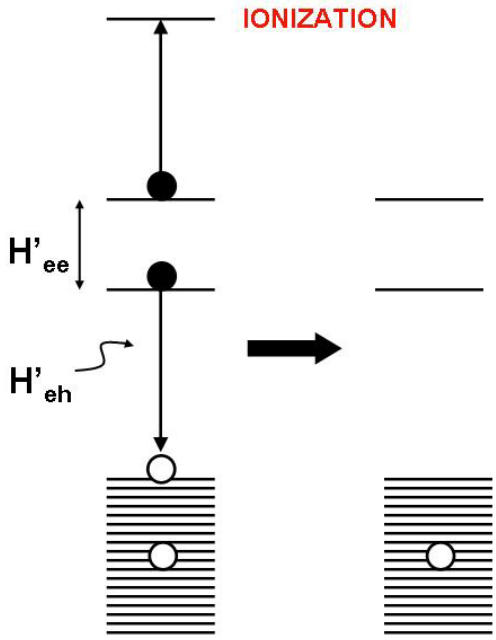

Figure 1-5: Nonlinear Auger process (two photons absorbed per particle) indicating the relaxation of excited electron and the energy released is used to ionize other excited electron.

Intraband Energy Relaxation Dynamics

Femtosecond broad band transient absorption can be used to study intraband relaxation and depopulation dynamics in semiconductor nanoparticles. It is shown that the electron relaxation dynamics in semiconductor nanocrystals from the upper states to the 1S state is very much dependent on the size of the nanocrystal and surface quality as well as the laser pump intensities and the molecules adsorbed on the surface (43-47).

Firstly, transient absorption spectra taken at different time intervals reveal the decay and growth of different bands as shown in figure 1-6. Comparing the transitions in the bleach spectra with that of the linear absorption spectra, B1, B2 and B3 were assigned to 1S, 2S and 1P transitions, respectively (43-45).

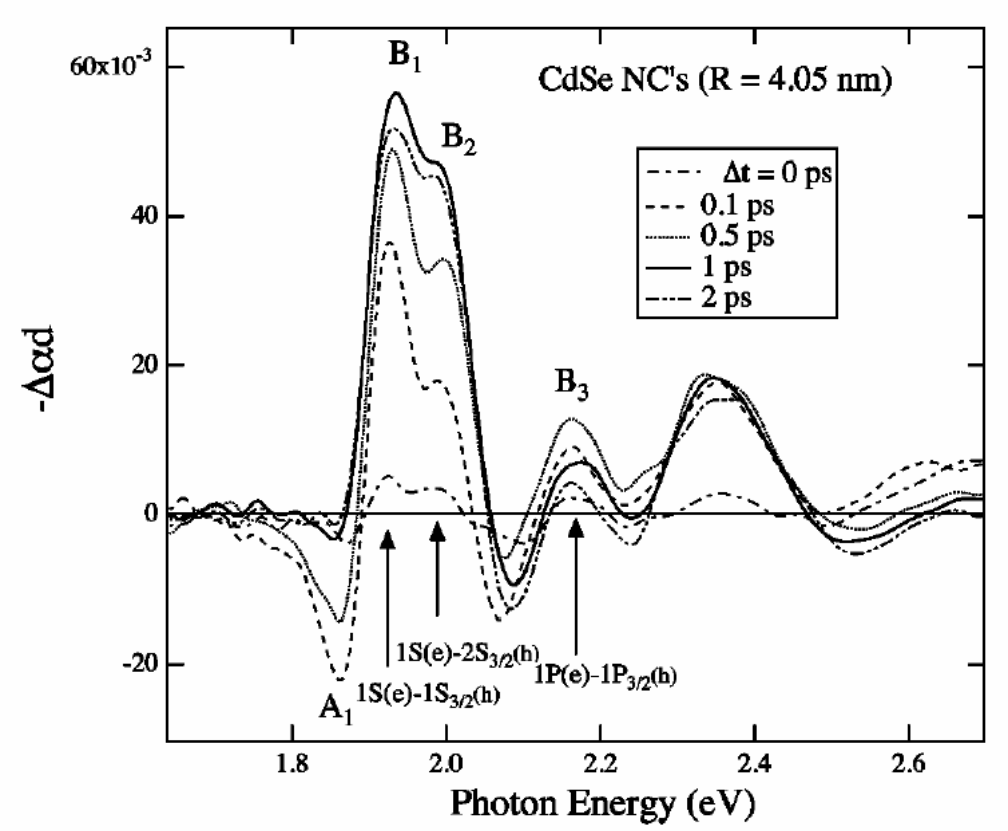

Figure 1-6: Transient absorption spectra for CdSe nanocrystals (R=4.05nm) recorded at different time delays between pump and probe pulses, from ref. 44.

Figure 1-6 also shows that the growth of B1 is accompanied by the decay of B3 band associated with the 1P transition. A femtosecond pump-probe experiment can be used to monitor the time for the decay and growth of 1P and 1S transitions, respectively.

Figure 1-7 shows the time transients recorded at the positions of the 1S and 1P transitions for R= 4.05, 2.77 and 2.33 nm CdSe nanocrystals. For the 4.05 nm sample (figure 1-7(a)), the B3 feature decays with a time constant of 540fs, which is attributed to the depopulation of the 1P state. The B1 time transient shows biexponential rise with the fast initial rise being due to a biexciton effect, followed by a slower rise with a time constant of 530fs (44). The secondary B1 rise time is complementary to the decay of the B3 state and is associated with the increase of the 1S population, due to 1P→1S relaxation. Similarly, the rise and decay of other size CdSe nanoparticles are shown in figures 1-7(b) and 1-7(c). For both the 2.77 and 2.33 nm CdSe nanoparticles, the rise of the 1S state is complementary to the decay of the 1P state.

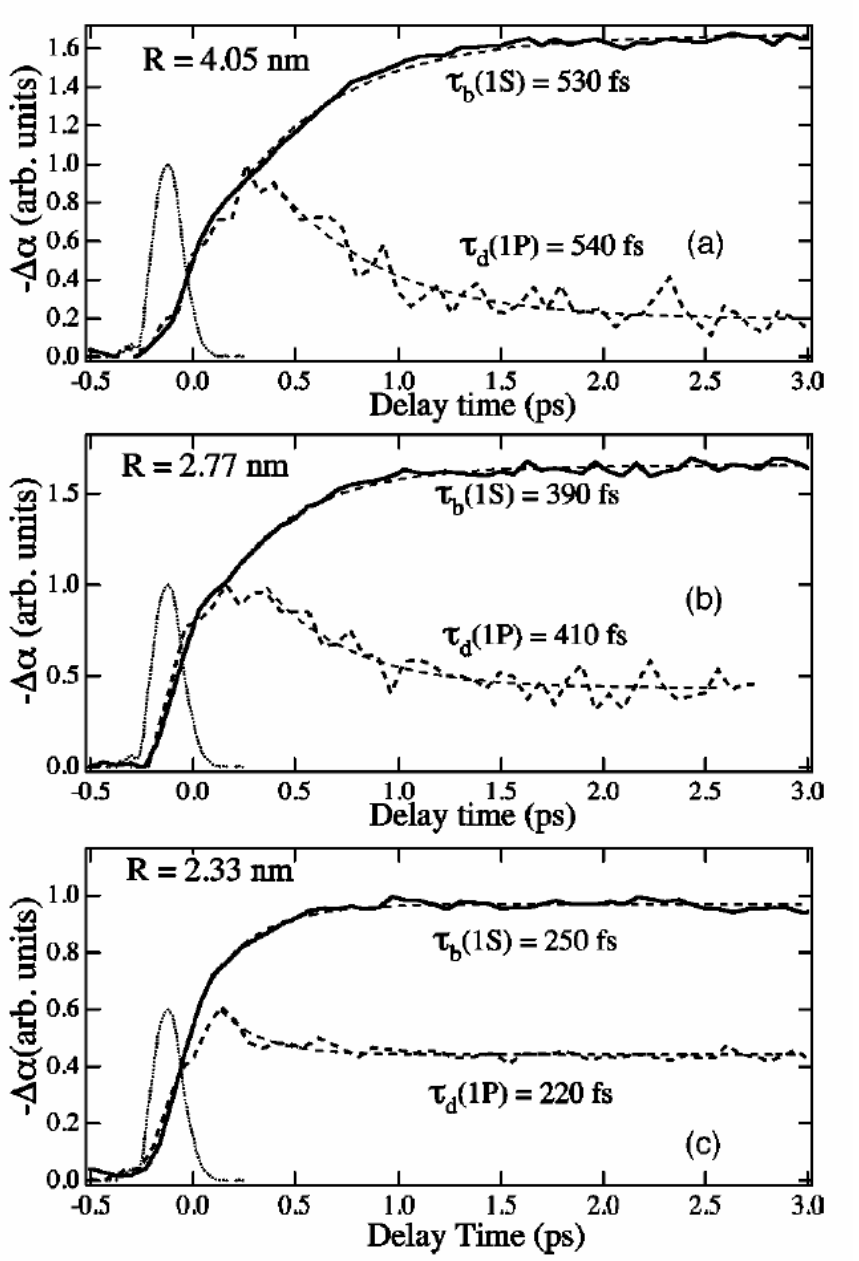

Figure 1-7: Transient absorption dynamics recorded at the positions of the 1S (thick solid lines) and the 1P (thick dashed line) transitions for TOPO-passivated CdSe NC's with R= 4.05 nm (a), 2.77 nm (b), and 2.33 nm (c). Thin dotted line is a pump-probe cross-correlation. Thin dashed lines are fits to a single-exponential decay (build-up) (τ_d and τ_b are corresponding time constants), from ref. 44.

Unless CdSe nanoparticles have near to perfect surfaces, it is very difficult to avoid surface contribution to the electron relaxation rates (42). At high pump intensity, it is very easy to excite more than 1 e-h pair per particle and therefore nonlinear Auger type relaxation processes would dominate the overall electron relaxation mechanism.

The size dependent relaxation dynamics are shown in figure 1-8a below. As the size of the nanoparticles decreases, the rise time of the 1S state becomes faster (43-44). The reduction is evident in figure 1-8b where the relaxation data for five colloidal samples are plotted as τ_b against radius of the particles (R). τ_b shortens from 530 fs for R=4.1 nm to 100 fs for R=1.2 nm, roughly following a linear size dependence (44). This observation is reverse of what was predicted from the quantum size effect. When the nanocrystal's size decreases, the energy band gap between the excited states increases and therefore an electron would require much higher energy rate loss than possible by multiphonon emission. This clearly suggests that the energy relaxation occurs via mechanisms other than electron-phonon interactions (43). The detailed nature of the energy relaxation processes is still unclear and more work is needed to fully understand these processes. Although quantum confinement is one aspect that leads to size dependent relaxation, we have shown that the nanocrystal surfaces also play an important role in thermaliazation of hot electrons (22).

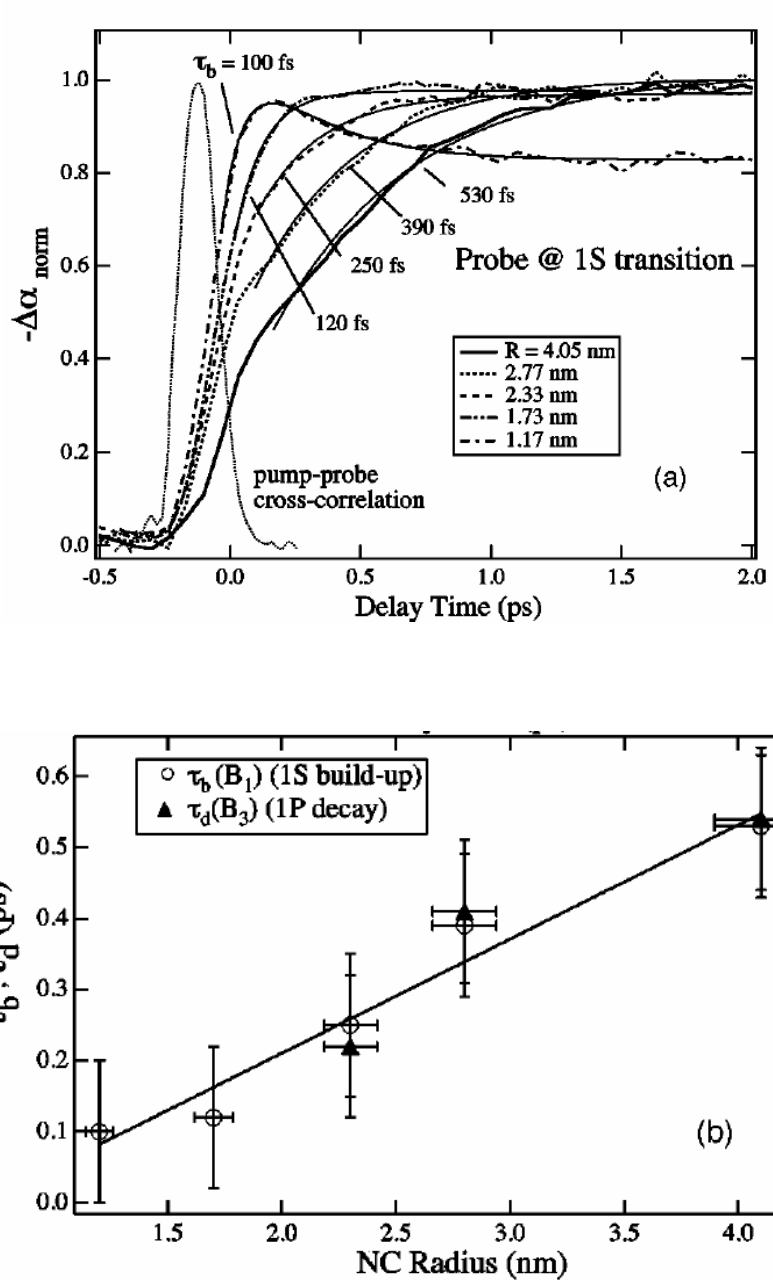

Figure 1-8: (a) The transient bleaching dynamics of the 1S state for colloidal CdSe nanoparticles of different size (thick lines) fit to a single exponential growth (thin solid lines). (b) The dependence of the 1P decay (triangles) and the 1S build-up (circles) times on the NC radii, fit to a linear size dependence (line), from ref. 44.

Optical properties and ultrafast dynamics of metallic nanoparticles

When the electromagnetic wave interacts with metal nanoparticles, it causes a collective oscillation of electrons on the surface of the particles, termed surface plasmon resonance (48-49) (figure 1-9). Noble metal nanoparticles show brilliant colors which led to their use in stained glasses and decorating ornaments during ancient Chinese and Egyptian times (50). Recent examples stained glasses where gold nanoparticles were incorporated to give brilliant colors can be found at the cathedral of Notre Dame in Paris, France.

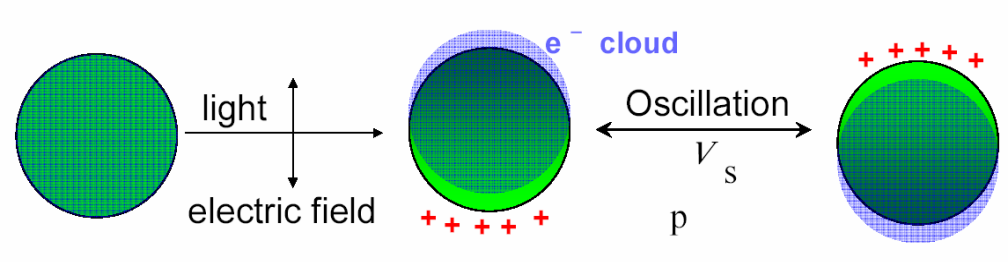

Figure 1-9: Collective oscillation of electrons in spherically shaped particle due to its interaction with an electromagnetic field.

Faraday was first to recognize the surface plasmon phenomenon (51) and Mie, by solving the Maxwell's equations, was able to explain this phenomenon theoretically in 1908 (52).

For nanoparticles much smaller than the wavelength of interacting light (<20nm), only the dipole approximation contributes to the extinction cross-section and therefore Mie theory is reduced to (48-49):

$$\sigma_{ext}(\omega) = 9\frac{\omega}{c}\varepsilon_m^{3/2} V \frac{\varepsilon_2(\omega)}{[\varepsilon_1(\omega)+2\varepsilon_m]^2+\varepsilon_2(\omega)^2}, \quad (1.3)$$

Where V is the volume of the particle, ω is the angular frequency of the interacting light, and *c* is the speed of light, and ε_m and $\varepsilon(\omega) = \varepsilon_1(\omega) + i\varepsilon_2(\omega)$ are the dielectric functions of the surrounding medium and the metal, respectively.

Experimentally (48), size dependence of the plasmon band is observed for metallic nanoparticles much smaller than 10 nm in contradiction to the above dipole approximation (Equation 1.3). The plasmon band is dampened and even disappears for very small nanoparticles (<2nm). It is argued that the dielectric function needs to be modified to account for the smaller particle size before Mie theory is applied (53).

Ultrafast Dynamics: Electron-Phonon and Phonon-Phonon relaxation in nanocrystals

Femtosecond pump-probe experiments allow one to follow the electron relaxation dynamics. The initially created electron distribution by femtosecond pulse laser is highly non-thermal, and the first relaxation step is the electron thermalization by electron-electron scattering, which is extremely fast in bulk metals (54-55).

The electron thermalization is followed by the energy exchange between the electrons and the lattice via electron-phonon coupling. Calculations show that the electron-phonon coupling should be size dependent due to electron-surface phonon contribution for gold nanoparticles in the size range of 2 to 100 nm (56) but was not found experimentally. (57-60)

Hartland and co-workers (61) showed that the coupling between the electrons and the surface phonon is determined by the ratio of the number of valence electrons in the atom to the atomic mass of the metal. In gold, because of a small number of valence electrons (one) and a large atomic mass, the contribution of the electron-surface scattering to the overall electron-phonon scattering cross section is very small. We have shown that if we use metal (copper) that has a much smaller atomic mass than gold, we can determine the electron- surface phonon coupling constant as a function of particle size (62).

The final step in electronic relaxation involves heat transfer to the surrounding medium through phonon-phonon interactions in 10's to 100's of picoseconds. It is found that the electron relaxation or the bleach recovery is faster in a more conductive surrounding as shown by Bigot et al (63) and El-Sayed et al (64). I will present the phonon-phonon relaxation dynamics in copper nanoparticles in two solvents with different thermal conductivities.

Some recent advances in the field of semiconductor and metal nanoparticles

One of the greatest advancements in the field of semiconductor research has been the synthesis of high quality and monodispersed nanosized samples in solution (22-24, 67-69). A lot of work has been done to understand the optical and electronic properties of semiconductor nanoparticles as discussed above. The flexibility to change the passivating molecules allows one to incorporate these nanoparticles into various applications. Most notably, making these particles water soluble, by replacing the TOPO with mercaptoacetic acid has been useful in covalently coupling them with biomolecules (70). A class of nonisotopic detection labels is developed by coupling water soluble ZnS capped CdSe quantum dots to biological molecules. The attached molecules identify specific analytes, such as proteins, DNA, or viruses, through photoluminescence.

Nie et al. have also embedded different size ZnS capped CdSe nanoparticles into polymeric microbeads at precisely controlled ratios for multicolor optical coding of biological assays (71). They predict that by using 10 different intensity levels and 6 colors, one could theoretically code one million nucleic acid or protein sequences. They show that their quantum dot tagged beads are highly uniform and reproducible, yielding bead identification accuracies as high as 99.99% under favorable conditions. Studies on DNA hybridization show that the coding and target signals can be simultaneously read at the single-bead level.

This spectral coding technology is expected to open new opportunities in gene expression studies, high throughput screening, and medical diagnostics.

Similarly, Bawendi et al. have used quantum dots as bioactive fluorescence probes for sensing, imaging, immunoassay, and other diagnostics applications (72). Colloidal semiconductor nanocrystals have the potential to overcome problems encountered by organic small molecules in certain fluorescent tagging applications by combining the advantages of a high photobleaching threshold, good chemical stability, and readily tunable spectral properties. Combining the advantages of lipoic acid capped CdSe-ZnS quantum dots with facile electrostatic conjugation of bioactive proteins, this type of hybrid bioinorganic conjugate represents a powerful fluorescent tracking tool for diverse applications.

Metal nanoparticles have also shown great promise for medical diagnostics and therapy (9, 73, 74). Halas et al. have shown that the optical properties of gold can be tuned by varying the shell thickness over silica spheres (75). By tuning the nanoshells to strongly absorb light in the near infrared, where optical transmission is optimal, a distribution of nanoshells deep inside the tissue can be used to deliver a therapeutic dose of heat by using near infrared light (74). Cells incubated with nanoshells were found to have undergone a change after exposure to near IR light. They show an increase in temperature after irradiation at a 4 W/cm^2 and 820 nm by 34ºC within 4-6 minutes. This temperature change was enough to cause irreversible damage in these cells.

El-Sayed et al. have taken advantage of optical tunability of gold nanorods with respect to the aspect ratio for cancer cell diagnostics and therapy (9). Gold nanorods with suitable aspect ratios can absorb and scatter light strongly in the NIR region (650-900 nm). The anti-epidermal growth factor receptor (EGFR) antibody-conjugated nanorods bind specifically to the surface of malignant type cells with a much higher affinity due to the over expressed anti- EGFR on the cytoplasmic membrane. Due to strongly scattered red light from gold nanorods in dark field imaging, the malignant cells are clearly identified and distinguished from nonmalignant cells. Laser power as low as 80 mW was found to destroy cancer cells incubated with gold nanorods.

Using metal nanoparticles can allow site specific diagnostics and therapy and can prove to be very useful for medical treatment in the future. Unlike semiconductor nanoparticles that are believed to be very toxic, gold nanoparticles are much safer to use for such purposes.

Semiconductor nanoparticles with their excellent optical properties and resistance to photobleaching are better suited for device application and for making high power lasers (12, 13, 15, 76). Klimov et al. have shown the development of optical gain in chemically synthesized semiconductor nanoparticles (13). Because of competing dynamical processes, they could only observe lasing by making CdSe films so as to minimize photoinduced absorption. Link et al. and Banin et al. have shown lasing from CdSe nanorods (15, 76).

Because the emission is red shifted from absorption, this reduces competing processes, therefore decreasing the gain threshold. Additionally, Link has shown that excitation at higher energy does not give optical gain. It is necessary to excite close to the band gap so as to minimize nonradiative relaxation and electron trapping processes from upper excited state.

Peng et al. have demonstrated experimental evidence of random lasing action in colloidal CdS/CdSe/CdS quantum dot quantum well heterostructures at 77 K (77). Threshold intensity, as low as 3 W/cm^2, was demonstrated with picosecond pulses as the excitation source and the lasing action can be seen in a broad spectral range. This indicates efficient gain and suppressed Auger processes in such colloidal CdSe quantum well system.

We have shown optical gain in the blue region from high quality and monodispersed CdS nanoparticles in solution at room temperature. The optical gain lifetime was found to be as long as 20 picoseconds under pump fluence as low as 0.77 mJ/cm^2. The low threshold is the result of the long lifetimes of electrons and holes and narrow emission band width. Solution based medium has an added advantage for a more efficient heat dissipation and photobleaching (12).

Thesis Focus and Organization

Before any studies can be done on these materials, the initial synthesis must be understood. Depending on the issue being addressed, the materials need to be selectively prepared and controlled. Chapter II, discusses different methods available to synthesize nanoparticles in solution. Both metallic and semiconductor nanoparticles are discussed in detail that were used for the majority of the work presented here. More importantly, the control and modifications over the surface quality, shape and size of both metallic and semiconductor nanoparticles is presented.

Importance of quantum confinement on the optical and electronic properties has been described above. Because the particle sizes are so small, surfaces play an extremely important role on both the optical and electronic properties. In chapter III, the effect of changing the size and shape of CdSe nanoparticles on the bleach recovery is presented. The electron density in the core and on the surface of the nanoparticles decreases with increasing size. Therefore, the slower relaxation of hot electrons in rods is attributed to a decreased interaction between excited electrons and a decreased electron coupling to both the surface species and surface defects.

To support our conclusion on the increase in the electron density with the excitation and coupling to the surface state, chapter IV discusses the effect of changing the excitation wavelength on the fluorescence quantum yield and fluorescence lifetime. Also, the effect of passivation on the steady state fluorescence and fluorescence lifetime is presented. It is found that the quantum yield decreases as the samples are excited at higher and higher energies where as the fluorescence lifetime is unaffected. This suggests that the trapping of the excited electrons results from higher energy states and not from the band gap state (lowest excited state).

Further more, chapter IV discusses the effect of changing the aspect ratio of CdSe nanoparticles. It is found that the fluorescence decay lifetimes decreases from ~37 ns to ~23 ns as the aspect ratio of CdSe nanorods increases above a critical value of 1.35. This is in accordance with the semi-empirical pseudopotential calculations by Alivisatos et al. that the excited electronic states cross at this aspect ratio allowing the transition to occur (65-66).

Chapter V discusses the effect of copper nanoparticles size on the electron-surface phonon coupling. The size dependence of the electron-surface phonon coupling is discovered for the first time in copper particles smaller than the mean free path of the electrons in copper. For gold nanoparticles, it was predicted that the electron relaxation dynamics would depend on the size of the particles but was not found to be experimentally true (57-61). Using metal nanoparticles with a

much smaller atomic mass, we show that the electron-surface phonon coupling is stronger in smaller nanoparticles. It is also found that copper nanoparticle fluorescence is much stronger than bulk copper metal ($>10^{-5}$). Additional mechanisms such as electron coupling to surface defects in smaller (12 nm) particles is needed to explain the faster relaxation rates observed than theoretically predicted.

In chapter VI, we show for the first time the optical gain from CdS nanoparticles in solution. Synthesis of high quality and monodispersed CdS nanoparticles is also discussed. Excellent quantum yield is observed in these particles without the need of surface passivation.

One of the most important applications for II-VI semiconductor nanoparticles is to make quantum dot based lasers because they have the ability to absorb and emit through most of the visible spectrum of light. Klimov has shown lasing from CdSe nanoparticles when incorporated in films (13). CdS particles in solution have an added advantage over CdSe in that they have a much wider band gap and therefore making a high power laser in the blue region becomes possible. Also, particles in solution can dissipate heat much more rapidly and the optical gain threshold in CdS is found to be much lower then reported for CdSe in films (13).

In chapter VIII, the effect of particle aggregation on the overall transient absorption dynamics is presented. It is found that the relaxation is faster when the samples are aggregated or when the particles form a close packed network in films. These results are obtained by monitoring the rise time of the 1S state signal. When more than one nanoparticle is involved, the excited electrons can relax by giving energy to the excited electrons in the neighboring particle. This process will become even more efficient if there are numerous particles in the aggregates.

As prepared quantum dots have fluorescence quantum yield of about 2-10% and therefore one of the most important question that remains is the nature and origin of the electron quencher. Chapter VII will discuss the effect of photo-oxidation on the fluorescence and fluorescence lifetimes of CdSe nanoparticles. It is found that the fluorescence quantum yield decreases with increasing UV light irradiation. The amplitude of the fast decay component increases with decreasing emission quantum yield where as the decay time remains unaffected. What atoms or surface species are affected under UV irradiation is still in need of further investigation.

References

(1) Ditlbacher, H., Krenn, J. R., Lamprecht, B., Leitner, A., Aussenegg, F. R., **2000,** *Optics Letters,* 25(8), 563.

(2) A. Morinaka, S. Oikawa, and H. Yamazaki, **1983,** *Appl. Phys. Lett*. 43, 524.

(3) Baba, K., Yamada, R., Nakao, S., Miyagi, M., **1993,** *Appl. Opt.,* 32, 3137.

(4) Colvin, V. L., Schlamp, M. C., Alivisatos, A. P., **1994**, *Nature*, 370, 354.

(5) Cassagneau, T., Mallouk, T. E., Fendler, J. H., **1998,** *J. Am. Chem. Soc.,* 120 (31), 7848.

(6) Dabbousi, B. O., Murray, C. B., Rubner, M. F., Bawendi, M. G., **1994,** *Chem. Mater.* 6, 216.

(7) Dabbousi, B. O., Bawendi, M. G., Onitsuka, O., Rubner, M. F. **1995,** *Appl. Phys. Lett.* 66, 1316.

(8) Kumar, N. D., Joshi, M. P., Friend, C. S., Prasad, P. N., Burzynski, R., **1997,** Appl. Phys. Lett., 71, 1388.

(9) Huang, X. H., El-Sayed, I. H., Qian, W., El-Sayed, M. A., **2006,** *J. Am. Chem. Soc.,* 128 (6), 2115.

(10) Alivisatos, A. P., **2004,** *Nat. Biotechnol.,* 22, 47-52.

(11) Chan, W. C. W., Maxwell, D. J., Gao, X., Bailey, R. E., Han, M., Nie, S., **2002,** *Curr. Opin. Biotechnol.*,13, 40-46.

(12) Darugar, Q., Qian, W., El-Sayed, M. A., *Appl. Phys. Lett.* (in press), 2006.

(13) Klimov, V. I., Mikhailovsky, A. A., Xu, S., Malko, A., Hollingsworth, J. A., Leatherdale, C. A., Eisler, H.-J., Bawendi, M. G., **2000,** *Science,* 290, 314-317.

(14) Sundar, V. C., Eisler, H. J., Bawendi, M. G. **2002,** *Advanced Materials***,** 14**,** 739.

(15) Link, S., El-Sayed, M. A., **2002,** *J. Appl. Phys.*, 92**,** 6799-6803.

(16) Knoxy. R. S. Theory of exciton; *Solid State Physics*, Supplement 5; Academic Press: New York, 1963.

(17) Kamat, P.V. *Progess in Reaction Kinetics* **1994**, 19, 277.

(18) Ekimov, A. L.; Hache, F.; Schanne-Klein, D.; Ricard, D.; Flyzanis, C.; Kudryavtsev, I. A.; Yazeva, T. V.; Rodina, A. V.; Efros, Al. L. *J. Opt. Soc. Am. B*. **1993**, 110, 100.

(19) Efros, Al. L; Efros A. L. *Sov. Phys. Semicond.,* **1982**, 16, 772.

(20) Ekimov, A. L.; Efros, Al. L.; Ivanov, M. G.; Onushchenko, A. A.; Shumilov, S. K.; *Solid State Commun*., **1989**, 69, 565.

(21) Efros, Al. L.; Rosen, M.; *Annu. Rev. Mater. Sci.* **2000**, 30, 475.

(22) Murray, C. B.; Norris, D. J.; Bawendi, M.G. *J. Am. Chem. Soc*., **1993**, 115, 8706.

(23) Peng, Z. A.; Peng, X. *J. Am. Chem. Soc*. **2001**, 123, 183.

(24) Peng, Z. A.; Peng, X. *J. Am. Chem. Soc*. **2002**, 124, 3343.

(25) Nirmal, M.; Norris, D. J.; Kuno, M.; Bawendi, M. G.; Efros, Al. L.; Rosen, M. *Phys. Rev. Lett*. **1995**, 75, 3728.

(26) Norris, D. J.; Efros, Al. L.; Rosen, M.; Bawendi, M. G. *Phys. Rev. B*. **1996**, 53, 16347.

(27) Norris, D. J.; Bawendi, M. G. *J. Chem. Phys*. **1995**, 103, 5260.

(28) Norris, D. J.; Bawendi, M. G. *Phys. Rev. B.* **1996**, 53, 16338.

(29) Qu, L. H.; Peng, X. G. *J. Am. Chem. Soc*. **2002**, 124 (9), 2049.

(30) Micic, O, I.; Sprague, J. R.; Lu, Z.; Nozik, A. J.; **1996**, *Appl. Phys. Lett*. 68, 3150.

(31) Zhang, J. Z. *Acc. Chem. Res*. **1997**, 20, 423.

(32) Roberti, T.W.; Cherepy, N.J.; Zhang, J.Z. J. Chem. Phys. **1998**, 108, 2143.

(33) Zhang, J.Z. *J. Phys. Chem. B* **2000**, 104, 7239.

(34) Underwood, D.F.; Kippeny, T.; Rosenthal, S.J. *J. Phys. Chem. B*, **2001** 105, 436.

(35) Klimov, V.; Bolivar, P.B.; Kurz, H. *Phys. Rev. B* **1996,** 53, 1463.

(36) Hines, M.; Guyot-Sionnest, P. *J. Phys. Chem*. **1996**, 100, 468.

(37) Brus, L. *J. Chem. Phys*. **1984**, 80, 4473.

(38) Benisty, H.; Sotomayer-Torres, C.M.; Weisbuch, C. *Phys. Rev. B*, **1991,** 44, 10945;

(39) Inoshita, T.; Sasaki, H. *Phys. Rev. B*, **1992**, 46, 7260.

(40) Efros, A.L.; Kharchenko, V.A.; Rosen, M. *Solid State Commun*. **1995**, 93, 281.

(41) Gelmont, B.L.; Kharchenko, V.A.; Yasievich, I.N. *Sov. Phys. Solid State*, **1989**, 29, 1355.

(42) Darugar, Q.; Landes, C.; Link, S.; Schill, A.; El-Sayed, M.A. *Chem. Phys. Letters*, **2003**, 373, 284-291.

(43) Kilmov, V. I. *J. Phys. Chem. B*, **2000**, 104, 6112 Feature Article.

(44) McBranch, D. W.; Klimov, and V. I.; Leatherdale, C. A.; Bawendi, M. G. *Phys. Rev. B*, **1999,** 60 (19) 13740.

(45) McBranch, D. W.; Klimov, and V. I.; Leatherdale, C. A.; Bawendi, M. G. *Phys. Rev. B*, **1999,** 60 (4) R2177.

(46) Burda, C.; Link, S.; Mohamed, M.; El-Sayed, M. A. *J. Phys. Chem. B*, **2001,** 105, 12286

(47) Wehrenberg, B. L.; Wang, C.; Guyot-Sionnest, P. *J. Phys. Chem. B*, **2002,** 106, 10634.

(48) Kreibig, U.; Vollmer, M. *Optical properties of Metal Clusters*, **1995,** Berlin: Springer.

(49) Papavassiliou, GC. *Prog. Solid State Chem*, **1979,** 12, 185.

(50) Burda, C.; Chen, X.; Narayanan, R.; El-Sayed, M. A. *Chem Rev.* **2005,** 105, 1025.

(51) Faraday, M. *Phil. Trans. R. Soc*., 147, 145, 1857.

(52) Mie, G. *Annu. Phys*. **1908,** 25, 329.

(53) a. Kreibig , U.; Von Fragstein, C. Z. *Phys*. **1969,** 224, 307.

b. Kreibig, U. Z. *Phys*. **1970**, 234, 307.

(54) Sun, C. K.; Vallee, F.; Acioli, L. H.; Ippen, E. P.; Fujimoto, J. G. *Phys. Rev. B*, **1994,** 50, 15337.

(55) Del Fatti, N.; Voison, C.; Achermann, M.; Tzortzakis, S.; Christofolis, D.; Vallee, F. *Phys. Rev. B*. **2000**, 61, 16956.

(56) Hodak, J. H.; Henglein, A.; Hartland, G. V. *J. Phys. Chem. B*. **2000**, 104, 9954.

(57) Hodak, J. H.; Martini, I.; Hartland, G. V. *J. Phys. Chem. B.* **1998**, *102*, 6958.

(58) Hodak, J. H.; Henglein, A.; Hartland, G. V. *Journal of Chemical Physics* **1999**, *111*, 8613.

(59) Hodak, J.; Martini, I.; Hartland, G. V. *Chemical Physics Letters* **1998**, *284*, 135.

(60) Link, S.; Burda, C.; Wang, Z. L.; El-Sayed, M. A. *Journal of Chemical Physics* **1999**, *111*, 1255.

(61) Hodak, J. H.; Henglein, A.; Hartland, G. V. *J. Chem. Phys*. **2000**, 112, 5942.

(62) Darugar, Q.; Qian, W.; Pileni, M-P.; El-Sayed, M. A. *J. Phys. Chem. B*. **2006,** 110 (1) 143.

(63) Halte, V.; Bigot, J. Y.; Palpant, B.; Broyer, M.; Prevel, B.; Perez, A. *Appl. Phys. Lett.* **1999**, *75*, 3799.

(64) Mohamed, M. B.; Ahmadi, T. S.; Link, S.; Braun, M.; El-Sayed, M. A. *Chem. Phys. Lett*. **2001**, *343*, 55.

(65) Hu, J.; Wang, L.; Li, L.; Yang, W; Alivisatos, A. P. *J. Phys. Chem. B* **2002,** 106*,* 2447-2452.

(66) Hu, J.; Li, L.; Yang, W.; Manna, L.; Wang, L.; Alivisatos, A. P. *Science*, **2001,** 292, 5524, 2060-2063.

(67) Petit, C.; Lixon, P.; Pileni, M. P; *Langmuir*, **1991,** 7, 2620.

(68) Lisiecki, I.; Billoudet, F.; Pileni, M. P. *J. Phys. Chem*. **1996,**100, 4160.

(69) Peng, X. G.; Manna, L.; Yang, W. D..; Wickham, J.; Scher, E.; Kadavanich, A.; Alivisatos, A. P. *Nature*, **2000,** 404, 59.

(70) Chan, W.; Nie, S. *Science,* **1998,** 281, 2016

(71) Han, M.; Gao, X.; Su, J.; Nie, S.; *Nature Biotechnology*, **2001,** 19, 631.

(72) Mattoussi, H,; Mauro, J.; Goldman, E.; Anderson, G.; Sundar, V.; Mikulec, F.; Bawendi, M. G. *J. Am. Chem. Soc.* **2000,** 122, 12142.

(73) El-Sayed, I.; Huang, X.; El-Sayed, M. A. *Nano Lett.* **2005,** 5, 5, 829.

(74) Hirsch, L. R.; Stafford, R. J.; Bankson, J. A.; Sershen, S. R.; Rivera, B.; Price, R. E.; Hazle, J. D.; Halas, N. J.; West, J. L. *PNAS,* **2003,** 100, 23, 13549.

(75) Oldenburg, S. J.; Jackson, J. B.; Westcott, S. L.; Halas, N. J. *App. Phys. Lett,* **1999,** 75, 19, 2897.

(76) Kazes, M.; Lewis, D. Y.; Ebenstein, Y.; Mokari, T.; Banin, U. *Adv. Mater.* **2002,** 14, 4, 317.

(77) Jianfeng, X.; Xiao, M. *Appl. Phys. Lett.* **2005,** 87, 173117.

CHAPTER II

SYNTHESIS AND CHARACTERIZATION OF METALLIC AND SEMICONDUCTOR NANOPARTICLES

Abstract

The field of nanotechnology depends greatly on what the properties of nanoparticles have; this is the field of nanoscience. In order to study the properties of nanomaterials, one needs to be able to synthesize them in different sizes and shapes.

In this chapter, the different methods that were used to make metallic and semiconductor nanoparticles in colloidal solutions are described. Metallic nanoparticles that were prepared include platinum, palladium, cobalt, and copper. Semiconductor nanoparticles include cadmium selenide (CdSe), cadmium sulfide (CdS), and cadmium telluride (CdTe). The synthetic method can be manipulated to grow particles from a few nanometer in size to as large as 100's of nanometers. The particle surfaces can be functionalized with different molecules during or after their synthesis. Furthermore, particles of specific shapes can be synthesized and controlled by changing the experimental conditions and by using different surfactant molecules. The synthesis of CdSe nanorods was particularly modified from the standard method to grow rods as long as 40 nm. Also, synthesis of copper nanoparticles was achieved by modifying experimental conditions and chemical used so as to grow different size particles from 10 nm to 60 nm in diameter.

Synthesis of high quality CdS nanoparticles is also presented. Optical characterization using UV-Vis absorption and fluorescence spectroscopy in steady state and in the transient modes together with transmission electron microscopy images are presented for different metals and semiconductor nanoparticles.

Introduction

Synthesis of nanoparticles is not a new concept and dates back to as early as the ancient Egyptian time period. Colloidal gold nanoparticles were incorporated into stain glass windows giving them their brilliant colors used in windows of cathedrals and churches. It is believed that the Romans and Chinese used colloidal gold particles as well for decorating ornaments and vases (1a). Figure 2-1 shows a photograph of stain glass inside Notre Dame Cathedral in Paris. These bright colors were later suggested by Faraday to be colloidal gold nanoparticles that were synthesized back in the 17^{th} century (1b). Once transmission electron microscopy became available, it was found that the size of these particles is on the nanometer scale. Over the past couple of decades, synthesis of colloidal nanoparticles and clusters (2-20), as well as their applications in different fields (12, 21-30) has been one of the most active research fields in science and technology.

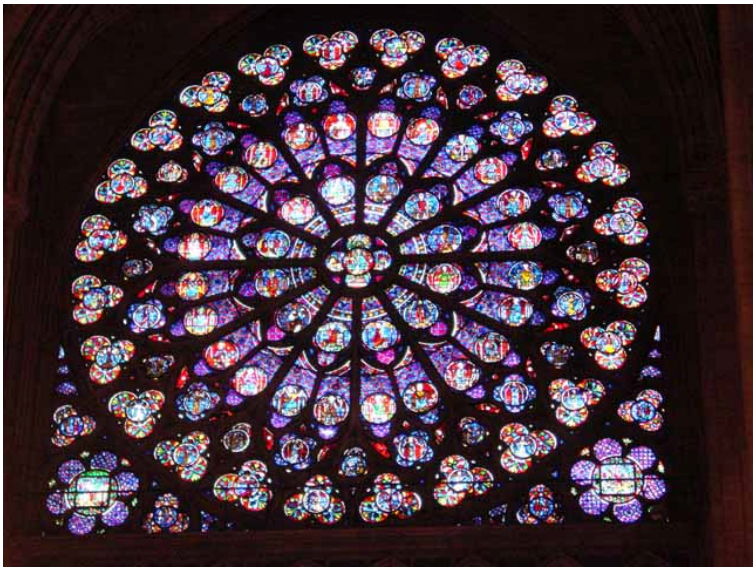

Figure 2-1: Gold nanoparticles deposited/incorporated on glass inside Notre Dame to give brilliant color effects.

Controlling the physical size of materials can be used to tune the material's properties. Because the particle's size is smaller than the length scale of the properties in the bulk materials, new physical phenomena in metallic and semiconductor nanoparticles can be discovered. Nanoparticles have electronic structure which is in the transition between atomic-like, molecular and bulk-like structures. Electronic and optical properties of metals (31-37) and semiconductors (8, 9, 12, 15, 38) strongly depend on crystallite size and shape in the nanometer size regime.

Size and shape monodispersity is very important to carefully reveal the dependence of the material's properties on size or shape and therefore requires synthetic routes to prepare monodispersed nanocrystals. Pileni et al (2, 13, 18, 39-41) have demonstrated shape and size control of metallic and semiconductor

particles in micelles by varying the surfactant concentration. Pileni has shown that the particle size can be controlled from 1-12 nm in diameter by varying the water content ([H2O]/[AOT]=w) during copper ion reduction. Figure 2-2 shows an example of copper nanoparticles prepared by the reverse micelle technique.

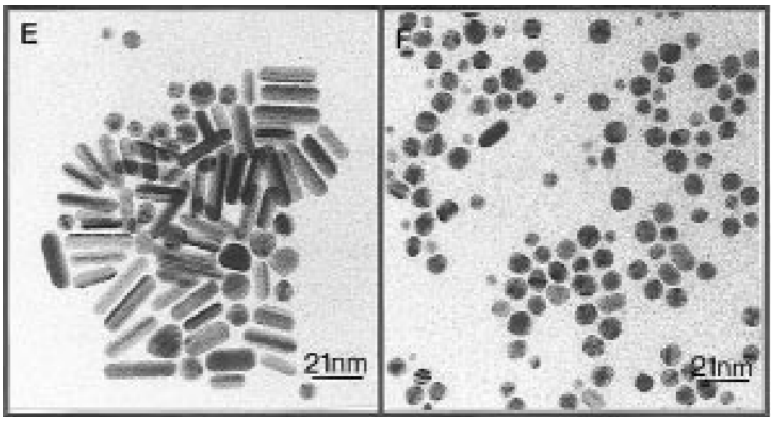

Figure 2-2: Spherical and cylindrical shaped copper nanoparticles prepared by using [H2O]/[AOT]=44=w and spherical particles using w=4 (42).

Reverse micelle methods have also been used to make monodispersed silver, gold, cobalt, cadmium sulfide and cadmium selenide nanoparticles by Pileni and co-workers (13, 18, 39-41). Metallic nanoparticles such as copper, gold and silver have been prepared by reducing the respective metal salt (or complex) in solution by UV light (64-69) in the presence of capping materials. Even though the size distribution is not as good as other known methods, the photochemical method does provide better control over the final average size, it is cheaper and simplistic in nature.

For most metallic nanoparticles used in catalysis, the size and shape becomes important in determining the rates of chemical reactions. Because of the shapes, the crystal facet also becomes important in determining the catalytic activity of a metal. Somorjai et al have done extensive work using sum frequency generation (SFG) experiments to show that the rate of the reactions and the final products depend on the type of crystal facet at the reaction surface (44-47).

El-Sayed et al demonstrated shape controlled synthesis of platinum nanoparticles (7) by changing the concentration ratio of the capping material to the cations used in the reductive process in solution. Figure 2-3 shows cubic and tetrahedral shaped particles prepared in aqueous solution (7).

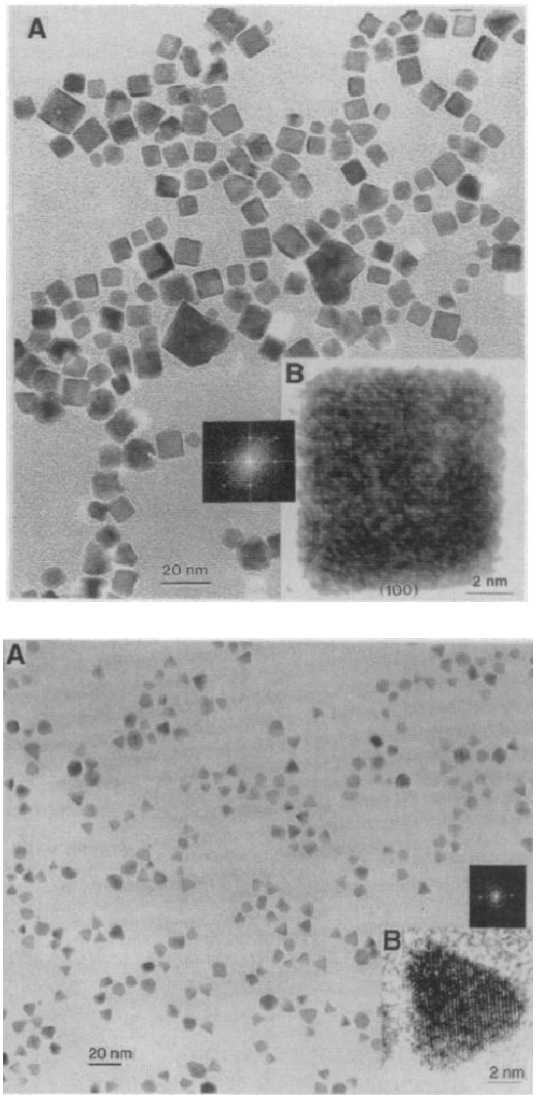

Figure 2-3: TEM images of cubic (upper) and tetrahedral (lower) shape platinum nanoparticles, from ref. 7.

As discussed above, cobalt nanoparticles can be prepared using the reverse micelle method and recently Alivisatos et al demonstrated the synthesis of cobalt nanoparticles by reducing a cobalt complex ($Co_2(CO)_8$) in a hot surfactant solution of tri-n-octylphosphine oxide (TOPO) (48). This method provides a simple one step synthetic route to produce monodispersed nanoparticles. Figure 2-4 shows a TEM image of 16nm cobalt particles prepared by Alivisatos et al. Since cobalt nanoparticles are magnetic and possess a high surface to volume ratio, these species are interesting to study and could be used as high density storage devices and other technological applications

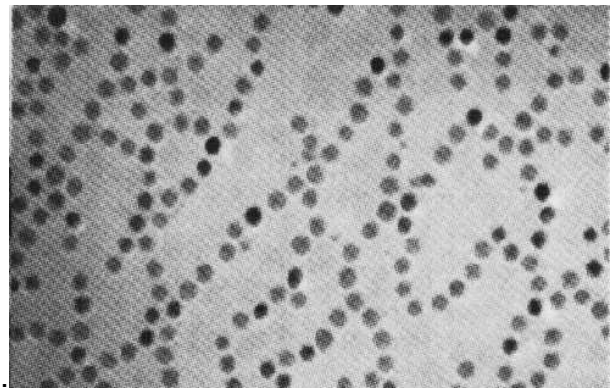

Figure 2-4: TEM image of 16 nm Cobalt nanoparticles produced by rapid injection of $Co_2(CO)_8$ in a non coordinating solvent (TOPO), from ref. 48.

The idea of synthesizing cobalt nanoparticles came from the synthesis of CdSe nanoparticles in which cadmium and selenium precursors were rapidly injected into hot surfactant solution of TOPO (15). This method of making semiconductor particles revolutionized the field of colloidal nanoparticles and nanoscience over the past decade. More and more researchers are using this method in order to make high quality and monodispersed samples. Another advantage of using Murray and Bawendi's method for particle synthesis is the ability to control the size by merely changing the reaction temperature and/or the reaction time. The size of semiconductor particles can be controlled to be smaller than the exciton Bohr radius and therefore show quantum confinement effect. What made CdSe so successful was its ability to absorb and emit light through most of the visible region of the spectrum (15). Figure 2-5 shows the absorption spectra of different size CdSe nanoparticles. The first absorption peak is from the smallest particles and as the particle size increases, the absorption peak shifts further and further to the red. Even though the synthesis, absorption and emission characterization was the major part of understanding the properties and the potential use of this system, there is still a wealth of information yet to be determined. These particles are very small in size and therefore large fractions of atoms are on the surface. For this reason, surfaces of these particles play a very important role in the optical and electronic properties.

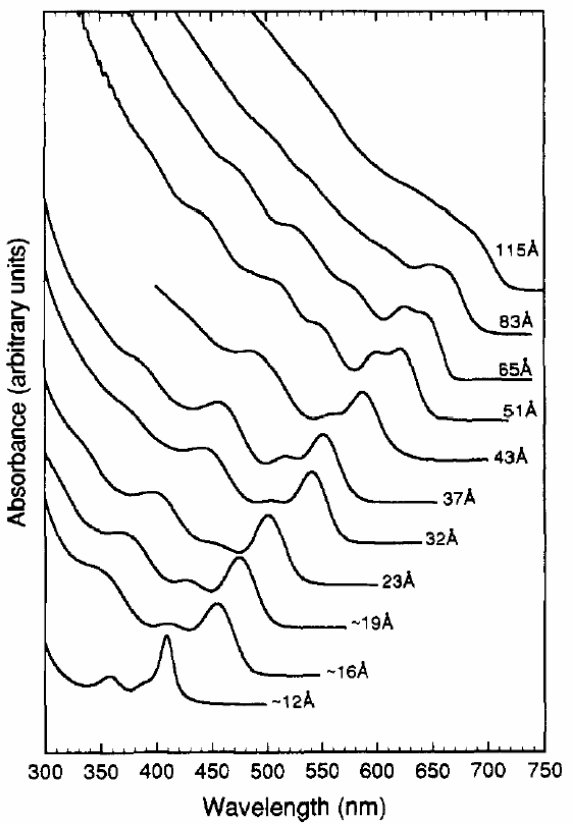

Figure 2-5: Room temperature optical absorption spectra of CdSe nanocrystals dispersed in hexane and ranging in size from 12 to 115A, from ref 15.

Colloidal CdSe nanoparticles synthesized in hot surfactant solution is the best known method at the moment for the bottom up technique in making colloidal nanoparticles. The surface states and traps can still quench most of the emission for particles synthesized by this method (15). The surface can be improved by passivating CdSe with an inorganic material such as zinc sulfide (ZnS) that has a larger bad gap than CdSe as demonstrated by Hines et al (49). Passivation helps improve the particle's surfaces from defects that could act as trapping sites for charge carriers or it could fill the deficiencies in electron or hole density.

Thus, passivation decreases the concentration of the surface traps somehow allowing more charge carriers to reach the band gap state and combine to give fluorescence. Figure 2-6 shows a 6 fold increase in the emission intensity after ZnS passivation as well as reduced deep trap emission at longer wavelengths (49).

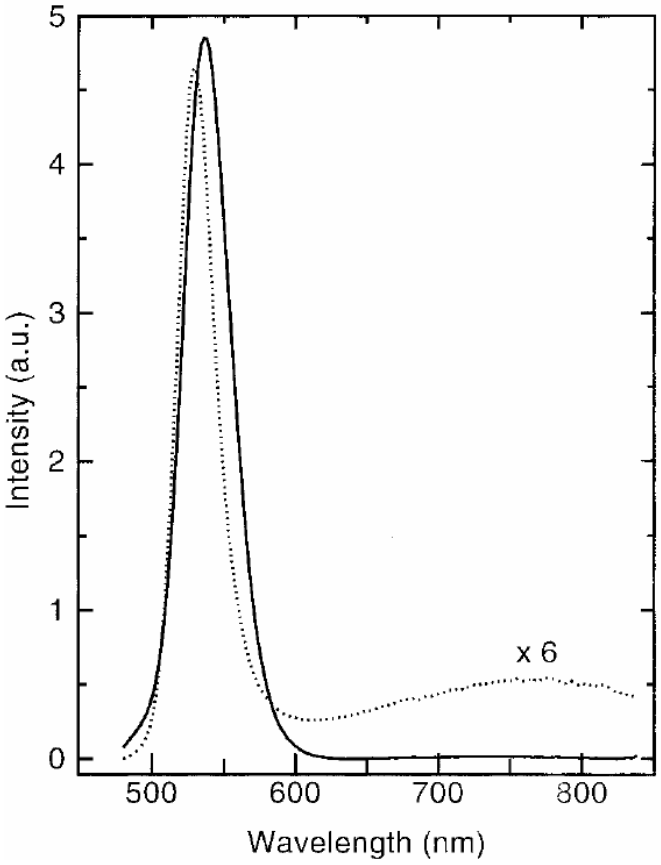

Figure 2-6: Fluorescence of the (CdSe)TOPO (dotted line) and (CdSe) ZnS (solid line) nanocrystals normalized by their absorption at the excitation wavelength (470 nm), from ref. 49.

Systematic control of shape in metallic particles was demonstrated by El-Sayed in 1996 (7) but there were no methods to selectively control the growth of semiconductor particles in solution within their confinement region until Alivisatos et al published their findings in 2000 on making rod shape CdSe nanoparticles with two-dimensional confinement (19). In their method, which is an extension of Bawendi's method of making spherical CdSe particles (15), they added co-surfactants to the hot solution of TOPO. This allowed CdSe to grow faster in one direction resulting in a rod shaped nanoparticle. Two dimensional control affords researchers the opportunity to investigate fundamental properties both experimentally and theoretically that they would not otherwise have. Alivisatos et al also measured polarized emission along the c-axis of these rods (50) and later showed using semi-empirical pseudo potential calculations that the two excited energy levels crossed when the aspect ratio increased to more than 1.3. Because of this energy state crossover, the lowest state is now the allowed state to radiate polarized emission in the direction observed experimentally.

Furthermore, other shapes of semiconductor nanoparticles such as tetra and tri-pods can be synthesized (figure 2-7), though the nature of the required experimental conditions is still not very clear (51-54).

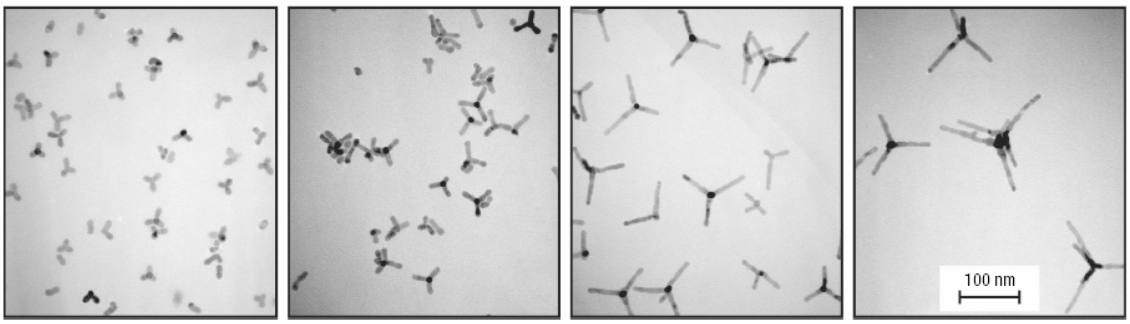

Figure 2-7: TEM images of different size CdTe tetrapods prepared by varying the amount of Cd:Te, from ref. 51.

Korgel et al. used the method of preparing nanorods discussed above to grow semiconductor heterostructures (32). Instead of multiple injections of the same precursors, they injected different anions to grow sequential layers of respective materials.

Great amount of work in the field of metallic and semiconductor nanoparticles synthesis and characterization has been done in our group and at other institutions around the world. It becomes very important to be able to make materials from known methods and/or by improving existing methods to accommodate our research needs. It's been more than ten years since Murray and Bawendi first prepared high quality semiconductor nanoparticles and there remains plenty of opportunity to still study more of their fundamental properties and their compatibility with other systems and their applications.

Experiemntal

2.1 Synthesis of Metallic Nanoparticles.

a. Cubic Platinum Nanoparticles

Chemicals:

K_2PtCl_4 (99.99%) and acrylic acid were obtained from Aldrich. All solutions were prepared using doubly deionized water. Hydrogen (99.995%) purchased from Matheson Company was used without further purification.

Catalyst Preparation:

Preparation method of the Pt catalyst is similar to that used by Rampino and Nord (55) and Henglein et al. (56). 2mL of 0.01M K_2PtCl_4 solution is added in 250mL of water together with 0.8mL of 1M acrylic acid. The pH of the solution was then adjusted to 7 with 0.1 M HCl and/or 0.1M KOH and purged with Ar for 20 min. Pt complexes were reduced by bubbling H_2 for 5 min. The solution was left for 24 h in the dark. For TEM imaging, a drop of final solution is spotted on a carbon coated copper TEM grid. Figure 2-8a and 2-8b show typical images of platinum nanoparticles of about 4-5 nm and 7-8 nm in size, respectively. The larger particles (7-8 nm) consist of about 80% cubic shaped particles.

(a)

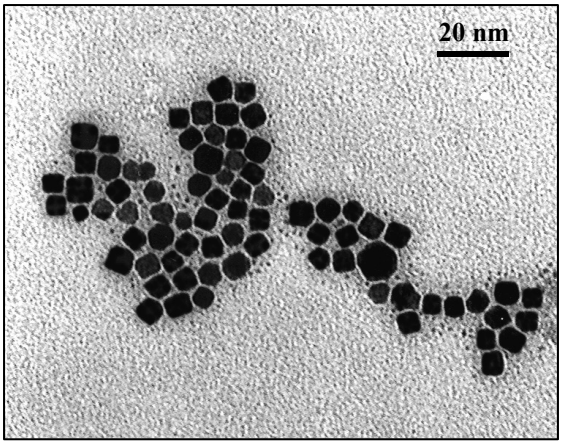

(b)

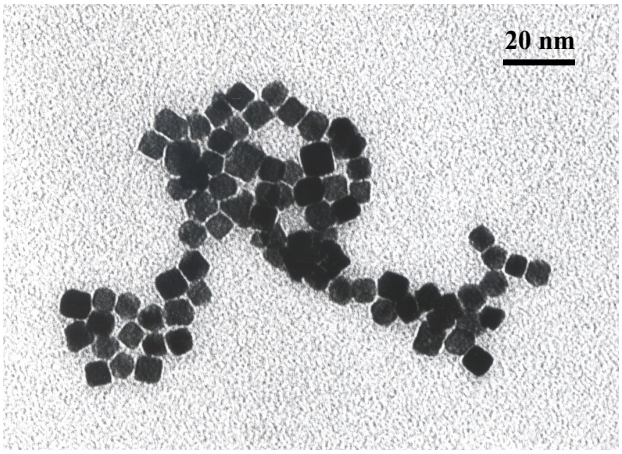

Figure 2-8: Cubic platinum nanoparticles (a) ~5nm and (b) ~8nm.

Capping materials such as poly(acrylic acid) (7, 57) and poly-(N-vinyl-2 pyrrolidone) (58,59) are typically used as stabilizers in making mono- or bimetallic nanoparticles to protect against self-aggregation of the metal nanoparticles. Specifically, poly(acrylic acid) can be used to control the shapes (tetrahedral, cubic, icosahedral) and sizes of Pt nanoparticles by changing the molar ratio of the capping material to the Pt cations in aqueous solution (7). Though the capping material has advantages that are described above, from a

viewpoint of its catalytic application, it is expected not to have a positive effect due to partial blockage of the active sites on the nanosized metal particle. Nevertheless a lot of work has been done on hydrogenation over metal nanoparticles in the presence of polymer (58-60).

Particles prepared in a way similar to that described above and others which were supported on alumina were used to study catalytic activities by Yoo et al (61-62) in our group.

b. Palladium Nanoparticles

Chemicals:

K_2PdCl_4 (99.99%) and polyacrylate were obtained from Aldrich. All solutions were prepared using doubly deionized water. Hydrogen (99.995%) purchased from Matheson Company was used without further purification.

Catalyst Preparation:

Palladium nanoparticles are prepared using a method very similar to the one used to make Pt (55, 56). 2mL of 0.01M K_2PdCl_4 solution is added to 250mL of water together with 1.5mL of 1M polyacrylate. The pH of the solution was then adjusted to 7 with 0.1 M HCl and/or 0.1M KOH and purged with Ar for 20 min. Pd complexes were reduced by bubbling H_2 for 5 min. The solution was left for 24 h in the dark. For TEM imaging, a drop of solution is dropped on a carbon coated copper TEM grid. Figure 2-7a below show a typical image of palladium

nanoparticles of about 10 nm in size, figure 2-9b is 15 nm and figure 2-9c is 5 nm particles.

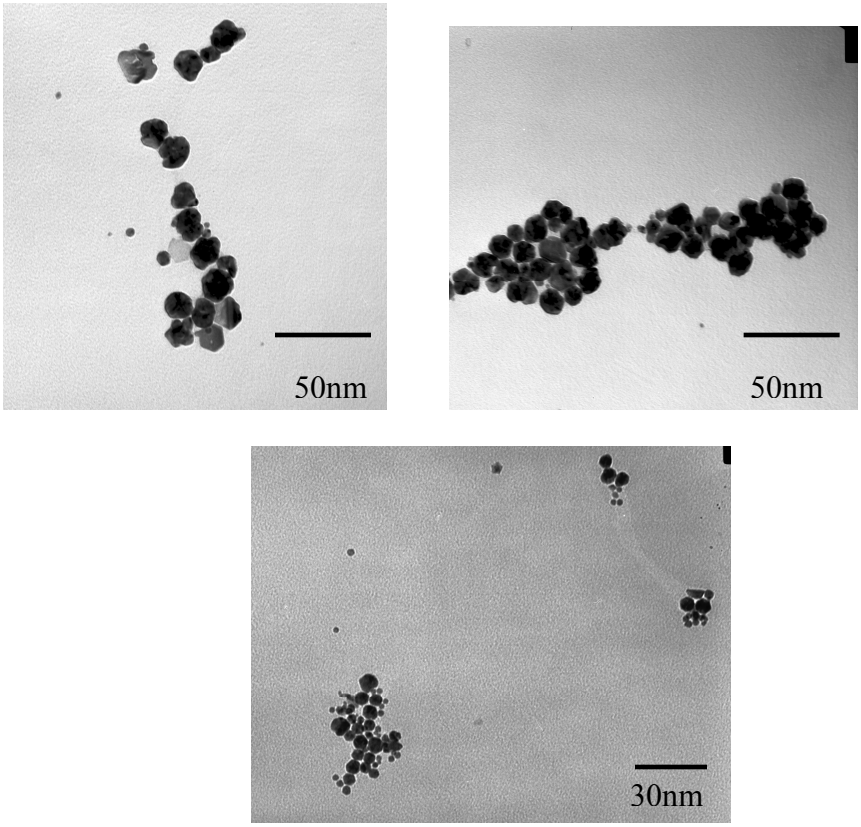

Figure 2-9: TEM image of palladium nanoparticles prepared by metal ion reduction using hydrogen; (a) 15 nm, (b), 10 nm and (c) 5 nm.

c. Copper Nanoparticles Using Reverse Micelles

Sodium bis(2-ethylhexyl) sulfosuccinate Na(AOT), dissolved in organic solvents forms reverse micelles (41). Water is readily solubilized in polar core forming a so called “water pool”, characterized by w, w=[H_2O]/[AOT]. Increase in the water content increases the size of the metal particles formed inside them.

To make copper particles by reverse micelle, we need to make $Cu(AOT)_2$ by exchanging sodium ions with copper ions in Na(AOT) (63). Detailed outline of the procedure is described below.

Chemicals:

Na(AOT) and hydrazine are obtained from Sigma. Bio-Rex 70 resin (100-200 mesh), Na form and AG-MP-50 resin (100-200 mesh), H^+ form were purchased from Bio-Rad. Isooctane was purchased from Fluka and used as received.

Procedure for making $Cu(AOT)_2$:

Set up two columns as described below.

1st Column:

1st column contains the resin to exchange cations that are strongly acidic. It is used to exchange AOT/Na into AOT/H^+.

1) Mix 75g of Bio-Rex 70 resin slowly with deionized water and put all of it in the column while stirring it to avoid forming air bubbles.
2) Add water to rinse the resin until the pH of the collected water is ~7.

3) Prepare excess (~200mL) of 0.2M Na(AOT) in a mixed solvent (50:50 water/ethanol).
4) Condition the resin by adding the mixed solvent.
5) Pour Na(AOT) slowly into the column and discard ~25mL of the first solvent collected.
6) The AOT/H^+ that progressively forms can be directly transferred to the second column.

<u>2nd Column:</u>

2nd column contains the resin to exchange cations that are slightly acidic. It is used to exchange AOT/H^+ into AOT/Cu^{2+}

1) Mix 75g of AG-MP50 resin slowly in water and place all of it into the column.
2) Add water to rinse the resin until the pH of the water collected is 9.
3) Prepare excess of 0.2M of $CuSO_4$ (~1L) in water.
4) Add $CuSO_4$ slowly to the column until all the sites are exchanged (can be monitored by measuring the absorption spectra of the original $CuSO_4$ solution with the one collected from the column.)
5) Rinse the resin with water to remove any Cu^{2+} from the column (Blue color will disappear).
6) Condition the resin by adding the water/ethanol solvent.
7) At this point the column is ready to receive AOT/H^+ from column one.

The collected $Cu(AOT)_2$ in the mixed solvent has to be evaporated and washed several times with the chosen solvent (Isooctane).

Reduction of $Cu(AOT)_2$ to Make Copper Nanoparticles:

Measure 0.3mL of 0.1M $Cu(AOT)_2$ into a cuvette with 0.96mL of 0.25M Na(AOT) and 1.74mL of Isooctane. Measure the require amount of water as needed depending on the w = [H2O]/[AOT] value calculated. Inject rapidly, 4.4µL (excess) of hydrazine into the $Cu(AOT)_2$ solution and shake vigorously. The blue tinted solution will immediately turn brown to reddish in color. The cuvette was allowed to sit for a couple of hours and a drop of the solution was spotted on a carbon coated copper TEM grid for imaging as shown in figure 2-10 for three different nanoparticle samples. The sizes were examined by using a JEOL 100CX II transmission electron microscope (TEM). Figure 2-11 shows the absorption spectra of two different size copper nanoparticles.

(a)

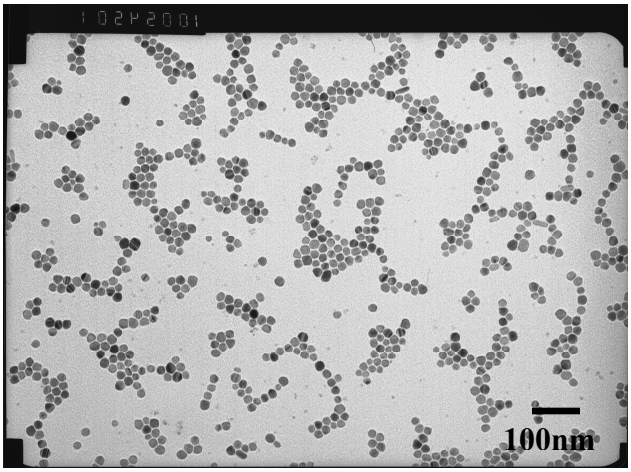

(b)

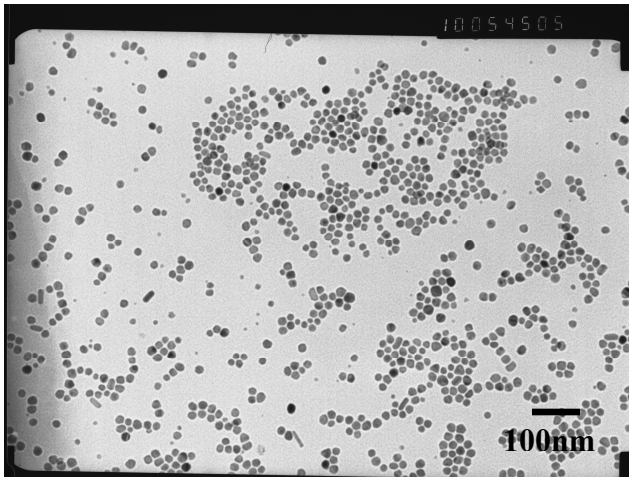

Figure 2-10: TEM images of different size copper nanoparticles prepared using the reverse micelle method. (a) 16nm copper particles (w=10), (b) 11nm copper nanoparticles (w=4), and (c) ~9nm copper particles (w=1),. (d) Close look at the copper particles shows very nice self-assembles and monodispersed 16 nm copper nanoparticles.

(c)

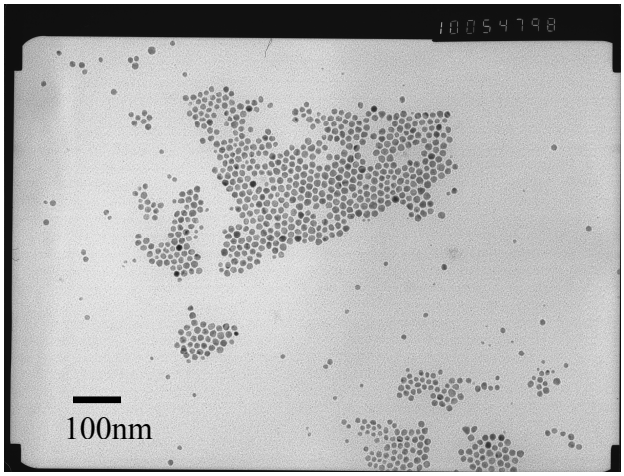

(d)

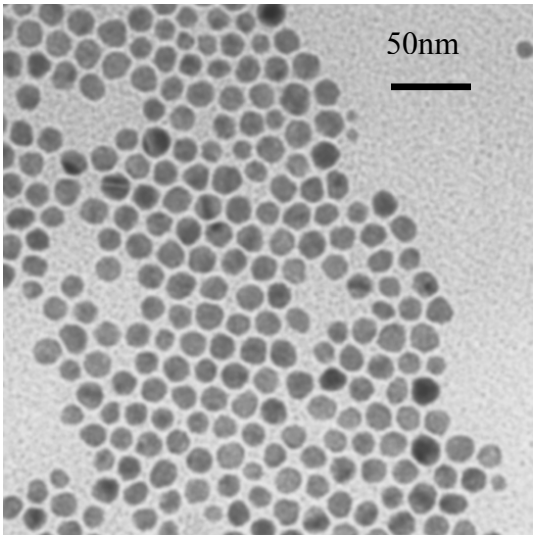

Figure 2-10 Continued.

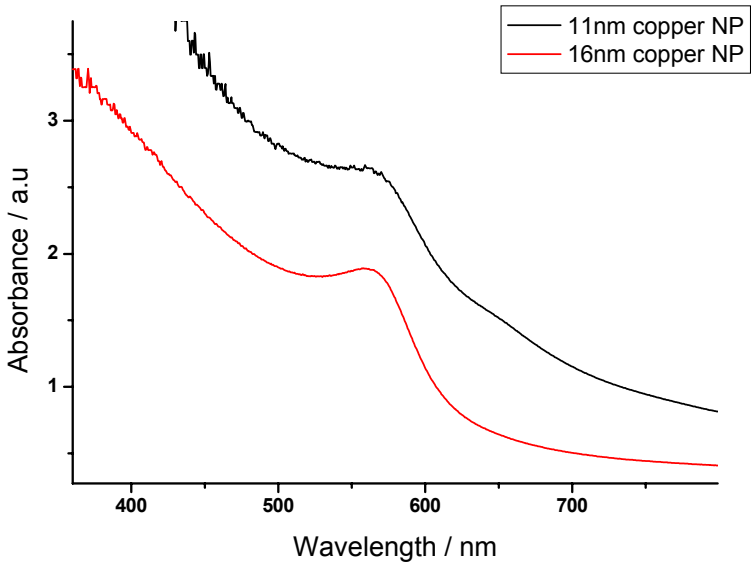

Figure 2-11: Absorption spectra of 16 and 11nm copper NP with the plasmon band at 564 nm.

Comments on the method and the particles stability:

It is necessary to do the reduction of copper ions in the glove box under inert atmosphere. Any trace of oxygen can affect the sample and oxidize the surface. Also, it is critical to monitor the amount of water added. Too much water can cause micelles to break and aggregate the copper nanoparticles. Also, it is very important to wash $Cu(AOT)_2$ carefully with isooctane to remove any trace of water so that it does not affect the calculated amount of water added during reduction.

d. Copper Nanoparticles Using Photochemical Reduction Method:

Chemicals:

Bis(2,4-pentanedionato)copper(II), [$Cu(acac)_2$] and poly(N-vinylpyrrolidone) (PVP) were purchased from Sigma-Aldrich and Ethanol was purchased from Fisher Chemicals. All chemical were used as received.

Experimental:

The copper nanoparticles in ethanol solution are synthesized by photochemically reducing the commercially available precursor bis(2,4-pentanedionato)copper(II), [$Cu(acac)_2$] with UV light as proposed by Giuffrida et al (64). In a typical copper nanoparticle synthesis, $5\times10^{-4}M$ $Cu(acac)_2$ in deoxygenated ethanol is irradiated at 254 nm at an intensity of 5 mW/cm^{-2} under anaerobic conditions. Growth of copper nanoparticles is monitored by the appearance of an absorption peak around 570 nm, which is characteristic of the plasmon band of copper nanoparticles (32, 39). The irradiation is stopped when a maximum value of plasmon absorption is observed. Copper nanoparticles prepared this way are very unstable. In order to increase their stability, poly(N-vinylpyrrolidone) was added to the solution before irradiating with UV light. This allowed the formation of isolated copper nanoparticles that were stable for days when left in an inert atmosphere. Particle size variation was very critical for our research and was difficult to obtain by only controlling the parameters of one-step photochemical reduction (such as concentration of solution, irradiation light intensity, and

irradiation time). With previously synthesized nanoparticles (about 10 nm) as seeds, the seed-mediated growth method was used to successfully grow copper nanoparticles in ethanol with an average diameter of 50 nm.

The size and morphology were examined by using a JEOL 100CX II transmission electron microscope (TEM) and the linear absorption spectrum of our samples was measured by using a Shimadzu UV-3101-PC spectrophotometer. The TEM images of two samples, Cu1 and Cu2, are shown in figure 2-12a and 12b, respectively. The average diameters of Cu1 and Cu2, determined by measuring the sizes of roughly 200 particles, were 12 nm and 30 nm, respectively. The linear optical absorption spectrum of Cu1 and Cu2 are shown in figure 2-13. A nice plasmon absorption band is clearly seen in both samples with a slight blue shift from 568.5 nm for Cu1 to 565.0 nm for Cu2. The blue shift of the surface plasmon absorption of copper nanoparticles as increasing their sizes is consistent with the theoretical prediction made by Pileni's group (70). By using the Mies' theory and taking into account the size dependence of the dielectric constant $\varepsilon_2(R)$, they demonstrated that there is a progressive blue shift of the surface plasmon absorption upon increasing the size of copper nanoparticles. Besides the TEM images, the absorption spectra also confirm that the size of Cu2 is larger than that of Cu1.

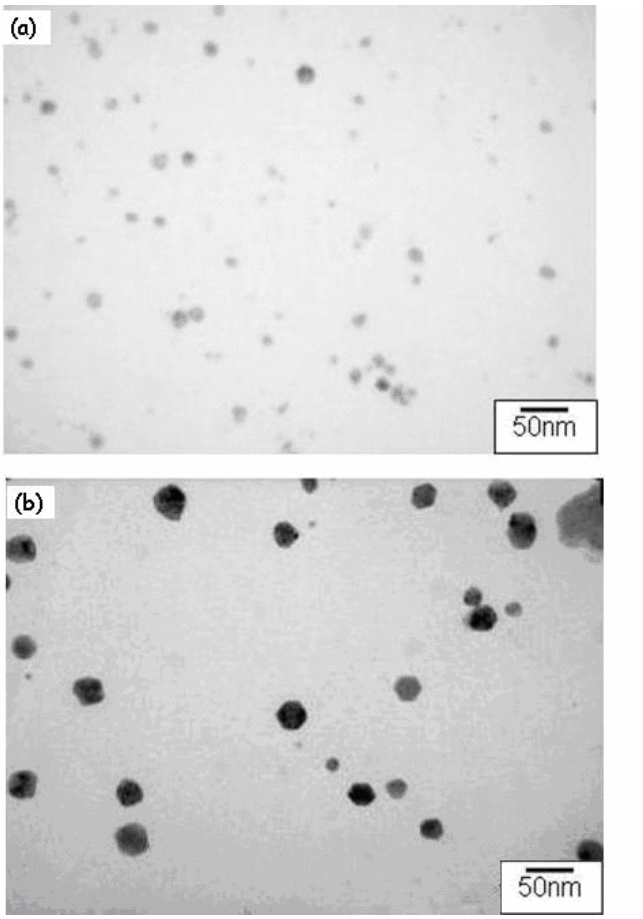

Figure 2-12: Transmission electron microscope images of (a) Copper 12 nm and (b) Copper 30 nm particles. The measured average diameter of these nanoparticles was determined by measuring sizes of roughly 200 particles. In (b), we also observed nonspherically shaped copper nanoparticles synthesized by photochemical method.

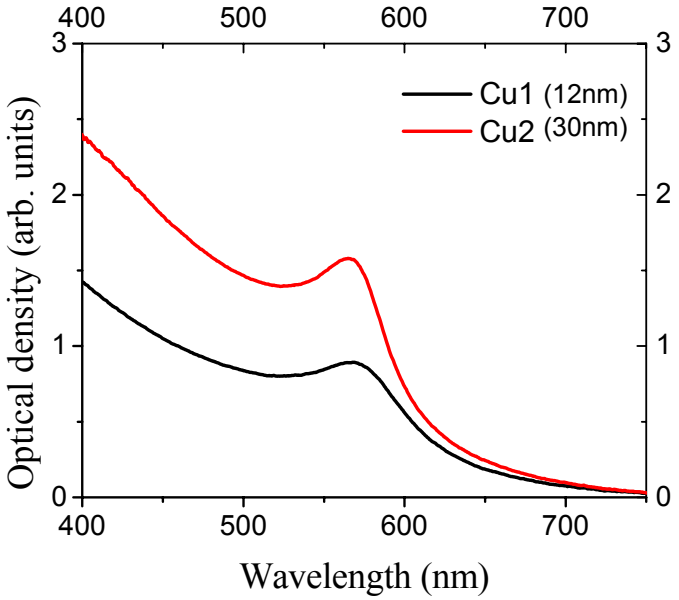

Figure 2-13. Absorption spectra of copper nanoparticles in ethanol solution synthesized by photochemical reduction of the precursor bis(2,4-pentanedionato)copper(II), [$Cu(acac)_2$] in ethanol in the presence of PVP with 254 nm UV radiation. The absorption around 570 nm is characteristic of the plasmon band of copper nanoparticles.

Comments on the method and the particles stability:

All the sample preparation and copper ion reduction needs to be done in the glove box. Any trace of oxygen would oxidize the particles immediately. Copper nanoparticles are transferred to the cuvette in the glove box and sealed tightly before removing. The sample is stable for weeks under inert atmosphere. Ethylene glycol instead of ethanol was also used as a solvent but did not form copper nanoparticles.

e. Synthesis of Cobalt Nanoparticles

Chemicals:

Dicobalt octacarbonyl ($Co_2(CO)_8$) was purchased from Strem Chemicals, trioctyl phosphine oxide, 1,2-dichlorobenzene and oleic acid were purchased from Sigma.

Experimental:

Synthesis of cobalt nanoparticles was carried out as described by Alivisatos et al (48). This method is an extension of the synthesis of CdSe nanoparticles in a hot surfactant solution of TOPO (15). In a typical synthesis of cobalt nanoparticles, 0.50g of $Co_2(CO)_8$ is dissolved in 3mL of 1,2-dichlorobenzene. In a separate 3 neck flask, 1.0g of TOPO is added with 20mL of 1,2-dichlorobenzene and 0.8mL oleic acid and the temperature is raised to 120˚C. At this temperature, the solution of $Co_2(CO)_8$ is rapidly injected into the flask. The color of the solution changes almost immediately from brown to greenish grey. Within 20 seconds from the injection time, a small portion of the sample is removed for TEM. The solution is heated for about 5 minutes longer (color changes to vibrant blue) and again a small portion of the sample is removed. Figure 2-14 shows TEM images of different cobalt nanoparticles samples. At early time, there is a mixture of spherical and rod shaped particles and after continued heating of the reaction flask, all the particles become spherical in shape.

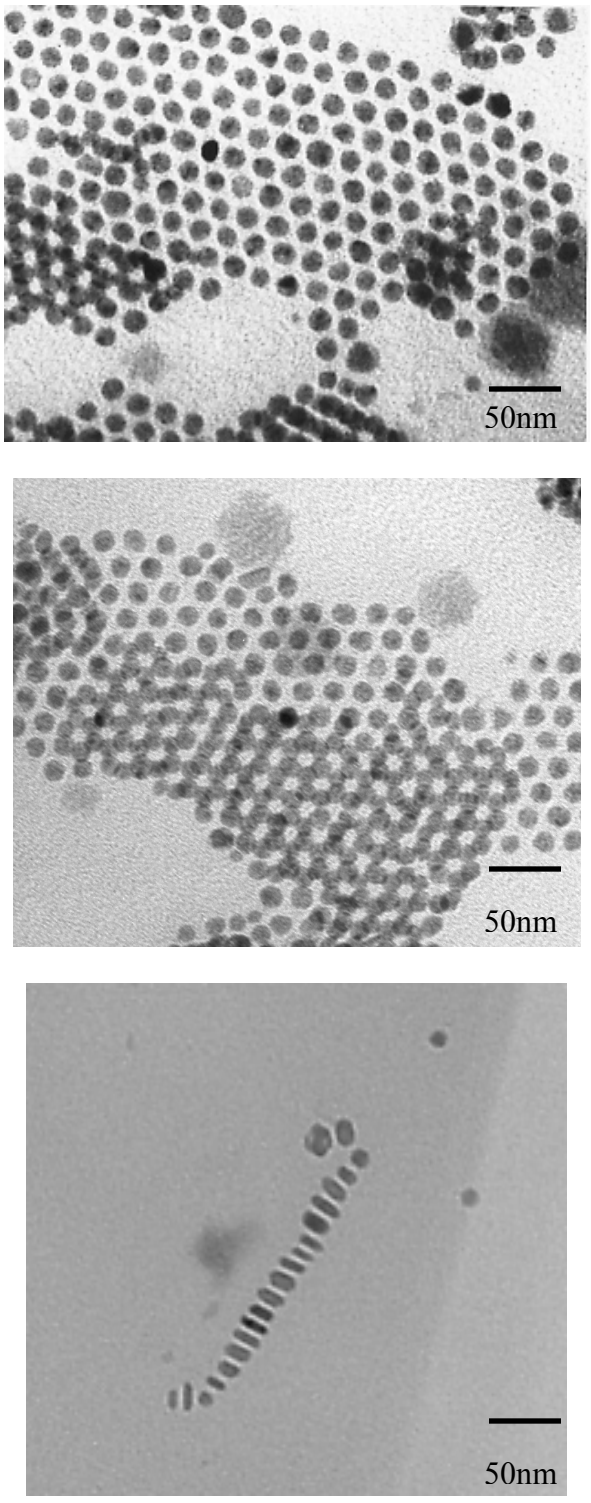

Figure 2-14: TEM image of (a) 15 nm Cobalt nanoparticles, (b) shows nicely assembled and stacked cobalt nanoparticles, and (c) shows TEM images of 15x5nm rods like cobalt nanoparticles.

Comments on the method and the particles stability:

In order to make rods or disc shaped cobalt nanoparticles, it is very important to not let the reaction go for more than a minute. After this time, most of the particles will change to spherical in shape. The absorption spectra show multiple peaks in the visible region. This is likely due to some cobalt/TOPO complex formed during the synthesis. Ideally, the solution containing cobalt nanoparticles is grey in color.

The sample prepared maybe washed from excess capping material and other impurities by adding alcohol and centrifugation and redissolving in 1,2-dichlorobenzene. Always purge the sample with argon or nitrogen before storing them in the dark.

2.2 Synthesis of Semiconductor Nanoparticles of Different Size and Shapes.

a. Spherical CdSe Nanoparticles

Chemicals:

Dimethylcadmium ($(CH_3)_2Cd$), Cadmium Oxide (CdO), Trioctylphosphine Oxide (TOPO) (90%), Trioctylphosphine (TOP) (90%), Selenium power (100 mesh, 99.99%), stearic acid and Hexyldecylamine (HDA) where purchased from Sigma-Aldrich. Toluene and Methanol were purchased from Fisher.

Experimental:

Synthesis of CdSe is well documented since it was first described by Murray and Bawendi. (15) It has been continuously modified in order to use less toxic, less expensive chemicals and to get particles with better size distribution and surface characteristics. I have been able to synthesize CdSe nanodots using the method of Murray (15) as modified by Peng et al (71-72). This modified method requires much higher temperatures compared to the original method since dimethylcadmium is replaced by less reactive Cadmium Oxide (CdO). The use of fatty acids (stearic acid) helps CdO react much faster and also gives better size distribution. The typical experimental setup is shown in figure 2-15 for synthesizing semiconductor nanoparticles.

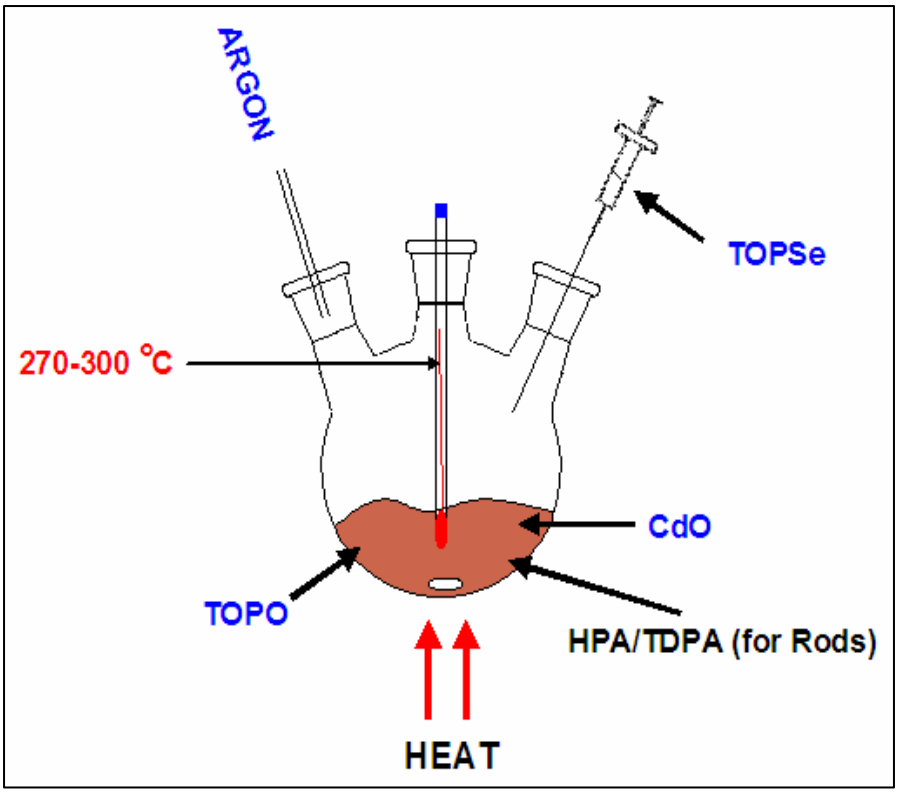

Figure 2-15: Experimental setup for synthesizing CdSe nanoparticles.

The amount of each precursor, capping materials, surfactants and temperature conditions can be varied from one experiment to another depending on the size, shape or surface quality desired. In a typical synthesis, 5 g of TOPO is preheated to 300˚ C with 0.20 g CdO (dimethyl cadmium was used initially before Peng introduced the use of CdO). After the solution become optically clear, 0.15 g Se dissolved in 3 ml trioctylphosphine (TOP) is quickly injected into the hot solution of TOPO/Cd. CdSe nanoparticles are instantaneously formed and the reaction flask is heated until desired particle size is obtained. Growth of the nanoparticles

is monitored by measuring the absorption of the aliquot during the synthesis. The typical linear absorption spectrum of our sample is shown in Figure 2-16.

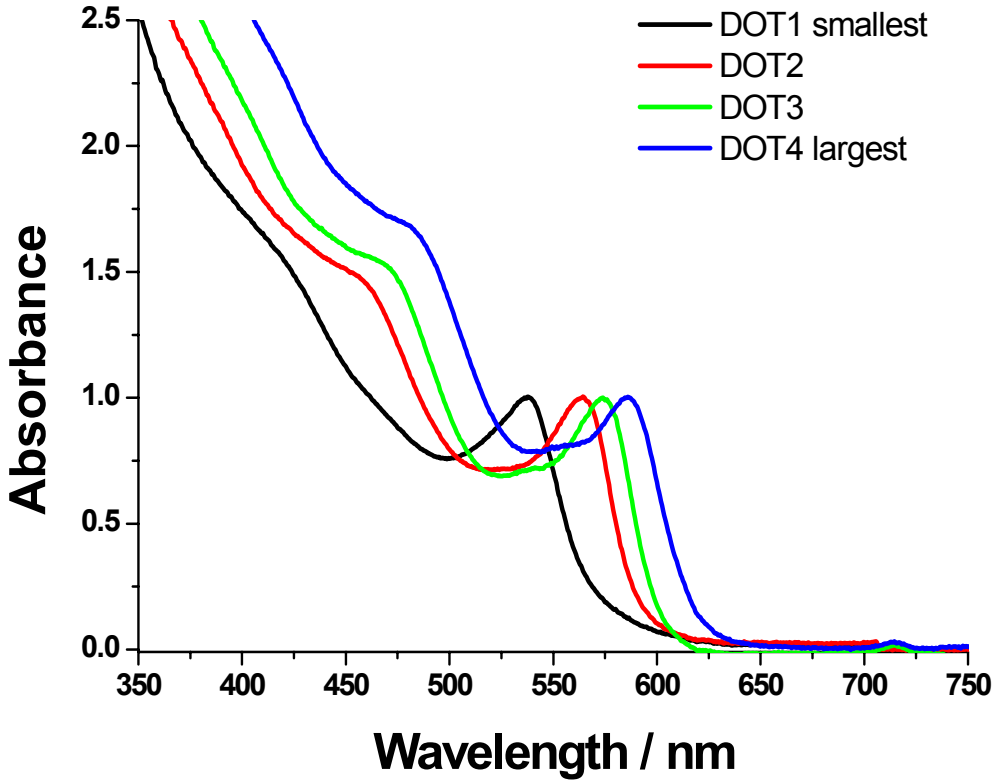

Figure 2-16: Normalized spectra of four CdSe nanoparticles samples taken at different intervals during the synthesis.

CdSe nanoparticles are washed from excess TOPO by adding alcohol (methanol). The addition of methanol precipitates the CdSe nanoparticles out of the solution which is then centrifuged and the solvent is discarded. CdSe particles are re-dissolved in toluene or chloroform as required. This process can be repeated multiple times to remove any trace of unreacted materials and excess capping materials. One thing to note is that excessive washing the sample with alcohol and redissolving in toluene can start stripping off the capping material on the particle's surface, so one has to be careful as to how many washes the sample goes through. TEM images of CdSe particles are taken by spotting a very dilute sample onto a carbon coated copper grid. Figure 2-17 shows an image of one of the synthesized CdSe samples. Sizes of the CdSe samples measured from the TEM images are often consistent with that calculated from the absorption spectra and their respective sizes provided by Murray and Bawendi (see figure 2-5 (15)).

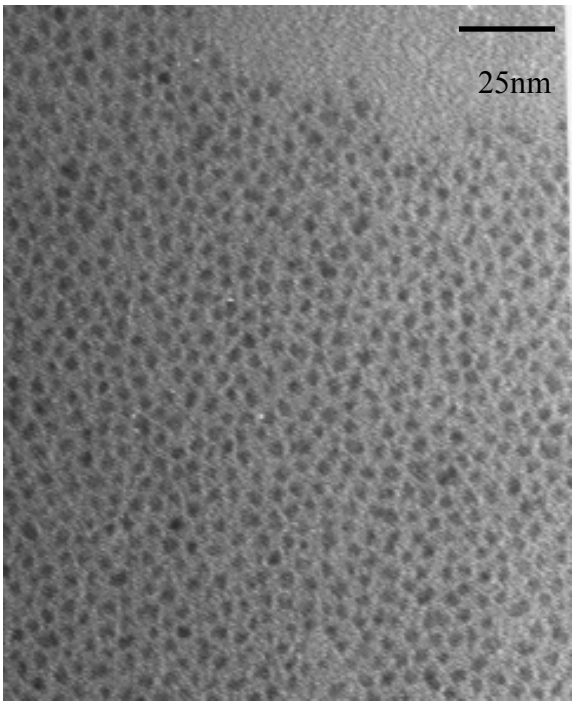

Figure 2-17: TEM Image of CdSe nanoparticles, 3.5 nm in diameter.

b Synthesis of CdSe Nanorods of Different Aspect Ratio

Chemicals:

Cadmium Oxide (CdO), Trioctylphosphine Oxide (TOPO) (90%), Trioctylphosphine (TOP) (90%), Selenium power (100 mesh, 99.99%), stearic acid, Hexyldecylamine (HDA), Tetradecylphosphonic acid (TDPA), and Hexylphophonic dichloride were all purchased from Sigma-Aldrich while toluene and methanol were purchased from Fisher.

Experimental:

The experimental setup for making rods is similar to the one described above for the dots. Preparation of CdSe dots was extended by Alivisatos and co-workers and later modified by Peng et al to grow rod shaped particles by adding co-surfactants such as TDPA and hexylphosphonic acid (HPA). HPA is made from the hydrolysis reaction of hexylphosphonic dichloride and then extracting HPA with diethylether.

In this method, CdO is added to a solution of a binary surfactant mixture of TOPO and HPA. In a typical reaction, 0.5g CdO is added to 4g of TOPO and 0.2g HPA at 300°C. 0.2g Se dissolved in TOP is quickly injected into the reaction flask and heated at 280°C. CdSe nanorods synthesized are washed from excess surfactants by the method described above.

Alivisatos et al have shown (19) that they can grow longer nanorods if they let the reactants age from a few days to up to weeks before adding Se. In this method, TOPO, CdO and TDPA are heated to about 270ºC until the solution turns optically clear. The solution is then cooled to room temperature and stored under argon for 3-4 days for aging. It is believed that aging slows down the nucleation process which in turn results in the growth of longer rods. Images were taken using low resolution TEM and show pretty good size distribution of rods that are about 12 nm in length and 3nm in diameter (see figure 2-18).

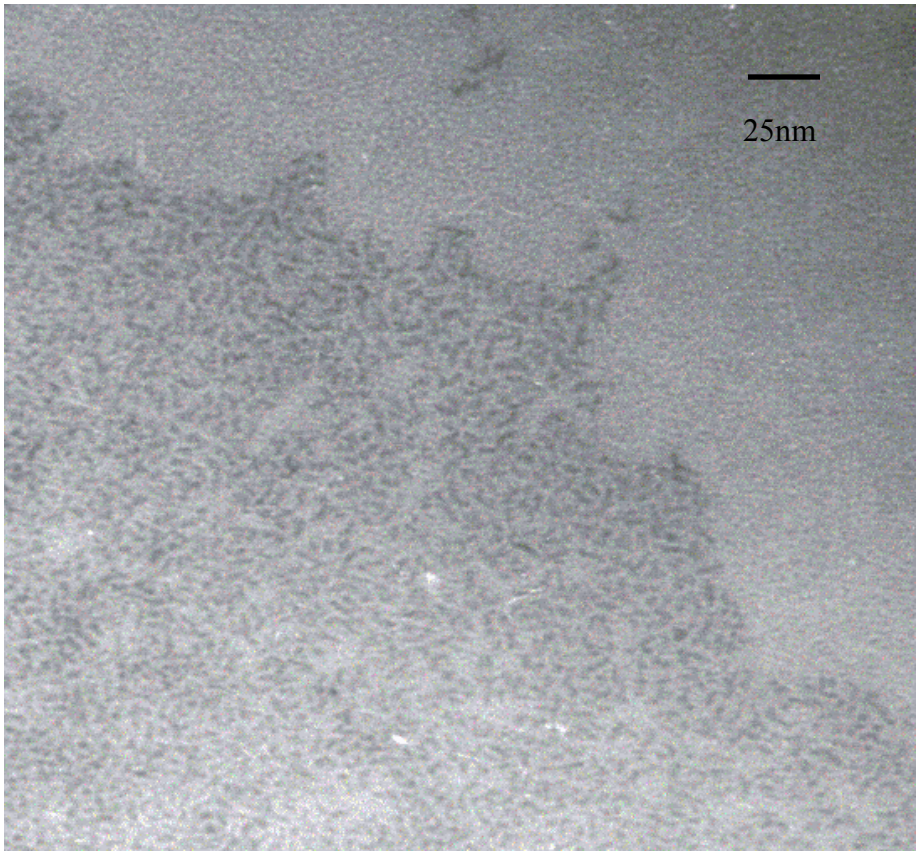

Figure 2-18: TEM image of CdSe nanorods that are about ~12 nm long and ~3 nm in diameter.

Single injection method allowed growing rods of about 15 nm in length. In order to grow rods longer than 15 nm, I used multiple injections of Se precursor after an initial Se injection. In this multiple injection method, excess Cd precursor is added to the reaction flask with TDPA/HPA and heated until the reactants turns optically clear. The temperature is then reduced to about 180ºC and followed by quick injection of TOPSe. After an initial quick injection, roughly 1 ml TOPSe is injected after a couple of minutes. Similar injections are repeated every two minutes. The Se stock solution is always less than 40% of the original reactants to avoid nucleation and formation of new particles. Figure 2-19 shows TEM

images of CdSe nanorods as long as 40 nm in length synthesized by multiple injections of the precursor. Figure 2-19 (a) shows rods which are 12 nm in length and 3 nm in diameter. Figure 2-19 (b) shows rods which are 15 nm by 3 nm in sizes. 2-19 (c) shows rods shows which are 22 nm by 3 nm in size and figure 2-19 (d) shows rods which are 40 nm long and 4 nm wide.

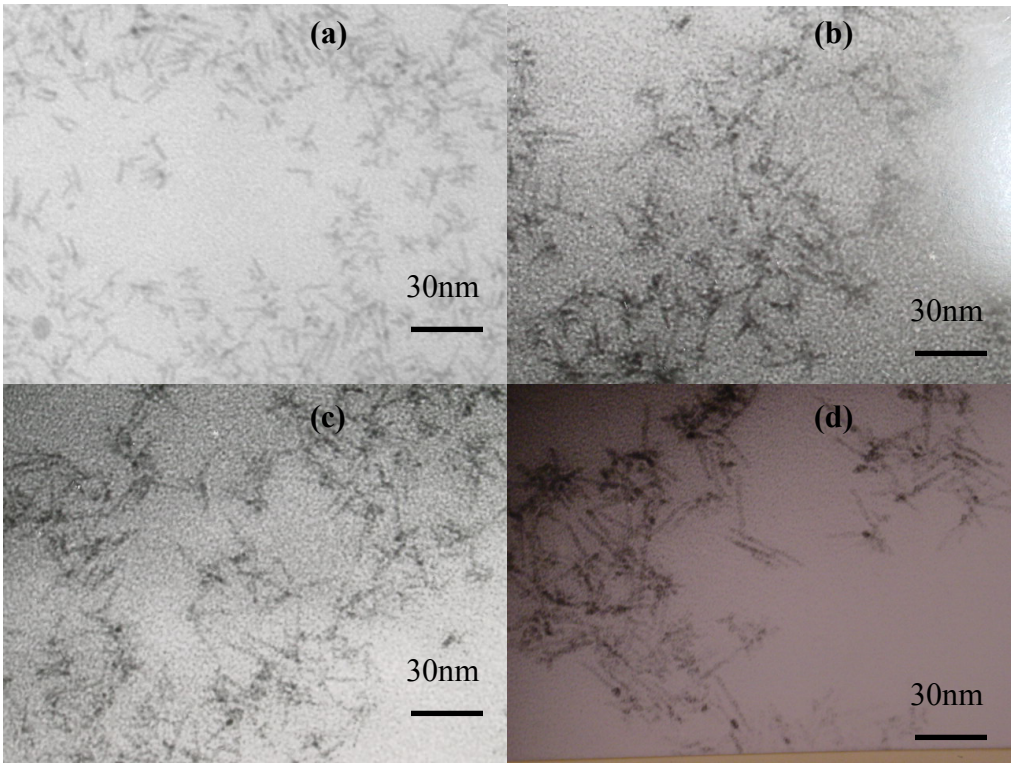

Figure 2-19: TEM images of different size CdSe nanorods prepared by the multi-injection method of TOPSe precursor. (a) Initial injection, (b) second injection (2 minutes apart), (c) fourth injection (6 minutes after first injection) and (d) sixth injection (10 minutes after first injection).

Other shapes of nanoparticles can be synthesized by changing the monomer concentration. It was possible to make tri and tetrapods shaped CdSe particles by using high concentrations of monomers. Figure 2-20 shows a TEM image of CdSe particles synthesized by using four times higher HPA concentration than the Cd/Se concentration. It is important to monitor the growth time in order to get multipod shaped nanoparticles. If the reaction is run for longer times (typically, 5-10 minutes), the particles formed are spherical in shape. The growth temperature is similar to the temperature used for making CdSe nanodots and nanorods.

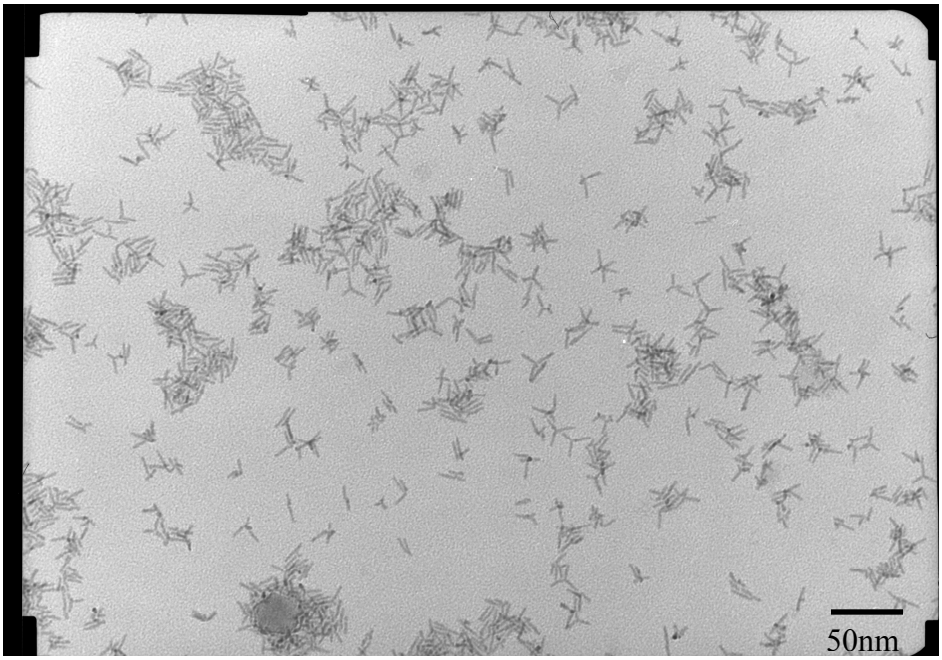

Figure 2-20: TEM images of CdSe rods, tri and tetrapods. The size of the particles is ~20 nm in length and 3 nm in diameter.

c. Synthesis of CdS nanoparticles:

Chemicals:

Dimethylcadmium ((CH3)2Cd), Cadmium Oxide (CdO), Trioctylphosphine Oxide (TOPO) (90%), Trioctylphosphine (TOP) (90%), bis(trimethylsilyl)sulfide [$(TMS)_2Se$] and stearic acid where purchased from Sigma-Aldrich. Toluene and methanol were purchased from Fisher.

Experimental:

Attempt to make CdS nanoparticles using Bawendi's method (15) failed multiple times. CdS nanoparticles did not form no matter what temperature or precursor concentration was used. One possible reason that came to mind was that CdO precursor may not be as reactive as dimethylcadmium which was used in Bawendi's synthesis. For this reason, instead of using more reactive cadmium precursor, a more reactive sulfur precursor to make CdS nanoparticles was used. The synthetic procedure is still similar to the one described for CdSe nanoparticles above. Instead of using more common sulfur and tri-n-octylphosphine (TOP) complex to make CdS nanoparticles, bis(trimethylsilyl)sulfide [$(TMS)_2S$] was used. In a typical synthesis, 0.2g CdO (Sigma) was added to a 3-neck round bottom flask together with 3g Tri-n-octylphosphine oxide (TOPO) and 1g Stearic acid and are heated to 280 ˚C.

Once the solution in the flask became optically clear, 0.5 ml of $(TMS)_2S$ was rapidly added. The solution turned yellow almost immediately and the synthesized CdS nanoparticles were monitored using a Shimadzu UV-3101-PC spectrophotometer. The first absorption peak for the smaller (CdS1) was determined to be at 425 nm and 445 nm for the larger CdS particles (figure 2-21). The size and morphology were examined using a JEOL 100CX II Transmission electron microscope (TEM). The TEM image of CdS nanoparticles is shown in figure 2-22 and the particle size was determined to be 3.8 nm in diameter. This method allowed growth of high quality nanocrystals with excellent fluorescence quantum yield without the need of large band gap passivation. Detailed study on these samples is given in chapter VI.

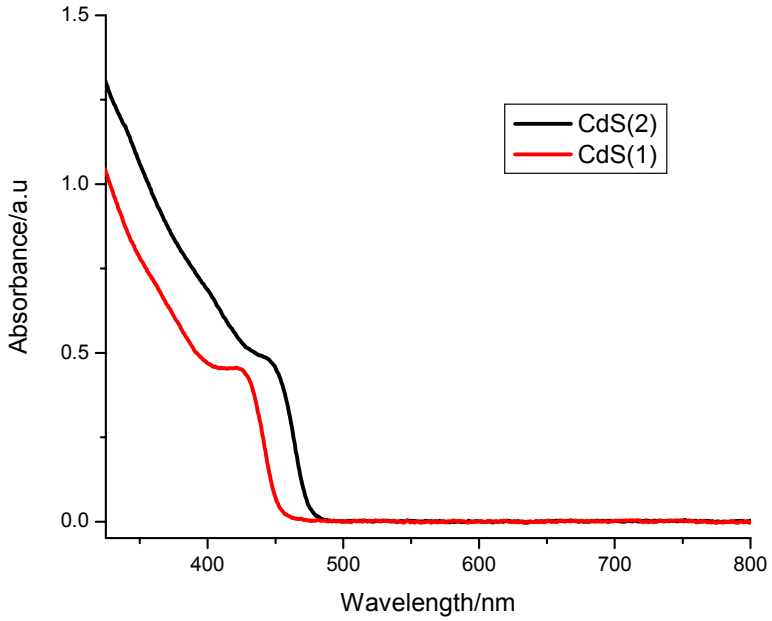

Figure 2-21: Absorption spectra of two CdS nanoparticle samples of 3.8 nm (red) and 4.8 nm (black) in diameter.

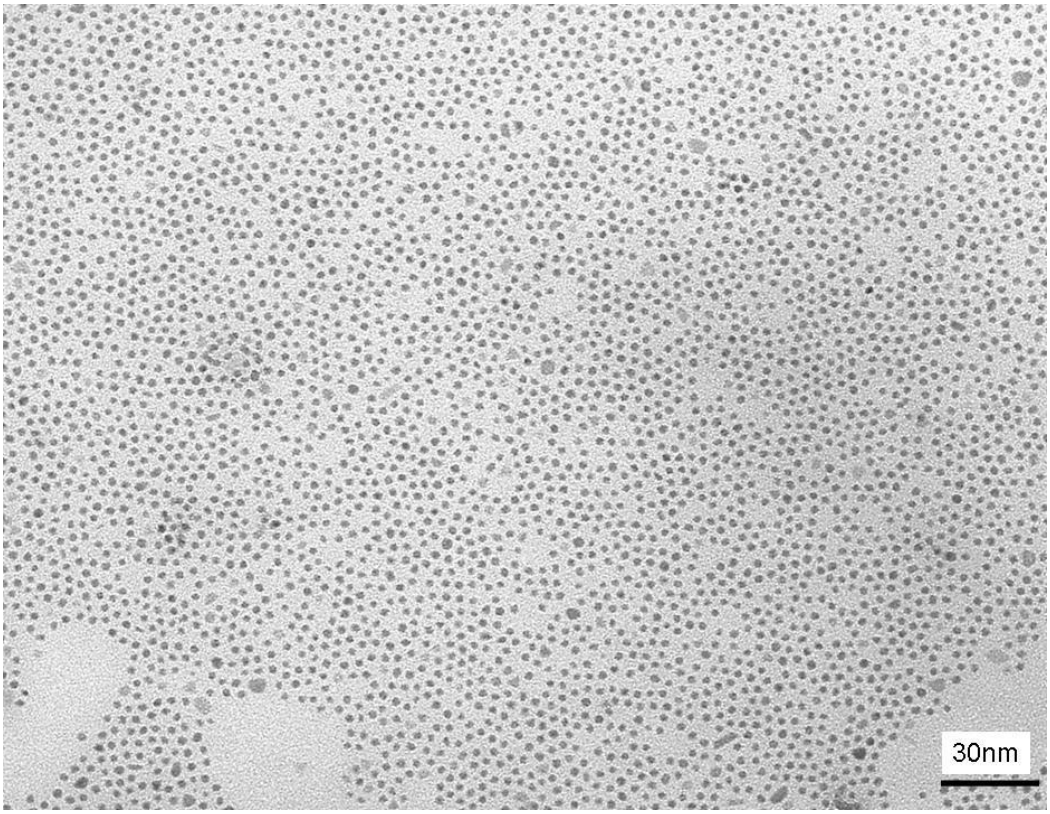

Figure 2-22: TEM image of 3 nm CdS nanoparticles.

d: Surface Passivation of CdSe with ZnS Layer

Chemicals:

DimethylZinc, TOP and TOPO were purchased from Sigma. Hexamethyldisilathiane was purchased from Fluka and CdSe nanoparticles were prepared as described above.

Experimental:

CdSe nanoparticles were passivated with a ZnS layer using the method of Hines and Guyot-Sionnest (49). In this method, dimethylzinc ($ZnMe_2$) and hexamethyldisilathiane ($(TMS)_2S$, Fluka) were used as zinc and sulfur precursors, respectively. CdSe nanoparticles in toluene are heated at 60˚C under argon flow until most of the toluene is evaporated. 5g of TOPO is added to the flask and the temperature is raised to ~130˚C (figure 2-23). Equimolar concentrations of $ZnMe_2$ and $(TMS)_2S$ are dissolved in TOP and added drop wise into the reaction flask. The amount of precursor added depends on the number of ZnS layers needed. The capped particles are washed using methanol and re-dissolving them in toluene. Figure 2-24 shows the emission spectra of CdSe nanoparticles before and after passivation. Note the increase in the fluorescence intensity for the dots after the particles are passivated (figure 2-24a). Similarly, CdSe rods can also be passivated with ZnS as shown in figure 2-24b. CdSe nanorods are much more difficult to passivated then CdSe nanodots.

Since reheating of the sample is required, the sample can undergo changes. Rods that are about 12 nm in length were successfully passivated with ZnS. Rods longer than 12 nm in length were much more difficult and rapidly changed size, shapes. To passivate rods, the temperature needs to be raised very slowly (few centimeter every minute to get to ~130ºC. Studies on passivated rods are described in chapter III.

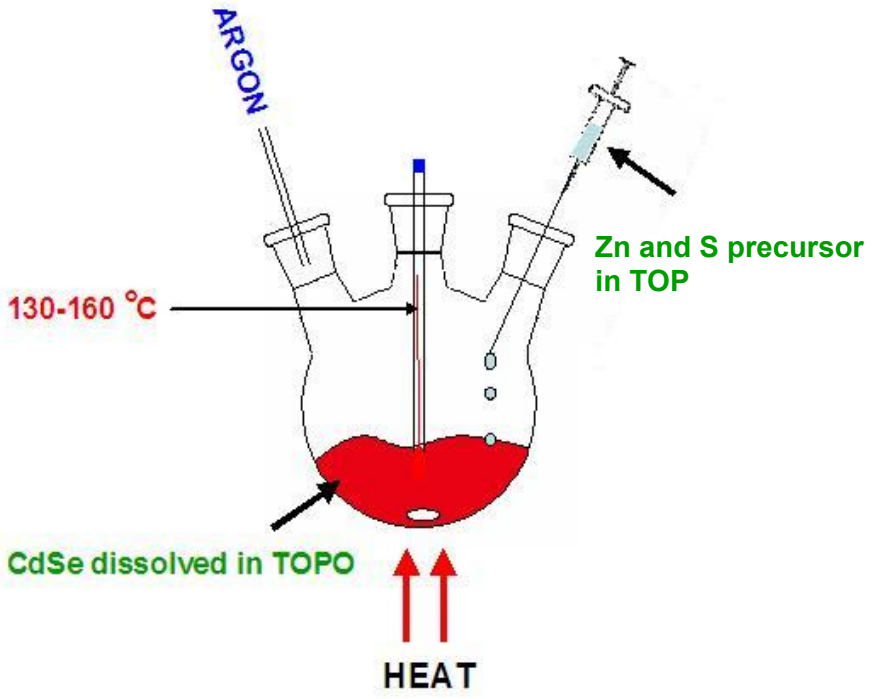

Figure 2-23: Setup for passivating CdSe with ZnS layer.

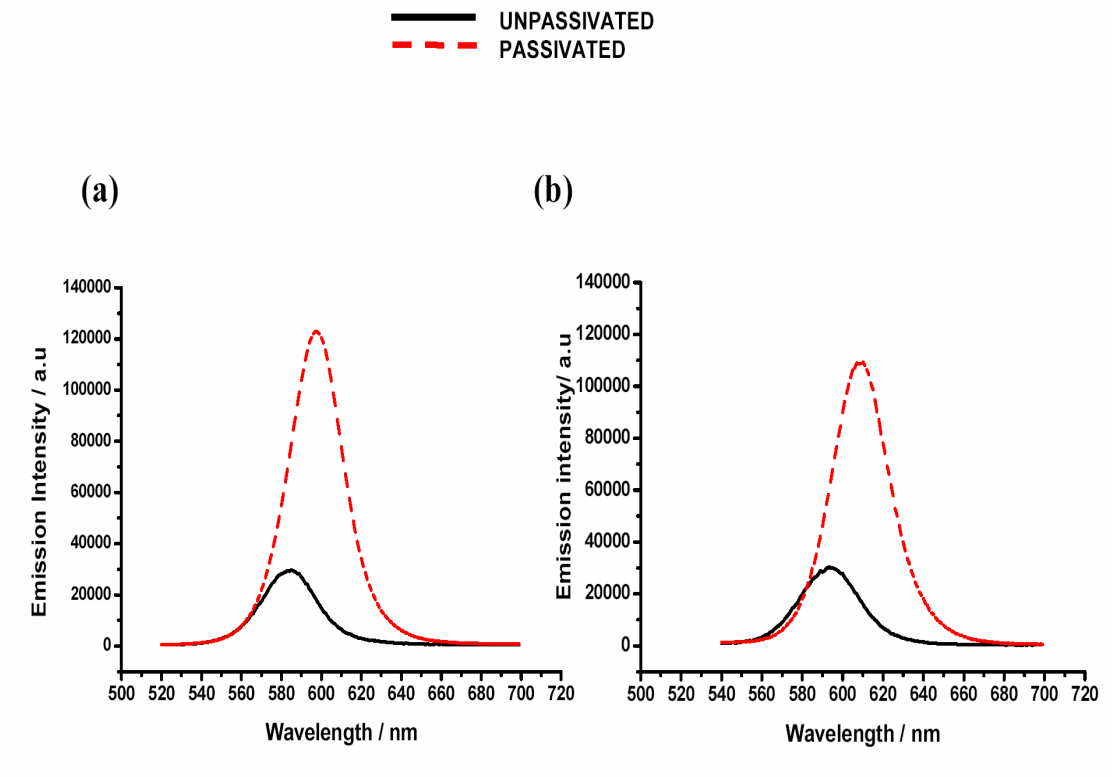

Figure 2-24: Band gap emission spectra of CdSe nanoparticles before and after ZnS passivation for Dots (a) and for Rods (b) excited at 400nm. This shows that passivation of rods and dots increases their band gap intensity by > 300%.

Comments on the method and the semiconductor nanoparticles stability:

The most difficult part in making cadmium containing semiconductor nanoparticles is to have reactive cadmium precursors. Though CdO is very stable, using fatty acids such as stearic acid helps react CdO rapidly at high temperatures. Attempts to make CdS using cadmium/stearic acid failed multiple times. This could be due to a more stable sulfur/TOP complex and stable Cd/stearic acid complex. Therefore it was necessary to use a more reactive sulfur precursor as described above.

For making CdSe rods, avoid using too much surfactant in order to avoid growing multi-pods shaped particles. Also, there is no need to use strearic acid when using HPA or TDPA during the synthesis of rods. CdO can react directly with these precursors to form cadmium ions.

Another important factor that needs to be considered is that all the glassware, specially the reaction flask needs to be cleaned very carefully with acid. Even if the flask is always used to make CdSe nanoparticles, washing the glassware carefully helps with the sample quality and size distribution.

Instrumentation

Experimental details for measuring Fluorescence quantum yield, Fluorescence Excitation and lifetimes in CdSe nanoparticle:

Steady state fluorescence was measured using a PTI Model C60 steady-state spectrofluorometer. Fluorescence lifetime measurements were done on a Photon Technology Instrument (PTI GL-3300) nitrogen laser with the fundamental excitation at 337 nm.

Measuring fluorescence is fairly straight forward. In order to obtain accurate quantum yield, the optical density of the sample needs to be very low. If the sample is too concentrated, there will likely be a filtering effect, lowering the detected emission intensity.

Fast and easy way to calculate the quantum yield is to measure and adjust the absorption optical density of the sample and the reference dye to be the same at the excitation wavelength. The quantum yield is then calculated by taking the ratio of the area under the emission peaks of the sample and the reference dye. The quantum yield of the reference dye is assumed to be 1 in the above case. If the quantum yield is not 1 then this factor needs to be multiplied to get the actual quantum yield of the sample.

In the case, when the absorption optical densities are not the same, then equation 2.1 can be used to calculate the quantum yield.

$$Q^S = \frac{Q^{ref} (F*n^2)^S (1-10^{-E})^{ref}}{(F*n^2)^{ref} (1-10^{-E})^S} \quad \text{----------(2.1)}$$

Where Q^{ref} is the quantum yield of the reference dye, F is the area under the emission peak, n is the respective refractive index of the respective solvents, and E is the extinction coefficient (Optical density at the excitation wavelength).

Measuring the excitation spectrum:

Every time we collect the excitation spectra, we need to correct it for the lamp. First, we need to make a correction file by using a high concentration rhodamine B dye as a photon counter. Using a flat cuvette at 45º, we get the correction file as shown in figure 2-25.

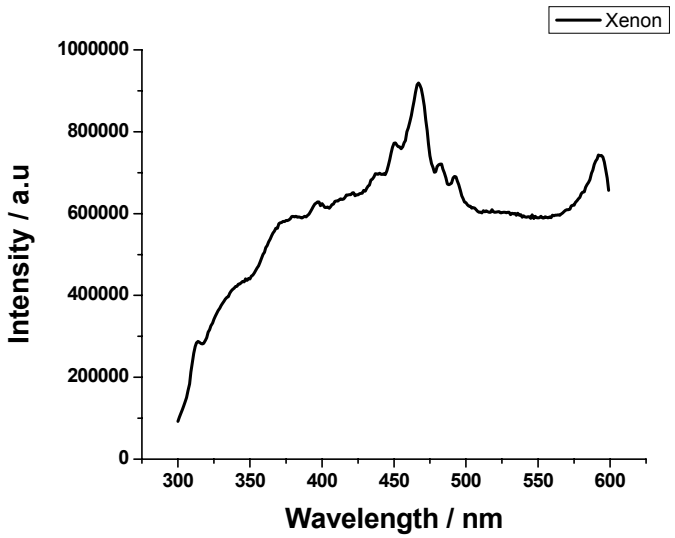

Figure 2-25: Excitation spectrum obtained using quantum counter.

The sharp peak at 467 nm is the characteristic peak of the xenon lamp and is visible in all excitation spectra collected and therefore needs to be corrected. Figure 2-26 (a) shows the uncorrected excitation spectrum of CdSe nanoparticles, and figure 2-26 (b) shows the corresponding corrected spectrum.

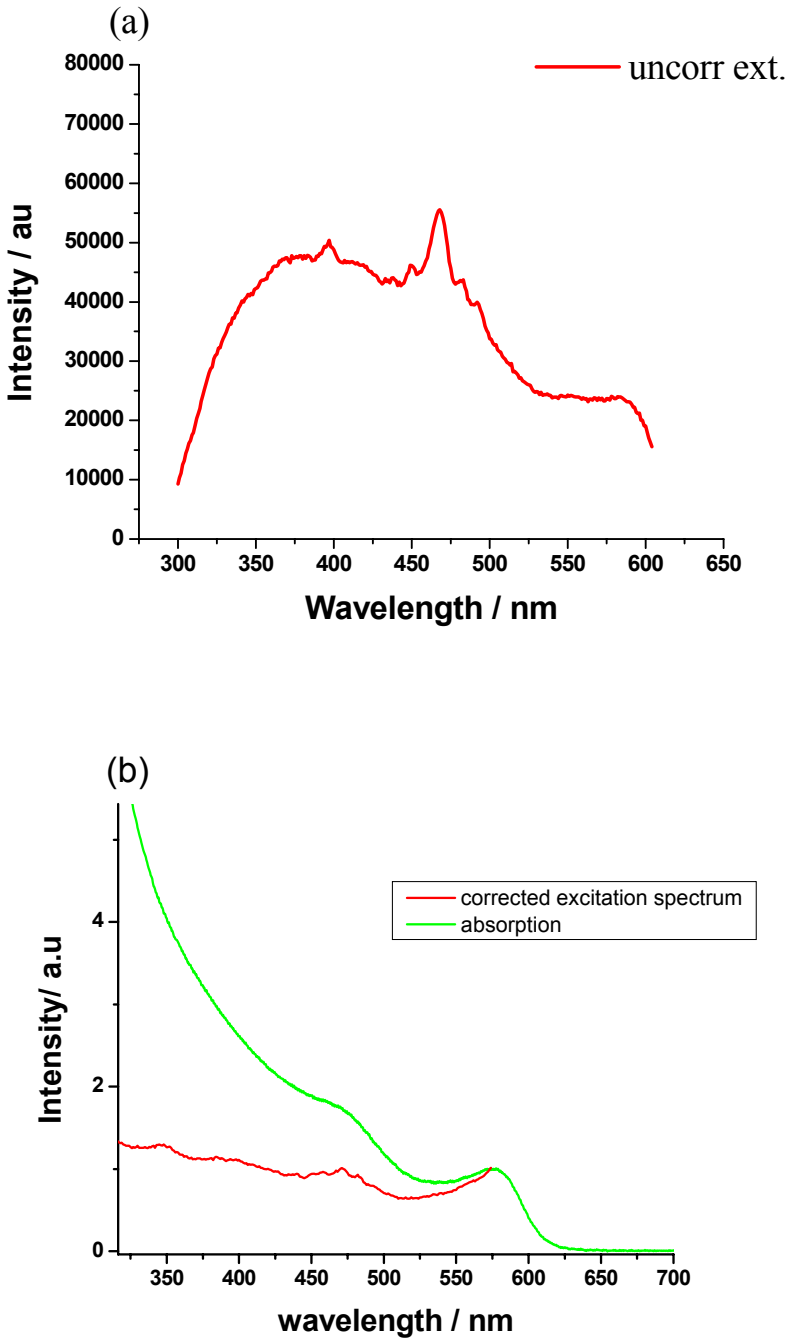

Figure 2-26 (a) shows the uncorrected excitation spectrum of CdSe dots and (b) shows the corresponding corrected excitation spectrum.

The excitation spectrum can be corrected for by taking the ratio of the raw excitation spectrum to that of the correction spectrum.

Fluorescence lifetime measurements:

Fluorescence lifetime measurements were taken by using a PTI GL-3300 nitrogen laser with the fundamental excitation at 337 nm. The excitation wavelength can be changed by using the desired laser dye. A list of dyes and the formula for making correct concentrations to generate a specific wavelength can be found at http://www.exciton.com.

During instrument startup, it is necessary to purge it with nitrogen to remove any trace of air before increasing to high voltage. Once, the recommended voltage is reached and the instrument is still misfiring the laser shot, do not increase the voltage. It is better to purge longer until consistent laser shots are achieved. If purging does not help, it maybe because the electrodes have become dirty with carbon deposits. At this point, these electrodes may need cleaning. Cleaning instructions maybe found at http://www.pti-nj.com/manual_gl-3300.html. One thing to note is that, when putting the electrodes back after cleaning, the distance between them needs to be adjusted exactly as specified. If the distance is not correct, the laser will not work at all.

Summary

Nanoparticles synthesis has tremendously advanced in the past couple of decades and a variety of materials are produced either on substrates or in solution. Particles produced in solution can have very narrow size distribution and can also be produced in large quantities compared to lithographic and laser ablation techniques. This provides an added advantage for practical use. A variety of metallic nanoparticles such as copper, cobalt and platinum of different sizes and shapes using different techniques have been shown. Furthermore, the synthesis of different sizes and shapes of semiconductor nanoparticles is also presented. Particle's properties can easily be manipulated during or after the synthesis by controlling their sizes and surface properties depending on the capping materials used.

One very important thing to learn from making different nanomaterials is that there is no perfect method. There is always room for improvement and one can only get better at making nanomaterials is by doing it over and over again and applying different techniques. Making metallic and semiconductor particles using different methods gives us broader view of different parameter that effect certain synthetic procedure and hence the final product. It makes it easier to apply methods already learned into making other nanomaterials or improving existing methods as I have shown for making long CdSe rods, different size copper nanoparticles and also making high quality CdS nanoparticles. Making monodispersed nanoparticles does not only depend on the precursors or the

temperature used, but also depends on the injection times of the precursors and the reaction quenching time.

After sample preparation, storing the samples under right conditions also becomes very important. The best way for longer shelf life, it is necessary to purge the sample with inert gas and tightly seal the vial carefully and store the sample in the dark. For semiconductor nanoparticles, drying the sample completely also is a good way to store and redissolve in appropriate solvent when needed.

References

(1a) Burda, C.; Chen, X.; Narayanan, R.; El-Sayed, M. A. *Chem Rev.* **2005,** 105, 1025.

(1b). Faraday, M. Phil. Trans. R. Soc., 147, 145, 1857.

(2) Pileni M. P. *Langmuir,* **1997**, 13, 3266.

(3) Rogach A. L.; Katsikas L.; Kornowski A.; Su D. S.; Eychmuller, A.; Weller, H. *Phys. Chem. Chem. Phys*., **1996,** 100, 1772.

(4) Watzky M. A.; Finke R. G. *J. Am. Chem. Soc*. 1997, 119 (43) 10382.

(5) Bradley, J. S, Hill, E. W., Klein, C., Chaudret, B., Duteil, A., 1993, Chem. Mater., 5 (3) 254.

(6) Henglein, A., 1993, J. Phys. Chem., 97, 8457.

(7) Ahmadi, T. S., Wang, Z. L., Green, T. C., Henglein, A., El-Sayed, M. A., 1996, Science, 5270, 1924.

(8) Alivisatos, A. P., 1996, J. Phys. Chem., 100, 13226.

(9) Manna, L., Scher, E. C., Alivisatos, A. P., 2000, J. Am. Chem. Soc., 122 (51): 12700

(10) Storhoff, J. J., Mirkin, C. A., 1999, Chem. Rev., 99, 1849.

(11) Brust, M., Fink, J., Bethell, D., Schiffrin, D. J., Kiely, C., 1995, J. Chem. Soc.-Chem. Comm., 16, 1655.

(12) Trindade, T., O'Brien, P., Pickett N. L., 2001, Chemistry of Materials, 13, (11), 3843.

(13) Taleb, A., Petit, C., Pileni M. P., 1997, Chemistry of Materials, 9, (4), 950.

(14) Jana N. R., Gearheart, L., Murphy C .J., 2001, Chemical communications, (7), 617.

(15) Murray, C. B., Norris, D. J., Bawendi, M. G., 1993, J. Am. Chem. Soc. 115, 8706.

(16) Aiken, J. D., Finke R. G., 1999, Journal of Molecular catalysis A-Chemical, 145, (1-2): 1-44.

(17) Zhao, M. Q., Crooks, R. M., 1999, Advanced Materials, 11 (3), 217.

(18) Petit, C., Taleb, A., Pileni, M. P., 1999, J. Phys. Chem. B, 103 (11), 1805.

(19) Peng, X. G., Manna, L., Yang, W. D., Wickham, J., Scher, E., Kadavanich, A., Alivisatos, A. P., 2000, Nature, 404, 59.

(20) Park, S. J., Kim, S., Lee, S., 2000, J. Am. Chem. Soc., 122, (35), 8581.

(21) Boal, A. K., Ilhan, F., DeRouchey, J. E., Thurn-Albrecht, T., Russell, T. P., Rotello, V. M., 2000, Nature, 404, (6779), 746.

(22) Schon, G., Simon, U., 2000, Science, 273 (2), 101.

(23) Kim, S. W., Kim, M., Lee, W. Y., 2002, J. Am. Chem. Soc., **124** (26), 7642.

(24) Narayanan, R., El-Sayed, M. A., 2005, J. Catalysis, 234, (2), 348.

(25) Narayanan, R., El-Sayed, M. A., 2005, J .Phys. Chem. B., 109, (26), 12663, Feature Article.

(26) Gref, R., Domb, A., Quellec, P., Blunk, T., Muller, R. H., Verbavatz, J. M., Langer, R., 1995, Adv. Drug Delivery Rev., 16 (2-3), 215.

(27) Brigger, I., Dubernet, C., Couvreur, P., 2002, Adv. Drug Delivery Rev., 54 (5), 631.

(28) Schmid, G., Corain, B., 2003, Eur. J. Ino. Chem., (17), 3081.

(29) Gao, X. H., Cui, Y. Y., Levenson, R. M., Chung, L. W. K., Nie, S. M., 2004, nature Biotechnology, 22 (8), 969.

(30) Pankhurst, Q. A., Connolly, J., Jones, S. K., Dobson, J., J. 2003, Phys. D-Appl. Phys., 36 (13) ,R167.

(31) Kubo, R., Kawataba, A., Kobayashi, S., 1984, Annu. Rev. Mater. Sci., 14, 49.

(32) Salzemann, C., Lisiecki, I., Brioude, A., Urban, J., Pileni, M. P. 2004, J. Phys. Chem. B., 108, 13242.

(32) Molina, R. A., Weinmann, D., Jalabert, R. A. 2002 ,Physical Review B, 65.

(33) Nisoli, M., Stagira, S., DeSilvestri, S. Stella, A. Tognini, P. Cheyssac, P. Kofman, R. 1997, Physical Review Letters, 78, 3575.

(34) Hodak, J. H., Henglein, A., Hartland, G. V. 1999, J. Chem. Phys., 111, 8613.

(35) Del Fatti, N., Flytzanis, C., Vallee, F. 1999, Appl. Phys. B-Lasers and Optics, 68, 433.

(36) Halte, V., Bigot, J. Y., Palpant, B., Broyer, M., Prevel, B., Perez, A. 1999, Appl. Phys. Lett., 75, 3799.

(37) Hodak, J. H., Henglein, A., Hartland, G. V. 2000, J. Chem. Phys., 112, 5942.

(38) Brus, L., 1998, J. Phys. Chem. Solids, 59, 459.

(39) Lisieki, I.; Pileni, M. P. 1993, J. Am. Chem. Soc., 115, 3887.

(40) Lisieki, I., Pileni, M. P. 1995, J. Phys. Chem., 99, 5077.

(41) Petit, C., Lixon, P., Pileni, M. P. 1990, J. Phys. Chem., 94, 1598.

(42) Pileni, M. P., 1997, Langmuir, 13, 3266.

(44) Su, X., Kung, K., Lahtinen, J., Shen, R. Y., Somorjai, G. A., 1998, Catal. Lett. 54, 9.

(45) McCrea, K., Somorjai, G. A. 2000, Adv. in Catalysis 45, 385.

(46) Kung, K. Y., Chen, P., Wei, F., Shen, Y. R., Somorjai, G. A., 2000, Surf. Sci, 463, 627.

(47) McCrea, K. R., Somorjai, G. A., 2000, J. Mol. Catal. A 163, 43.

(48) Puntes, V. F., Krishnzn, K. M., Alivisatos, A.P., Science, 2001, 291, 2115.

(49) Hines, M. A., Guyot-Sionnest P., 1996, J. Phys. Chem., 100, 468.

(50) Hu, J. T., Li, L. S., Yang, W. D, Manna, L., Wang, L. W., Alivisatos, A. P., 2001, Science, 292, 2060.

(51) Manna, L., Milliron, D. J., Meisel, A., Scher, E. C., Alivisatos, A. P., 2003, Nature Materials, 2, 382.

(52) Chen, M., Xie, Y., Lu, J., Xiong, Y. J., Zhang, S. Y., Qian, Y. T., Liu, X. M., 2002, J. mater. Chem., 12, 248.

(53) Manna, L., Scher, E. C., Alivisatos, A. P., 2000, J. Am. Chem. Soc., 122, 12700.

(54) Mohamed, M. B., Tonti, D., Al Salman, A., Chergui, M., 2005, ChemPhysChem, 6, 2505.

(55) Rampino, L. D.; Nord, F. F., 1942, J. Am. Chem. Soc., 63, 2745.

(56) Henglein, A., Ershov, B. G., Malow, M. J., 1995, Phys. Chem., 99, 14129.

(57) (25) Li, Y., Petroski, J., El-Sayed, M. A., 2000, J. Phys. Chem., 104, 10956.

(58) (27) Liu, M.; Yu, W.; Liu, H.; Zheng, J., 1999, J. Colloids Int. Sci., 214, 231.

(59) Shiraishi, Y., Nakayama, M., Takagi, E., Tominaga, T., Toshima, N., 2000, Inorg. Chim. Acta, 300, 964.

(60) Lu, P., Toshima, N., 2000, Bull. Chem. Soc. Jpn., 73, 751.

(61) Yoo, J. W., Hathcock, D., El-Sayed, M. A., 2002, J. Phys. Chem. A, 106 (10), 2049.

(62) Yoo ,J. W., Lee, S., Kim, T., El-Sayed, M. A., 2004, Bull. Korean Chem. Soc., 25, 843.

(63) Petit, C., Lixon, P., Pileni, M. P., 1991, Langmuir, 7, 2620.

(64) Giuffrida, S., Condorelli, G. G., Costanzo, L. L., Fragala, I. L., Ventimiglia, G., Vecchio, G., 2004, Chemistry of Materials, 16, 1260.

(65) Kapoor, S, Palit, D. K., Mukherjee, T, 2002, Chem. Phys. Lett., 355(3-4), 383.

(66) Kapoor, S, Mukherjee, T, 2003, Chem. Phys. Lett., 370(1-2), 83.

(67) Loginov, A. V., Gorbunova, V. V., Boitsova, T. B., 2002, J. Nano. Res., 4(3), 193.

(68) Kim, F., Song, J. H., Yang, P. D., 2002, J. Am. Chem. Soc., 124(48)14316.

(69) Callegari, A., Tonti, D., Chergui, M., 2003, Nano Lett., 3(11), 1565.

(70) Lisiecki, I., Billoudet, F., Pileni, M. P., 1996, J. Phys. Chem., 100, 4160.

(71) Peng, Z. A., Peng, X., 2001, J. Am. Chem. Soc. 123, 183.

(72) Peng, Z. A., Peng, X., 2002, J. Am. Chem. Soc. 124, 3343.

CHAPTER III

WHY IS THE THERMALIZATION OF EXCITED ELECTRONS IN SEMICONDUCTOR NANOPARTICLES SO RAPID? Studies on CdSe Nanoparticles[†]

Abstract

Quantum confinement of electronic motion in semiconductor nanoparticles leads to quantization of the conduction band continuum of the bulk. The relaxation between these levels by electron phonon coupling was expected to be slow due to the small phonon frequencies. Several mechanisms have been previously proposed. These mechanisms as well as new ones have been tested by studying the decay of the bleach observed at the band gap absorption and upper excited state absorption of CdSe nanodots and nanorods, passivated and unpassivated with and without the surface absorption of hole acceptor and at different laser powers. The results are found to be best understood if one considers the changes in the electron density of the excited electron in the core (thus affecting the nonlinear Auger processes) and on the surface (thus affecting relaxation via coupling to surface defects or adsorbed molecules).

[†] Qusai Darugar, Christy Landes, Stephan Link, Alexander Schill, Mostafa El-Sayed; Chem. Phys. Letters, **2003**, 373, 284-291.

Introduction

In large polyatomic molecules, nonradiative electronic relaxation from upper electronic excited states to the lowest excited state is usually very rapid, about four orders of magnitude faster than allowed radiative processes. This is the reason for the general observation that emission usually takes place from the lowest electronic excited state (band gap state). Due to its large energy separation from the ground state, relaxation from the band gap state to the ground state has a small nonradiative rate for transferring its electronic excitation energy to a large number of vibrational degrees of freedom. The fact that the energy separation between different electronic excited states is usually smaller than that between the lowest excited state and the ground state makes their electron-phonon relaxation so much faster (1). This enables very few quanta of the large vibrations (2000-3000cm^{-1}), to thermalize the electron in the upper state. Furthermore, the fact that the molecules and the surrounding media have small vibrations assist in making up for any energy mismatch between the electronic energy and the energy of the few large vibrational modes involved.

In bulk semiconductors, highly excited electrons in the conduction band also thermalize very rapidly (2). The reason for this is that the electron has continuum values of energy and can thus give the phonon bath one quantum at a time (which is a highly probable process) and cascades rapidly to the band gap state. If there is an impurity having quantized energy level structure in a bulk semiconductor, its excited electron relaxes very slowly. The reason for this is

that the electronic excitation energy is much larger than the single phonon energy of a semiconductor (~300cm^{-1}). It could require tens of phonon quanta to be transferred simultaneously to relax the excited electron energy from an upper to a lower level. As a result, the electronic relaxation of the excited electron of the impurity could have a long relaxation time. This is known as “phonon bottleneck (3).”

In a semiconductor nanocrystal, quantum confinement leads to quantization of its energy levels (4). The conduction band is replaced by quantized energy levels, like the molecular case. Unlike the large molecule case, semiconductors do not have large vibration quanta. As a result, the electronic energy separations become much larger than the phonon quanta. It was then expected that semiconductor nanoparticles could show phonon bottleneck in the thermalization process of their excited electrons (5). However, the relaxation of excited electrons in semiconductor nanoparticles is found to be very rapid (in the subpico-to-pico second time scale) as fast as in large molecules. What vibrations and what electronic mechanisms are involved in relaxing the electronic excitation in a semiconductor nanocrystal has been the topic of many research papers (6) and will be that of this report.

In order to explain the rapid thermalization of excited electrons in semiconductor nanoparticles, several mechanisms have appeared in the literature. The coupling between the electron and hole is proposed by Efros (7) to transfer

electronic excitation energy to hole excitation. The high density of the hole states allows it to accept any amount of energy the electron gives off in its thermalization process with no problem of energy mismatch.

In the dynamic studies of semiconductor nanoparticles (6, 8-11), femtosecond pulses are used. Under these conditions, the probability of absorbing more than one photon per particle is high. Nonlinear Auger (12) processes involving multiple electron-hole pairs lead to electron-hole recombination where the energy released is used to ionize other excited electrons. Klimov (13) has experimentally examined these processes at different amounts of absorbed energies per particle. Nozik (6, 15) and his group have shown that hot electrons in III-V nanoparticles are excited or captured at the surface or the interface of the nanoparticles.

In the present report, the effect of changing the size and shape of CdSe nanodot into nanorod, the effect of capping the nanoparticle, and the effect adding a hole acceptor on the rate of the bleach recovery monitored at the band gap absorption region (at 560nm) and at higher excitation energy (470nm) are examined for CdSe nanoparticles. The observed changes in the nonlinear and the linear relaxation rates are found to be generally explained by the quantum mechanical predicted changes in the excited electron density in the particle core and on its surface, respectively. These results suggest that Nonlinear Auger and coupling to

the surface seem to dominate electron relaxation in these colloidal type nanoparticles.

Experimental

CdSe nanospheres were prepared using the method of Murray and Bawendi (16) as modified by Peng et al (17, 18). In this modified method, dimethylcadmium is replaced by less toxic CdO precursor. In a typical synthesis, 0.5g CdO (Strem) is loaded into a 3-neck flask with 4g trioctylphosphine oxide (TOPO, Aldrich) and 2g stearic acid (Aldrich) and heated to 320°C. At this temperature, the reddish brown solution turns optically clear. 0.2g selenium dissolved in 4ml trioctylphosphine (TOP, Aldrich) is then quickly injected to the reaction flask and CdSe nanocrystals are instantaneously formed and the reaction flask is heated until desired particle size is obtained. CdSe nanocrystals are washed from excess TOPO by washing with methanol and then redesolving the particles in chloroform. CdSe nanoparticles were passivated with ZnS layer using the method of Hines and Guyot-Sionnest (19). In this method, dimethylzinc ($ZnMe_2$, Aldrich) and hexamethyldisilathiane ($(TMS)_2S$, Fluka) were used as zinc and sulfur precursors respectively. To the previously prepared CdSe nanoparticles, $ZnMe_2$ and $(TMS)_2S$ dissolved in TOP is drop wise added at ~130º C. The capped particles are once again washed using the method discussed above.

CdSe nanorods were prepared by using the method of Alivasatos et al (20) as modified by Peng (17). In this method, CdO is added to a solution of a binary surfactant mixture of TOPO and hexylphosphonic acid (HPA). In a typical reaction, 0.5g CdO is added to 4g of TOPO and 0.2g HPA at 300°C. 0.2g Se dissolved in TOP is quickly injected into the reaction flask and heated at 280°C. CdSe nanorods synthesized are washed from excess surfactants by the method described above.

Freshly prepared CdSe particles were analyzed by a Hitachi HF-2000 field emission transmission electron microscope operating at 200 kV. Optical characterization was done using Shimadzu UV-3101PC UV-VIS-NIR scanning spectrophotometer and PTI Model C60 steady-state spectrofluorometer.

For the amine studies, n-butylamine (Aldrich) was added to the CdSe samples in concentrations of ~0.2 M.

Femtosecond transient experiments were performed using an amplified Ti:Saph. laser system (Clark MXR CPA 1000) pumped by a ND-YVO ring loss (Coherent Verdi 5W) laser. This produces laser pulses of 100 fs (FWHM) with energies of ~1 mJ at 810 nm with a 1 kHz repetition rate. A small part of the fundamental was used to generate a white light continuum using a 1 mm sapphire plate. 405 nm light generated by second harmonic generation was used for excitation. The excitation beam was modulated with an optical chopper (HMS 221) yielding an

excitation frequency of 500 Hz. The probe light was split into signal and reference channels. After passing the monochromator (Acton Research) both beams were detected with photodiodes (Thorlabs). The kinetic traces were collected using sample-and-hold unit and lock-in-amplification (Stanford Research Systems).

Results and Discussion

a. The effect of adsorption of hole acceptor*

In collaboration with Dr. Christy Landes.

The effect of adsorption of hole acceptor is shown in figure 3-1. This figure shows the bleach recovery monitored at the maximum of the band gap absorption (560nm) of CdSe quantum dots (a) and quantum rods (b) with and without the absorption of n-butylamine.

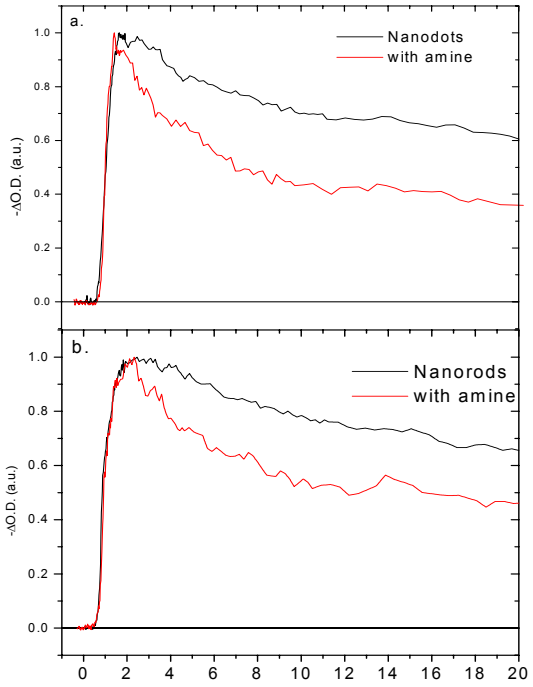

Figure 3-1. Bleach decay dynamics of dots (a) and rods (b) alone and in the presence of n-butylamine excited at 400 nm and monitored at the band edge at 555 nm. When amine is adsorbed to the particle surface, the band-edge bleach decays more quickly for both dot and rod samples.

Since hole relaxation is known to be 10 times faster than electron relaxation (21), bleach recovery rate thus measures the rate of excited electron relaxation. The observed results in figure 3-1 thus suggest a more rapid excited electron relaxation when the amine is adsorbed on the surface of the nanoparticle. Thus for both systems, the amine seems to increase the rate of the band edge relaxation.

The above results do not support the electron-hole mechanism (7). A hole acceptor is expected to decrease the concentration of excited holes in the nanoparticle. This will decrease the electron-hole coupling probability and is thus expected to decrease the relaxation rate of the excited electron. An explanation of the increase in the thermalization rate by the adsorption of amine could be the coupling of the excited electrons with its electronic system. This allows the excited electron of the nanoparticle to give its energy to the different large vibrations of the amine, which makes the relaxation in the nanoparticle-amine system resemble the large molecule system.

b. The effect of size and shape changes

Klimov and coworkers (13) have shown that increasing the radius of the quantum dots decreased the nonradiative rate of P→S excited state relaxation process in CdSe quantum dot by the nonlinear Auger mechanism. This is in agreement with previous theoretical and experimental studies (14) on CdS in glass in which the ionization rate from Auger processes are found to increase as the nanodot size decreases.

Figure (3-2a) shows the decay of the excited electrons in the band gap state of the nanodots (4nm) and nanorods (12x4nm). In these studies, the solution concentration of each sample is adjusted to an optical density of ~1 at the excitation wavelength (400nm). It is clear that in 100ps a larger fraction of the excitation (the bleach) recovers faster for the dot than for the rod at the same laser excitation energy. For example at 7nJ, 40% of the excitation recovers in 100ps while only 20% recovers for the rod in the same amount of time.

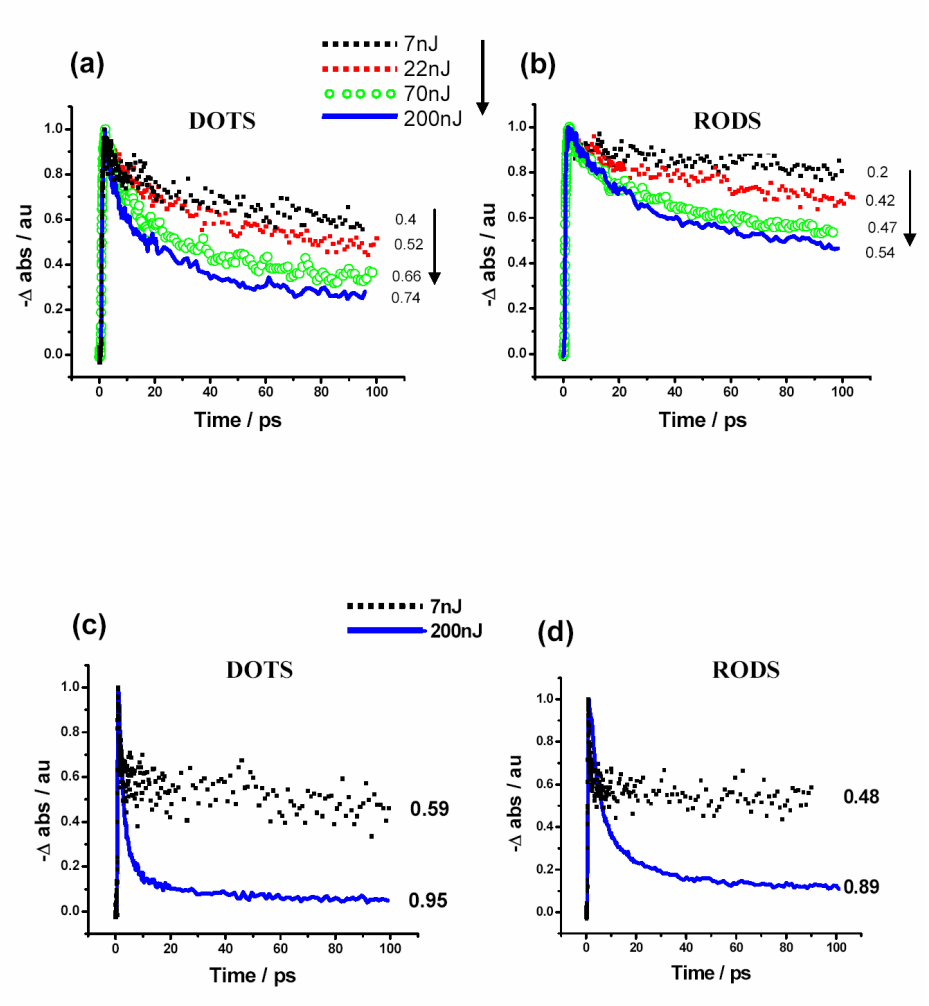

Figure 3-2. The bleach recovery in 100ps for Dots (a, c) and Rods (b, d) monitoring at the band gap absorption wavelength, 560nm (a, b) and at higher energy, 470nm (c, d) as a function of the laser pulse energy. This figure shows that the electron relaxation in the dot (4nm) is faster than in the rod (12nm x 4nm) for both the band gap and higher exited state. It also shows that relaxation of the higher excited state (470nm) is faster than at the band gap state (560 nm). In addition, the relaxation increases as the pulse energy increases due to more contribution of the Auger mechanisms.

Similarly at 200nJ, 74% of the excitation recovers in the dot while only 54% of the excitation recovers for the rods. Thus the relaxation rate is smaller for the rod than for the dot in the linear and the nonlinear region, i.e. at low and at high laser powers respectively.

It is assumed that at a standard optical density of 1 at the excitation wavelength, the rod should absorb at least as many photons per particle as the dot, because ε should scale with the volume. Thus for similar optical density, a rod would be expected to have a higher probability of non-linear Auger effects, and thus a larger contribution from the faster relaxation component. This is opposite to the observed results. This strongly suggests that both the linear and non-linear electron relaxation in the rod are intrinsically slower than that in a dot of similar diameter.

From the size and shape dependence studies, one main conclusion can be made. It is clear that as the nanoparticle volume increases, the relaxation rate of its excited electron decreases. This might be explained if the Auger mechanism is operative as follows. The nonlinear Auger mechanism depends on two terms in the Hamiltonian. The first term represents an electron-electron repulsion term: $e^2/\varepsilon(\mathbf{r}_i-\mathbf{r}_j)$; where ε is the dielectric constant. The second term represents the electron-hole attraction and has the form, $-e^2/\varepsilon(\mathbf{r}_i-\mathbf{r}_j)$. While the rate of the energy released in the electron-hole process is determined by the square of the second term, the rate of the electron relaxation is determined by the square of the

electron-electron repulsion (first) term. As the volume increases; the electron density of the charge carrier decreases and the distance between the interacting charge carriers increases. This leads to a decrease in the interaction energy leading to the coupling, whose square determines the relaxation probability. It is thus expected that the Auger rate decreases as the size of the nanodot increases or as the quantum dot changes its shape into a quantum rod of the same diameter (i.e. of larger volume) as has been observed for the CdSe nanodots.

c. Linear Relaxation mechanisms

It is possible that the Auger process is a strong participant in the relaxation even at low energies. However, let us examine the effect of volume or shape changes on the linear mechanism. Trapping of the electron is a viable mechanism of its relaxation. Another surface mechanism is one that involves coupling the excited electron with the electronic system of large molecules that have both large and small vibrations that thus can act as an effective heat bath.

Using wavefunctions obtained from solutions to the free-particle Schrödinger equation under spherical and cylindrical boundary conditions (22), the average location of excited electrons within spherical and rod shaped nanoparticles was estimated. Specifically, the fraction of the excited electron on the surface of a nanoparticle (within a shell 0.2 nm thick around the nanoparticle) has been calculated for nanoparticles of different sizes and shapes as a function of

excitation. Figure 3-3a shows that the fraction of the excited electrons at the surface depends upon the diameter of the nanoparticle and the degree of excitation. As the particle diameter increases from 3 nm to 4 nm, the fraction of the excited electron at the surface of the spheres and the rods drops by about 50 percent for any given excited state. Excitation of the electron from the ground state to the tenth excited state increases the fraction of the electron at the surface from ~2 percent to ~15 percent in a 3 nm sphere.

In addition to the fraction of the excited electron at the surface, it is also interesting to consider the electron density at the surface. Figure 3-3b shows that the density of excited electrons has a very strong dependence on the volume of the particle. For a sphere and rod of a given diameter and a given excited state, the rod will have a lower density of excited electrons at the surface as a result of the increased shell volume surrounding the particle.

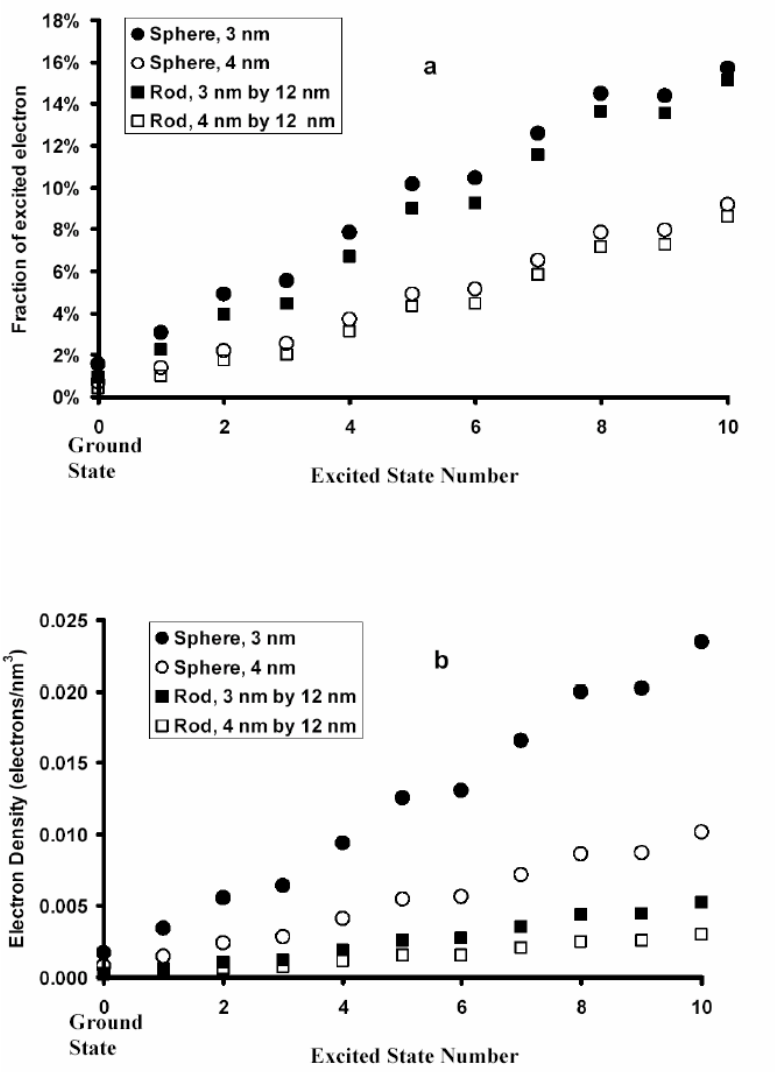

Figure 3-3. Quantum mechanical prediction of the fraction of the excited electron (a) and the excited electron density (b) at the surface of nanoparticles of various shapes and sizes. Results were obtained from calculations using the wavefunctions for a free-particle under spherical and cylindrical boundary conditions (In Collaboration with Mr. Alexander Schill)

As the aspect ratio of a nanoparticle of a given diameter increases, the density of excited electrons near the surface decreases. In this way, a long rod-shaped nanocrystal 3 nm in diameter will have less electron density at the surface than a 3 nm spherical particle.

The coupling to the defects, to other surface trapping sites, to the capping or other thermalizing adsorbed molecules on the surface is proportional to the square of the interaction energy between the excited electron and the electronic system of the surface species. This in turn is proportional to the electron density of the excited electron in the surface shell. It is thus expected that surface relaxation mechanisms increases in probability: 1) as the volume of the quantum dot decreases; 2) as the aspect ratio of the rod decreases or, 3) as the excitation level increases in energy. This is in agreement with the experimental results discussed above.

The dependence on the excitation level is observed if one compares the bleach recovery at 470nm (Fig. 3-2c) and at the band gap wavelength (Fig. 3-2a). For the quantum dots, excitation at 400nm with pulse energy at 7 and 200nJ monitored at 470nm is found to recover in 100ps to the extent of 59% and 95%, respectively. Similar excitations but monitored at the band gap absorption is found to recover to the extent of 40% and 74% in the same amount of time (100ps). This shows that the rate of bleach recovery is faster when higher excited states are monitored. In both cases, excitation with higher pulse energies causes

a higher percentage of recovery in a shorter time. This is due to the larger contribution of the Auger mechanism at higher laser powers (pulse energies).

It should be pointed out that the Auger process could benefit from the fact that the excited electron has a nonzero contribution at the surface. The ionization of one of the electron could be much faster if the ionized electron is trapped by a surface species. In this case, the energy needed for ionization will be reduced by the electron affinity of the trapping species as well as by the interaction energy between the negatively charged surface species and the positively charged nanoparticle resulting from the ionization of one of its electrons.

d. Effect of Passivating the Surface:

The effect of surface passivation on the deep trap emission and the quantum yield of the band gap emission was first demonstrated by Hines and Guyot-Sionnest (19). The passivation was carried out by covering the CdSe nanodots with ZnS, which has a larger band gap energy.

Figure 3-4 compares the effect of passivation on CdSe quantum dot (4nm) and quantum rod (12nm x 4nm). In both cases, the quantum yield increases by > 300%. For the smaller quantum dots, unpassivated particles showed deep trap emission which disappeared upon passivation. The interesting result was that while the observed yield increased by > 300%, the emission lifetime increased by

only ~15 percent. This suggests that the large increase in the quantum yield by passivation results from the increase in the population of the band gap excited state by eliminating electron trapping from higher excited states, and not by eliminating nonradiative processes involving excited electrons in the band gap state. This is consistent with the quantum mechanical results in figure 3-3 which shows that higher excited states have higher electron density on the surface and are thus more susceptible to trapping, especially as the particle size become smaller. Support of this conclusion can be derived from previous studies by Landes et al (23). In this report it is found that while the unpassivated 3.2nm CdSe nanodots have only band gap emission (with no deep trap emission), the 2.2nm dots show both types of emissions while the very small 1.2nm nanodots show only deep trap emission.

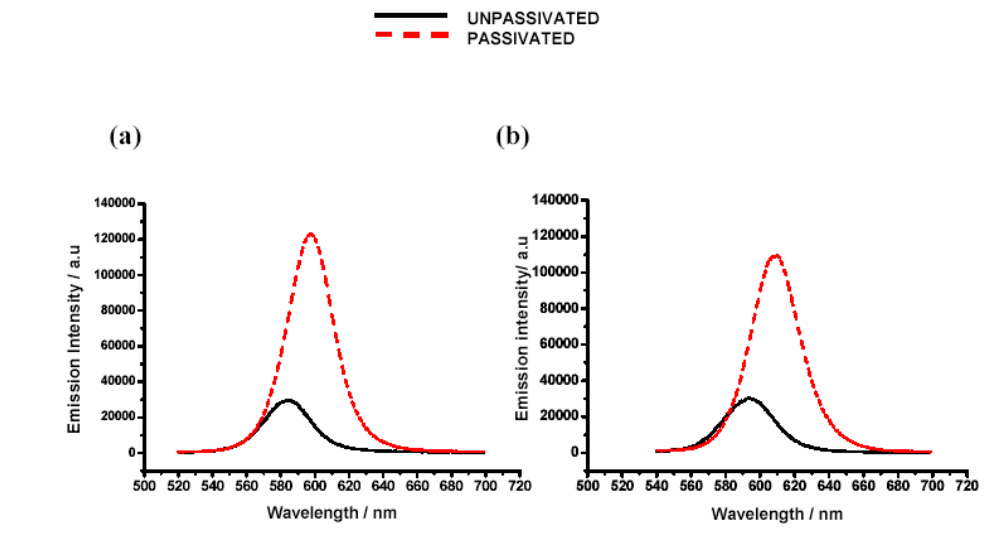

Figure 3-4. Band gap emission spectra of CdSe nanoparticle before and after ZnS passivation for Dots (a) and for Rods (b) excited at 400nm. This shows that passivation of rods and for dots increases its band gap intensity by > 300%.

Conclusion

A detailed study is carried out on the effect of different perturbations (such as changing the volume by changing the shape, passivating the surface or by adsorbing hole acceptors on it) on the linear and nonlinear thermalization of hot and band gap excited electrons in CdSe nanoparticles. From the results, a number of conclusions are made.

It is found that the electron-hole coupling mechanism cannot explain the observed results on the effect of adding hole acceptors on the surface. Being small, however, allows the excited electron in a nanoparticle to have nonzero amplitude on its surface. This increases its coupling to adsorbed molecules, traps or defects. These surface species can be an excellent heat bath for the linear thermalization processes or trapping sites for the ionized electrons in the nonlinear Auger process or the highly excited electrons in the linear process. The change in the excited electron density in the core by changing the nanoparticle volume (as the size or shape changes) can explain the dependence of the rate of the Auger process on these perturbations. The quantum mechanically predicted changes in the excited electron density on the surface with size, shape or by exciting different excited states is found to explain the observed dependence of the relaxation rate in these nanoparticles on these different perturbations.

I would like to thank the National Science foundation, Division of Material Research (Contract No. DMR-0138391) for their financial support on this project.

References

(1) Avouris, P.; Gelbart, W. M.; El-Sayed, M. A. *Chem. Rev*. **1977**, 77, 793

(2) Shah, J. *Ultrafast Spectroscopy of Semiconductors and Semiconductor Nanostructures*, **1999,** Springer.

(3) Landberg, P. T. *Recombintion in Semiconductors, Cambridge University Press* **1991**.

(4) Brus, L. *J. Chem. Phys*. **1984**, 80, 4473.

(5) a. Benisty, H.; Sotomayer- Torres, C. M.; Weisbuch, C.; *Phys. Rev. B* **1991,** 44, 10945.

b. Inoshita, T.; Sasaki, H.; *Phys. Rev*. **1992,** B 46, 7260.

(6) For the recent review see: Nozik, A. *J. Ann. Rev. Phys. Chem*. **2001**, 52, 193.

(7) Efros, A. L.; Kharchenko, V. A.; Rosen, M. *Solid State Commun.* **1995**, 93, 281.

(8) Zhang. J. Z. *J. Phys. Chem. B*, **2000,** 104, 7239.

(9) Logunov, S.; Green, T.; Marguet, S.; El-Sayed, M. A. *J. Phys. Chem. A*, **1998**,102, 5652.

(10) Burda, C.; Link, S.; Mohamed, M.; El-Sayed, M.A. *J. Phys. Chem. B*, **2001**,105, 12286.

(11) Klimov, V.I. *J. Phys. Chem. B* 104 (2000) 6112.

(12) Gelmont, B. L.; Kharchenko, V. A.; Yasievich, I. N. *Sov. Phys. Solid State*, **1989**, 29, 1355.

(13) Klimov, V. I.; Mikhailovsky, A. A.; McBranch, D. W.; Leatherdale, C. A.; Bawendi, M. G., *Science,* **2000**, 287, 1011.

(14) Chepic, D. I.; Ekimov, A. I.; Ivanov, M.G.; Kharchenko, V. A.; Kudriartsev, I. A.; Yazeva, T. V. *J. Luminescence*, **1990,** 47, 113.

(15) Ellingson, R. J.; Blackburn, J. L.; Yu, P.; Rumbles, G.; Micic, O. I.; Nozik, A. J. *J. Phys. Chem. B*, **2002**, 106, 7758.

(16) Murray, C. B.; Norris, D. J.; Bawendi, M.G. *J. Am. Chem. Soc.,* **1993**, 115, 8706.

(17) Peng, Z. A.; Peng, X. *J. Am. Chem. Soc*. **2001**, 123, 183.

(18) Peng, Z. A.; Peng, X. *J. Am. Chem. Soc*. **2002**, 124, 3343.

(19) Hines, M.; Guyot-Sionnest, P. *J. Phys. Chem*. **1996**, 100, 468.

(20) Peng, X.; Manna, L.; Yang, W.; Wickham, J.; Scher, E.; Kadavanich, A.; Alivasatos, A. P. *Nature*, **2000,** 404, 59.

(21) Braun, M.; Link, S.; Burda, C.; El-Sayed, M. A. *Chem. Phys. Lett*., **2002,** 361, 446.

(22) Liboff, R. L. Introductory Quantum Mechanics, New York: Addison-Wesley, **1998**.

(23) Landes, C. F.; Braun, M.; El-Sayed, M. A. *J. Phys. Chem. B***, 2001,** 105, 10554.

CHAPTER IV

EFFECT OF SHAPE, SURFACE PASSIVATION AND WAVELENGTH OF EXCITATION ON THE NONRADIATIVE PROPERTIES OF CdSe NANOPARTICLES OF DIFFERENT SHAPES

Abstract

We have studied the effect of capping the surface of CdSe nanodots with a material of larger band gap energy (ZnS) on their fluorescence quantum yield (QY) and lifetimes. We also studied the effect of changing the excitation wavelength on the steady state fluorescence emission intensity and lifetimes of these different samples. Additionally, the effect of changing the aspect ratio of CdSe nanorods on the fluorescence lifetime is presented. We observed that the fluorescence quantum yield, but not the lifetime, decreases as the excitation wavelength decreases. The quantum yield is found to increase by almost 400% after capping the CdSe core with a ZnS shell, while the fluorescence decay times change by <10% in dots and in rods. The quantum yield is found to decrease as the excitation wavelength decreases. These results suggest that surface trapping from higher energy excitation states leads to the observed quenching and that the probability of trapping increases as we increase the energy of the hot electron (i.e. as the excitation energy level above the band gap increases). Furthermore, we found that the fluorescence decay lifetimes decreases as the aspect ratio of CdSe nanorods increases above a critical value of 1.35. This is in

accordance with the semi-empirical pseudopotential calculations (1) that show that the excited electronic states cross at this aspect ratio, allowing a change in the nature of the lowest emitting state.

Introduction

Murray and Bawendi first published the synthesis of high quality CdSe semiconductor nanoparticles via chemical routes (2). This stimulated an active study of their physical and chemical properties as a function of different perturbations. Semiconductor nanoparticles have unique optical and electronic properties that make them potentially useful in a wide range of applications (3-7). CdSe nanoparticles become more interesting within the II-IV family of semiconductors for their ability to absorb and emit light through most of the visible spectrum simply by changing their size (2-4). The surfaces of these particles play a very important role in both their optical and electronic properties when the particle size is in the nanometer length scale. When the electrons are excited to higher energies, the relaxation of these excited electrons is greatly influenced by the surface quality, surface capping molecules, size of the particles and the degree of excitation (2, 3, 10, 16). In order to avoid electron trapping or mixing of the electronic wave functions of the nanoparticles with that of the surrounding medium or to the capping molecules, it is shown that capping nanoparticles with a material of a larger band gap such as ZnS can minimize surface effects (10). While the observed static fluorescence increases by changing or passivating the particle surface with higher band gap materials, little work has been done to understand the effect on the optical dynamics in such systems after passivation.

Alivisatos et al. have shown that the synthesis of CdSe nanodots can be altered to grow rod shaped nanoparticles (11). This provides a whole new direction for researchers to study the effect of particle elongation, both experimentally and theoretically, on their radiative and nonradiative properties. Alivisatos et al observed changes in the polarized emission of these elongated nanoparticles at a certain aspect ratio (length/width) (15). Using semi-empirical pseudopotential calculations, they found that the polarized emission is a result of having two high energy states ($4p_{x,y}$ and $4p_z$) crossover for particles that have an aspect ratio larger than 1.3 (1). The fluorescence is thus found to be polarized along the long axis. We explain our fluorescence lifetime results as a crossover between two high energy states, as explained by Alivisatos.

Little work has been carried out to explain the effect of particle shape on the fluorescence lifetime. In the present work, we carried out a detailed study of the fluorescence lifetime as a function of the aspect ratio of the rods. The effects of varying ZnS passivation and excitation wavelength on the emission quantum yield and lifetime are also presented.

Experimental

Two different methods were used to synthesize CdSe nanoparticles. Dimethylcadmium was used as a cadmium precursor for synthesis of dots and rods to study the effect of shape and aspect ratio on the fluorescence lifetime. CdO was used for the synthesis of particles used to study the effect of ZnS capping on emission quantum yield and fluorescence decay lifetimes. Typically, CdSe nanospheres were prepared using the method of Murray and Bawendi, were dimethylcadmium was used (2). In this method, dimethylcadmium is dissolved with selenium in trioctylphospine (TOP, Aldrich) and injected into a hot surfactant solution of trioctylphosphine oxide (TOPO, Aldrich). The above method modified by Peng et al. replaces dimethylcadmium with less toxic CdO as the precursor (8.9). In a typical synthesis, 0.5 g CdO (Strem) was loaded into a 3-neck flask with 4 g trioctylphosphine oxide and 2 g stearic acid (Aldrich) and heated to 320°C. At this temperature, the reddish brown solution turns optically clear. At ~280˚C, 0.2 g selenium dissolved in 4 ml trioctylphosphine (TOP, Aldrich) was quickly injected into the reaction flask and CdSe nanocrystals were instantaneously formed. The reaction flask was heated until the desired particle size was obtained. CdSe nanocrystals were washed from excess TOPO with methanol and then redesolved in toluene.

CdSe nanoparticles were passivated with ZnS using the method of Hines and Guyot-Sionnest (10). In this method, dimethylzinc ($ZnMe_2$, Aldrich) and

hexamethyldisilathiane ($(TMS)_2S$, Fluka) were used as zinc and sulfur precursors, respectively. To the previously prepared CdSe nanoparticles, $ZnMe_2$ and $(TMS)_2S$ dissolved in TOP was added drop wise at ~130º C. The capped particles were once again washed using the method discussed above.

CdSe nanorods were prepared by using the method of Alivasatos et al (11). This method is similar to that described above with the addition of co-surfactants hexylephosphonic acid (HPA) and tetradecylphosphonic acid (TDPA). The presence of co-surfactants allows a faster growth rate of particles in one direction, forming rod shaped particles. Rods can also be synthesized using the method modified by Peng et al. where CdO is used (9). Ideally, cadmium and selenium precursors were added at 280˚C and left to grow until the desired sizes were obtained. The synthesized CdSe particles were washed from excess surfactants by the method described above.

Freshly prepared CdSe particles were analyzed by a Hitachi HF-2000 field emission transmission electron microscope operating at 200 kV. Optical characterization was done using a Shimadzu UV-3101PC UV-VIS-NIR scanning spectrophotometer and PTI Model C60 steady-state spectrofluorometer. Fluorescence lifetime measurements were done on the PTI GL-3300 nitrogen laser with the fundamental excitation at 337nm. All the optical measurements were done in a square 1cm by 1cm cuvettes using colloidal solutions in toluene.

Results

a. Effect of changing the aspect ratio on the fluorescence lifetimes of CdSe nanorods:

The aspect ratios of the rods were determined by using TEM and ranged from 1.35 to 4.15 ($NR_{1.35,}$ $NR_{2.0,}$ $NR_{2.9,}$ $NR_{3.35,}$ and $NR_{4.15}$) with respective band gap absorptions at 490nm, 528nm, 535nm, 557nm and 573nm. The sizes of the nanorods are given in table 4.1.

Figure 4-1 shows the normalized absorption and fluorescence decay curves for five rod samples and a dot sample of 3.0 nm. The emission decay lifetimes for the dot sample and the $NR_{1.35}$ are much longer than the rest of the rod samples studied. The fluorescence time decay for the dot sample and $NR_{1.35}$ are 38 ns and 36 ns, respectively. The fluorescence lifetime becomes shorter as the aspect ratio becomes larger than 1.35, i.e. 25 ± 0.6 ns for $NR_{2.0}$ and 22 ± 0.8 ns for $NR_{4.15}$.

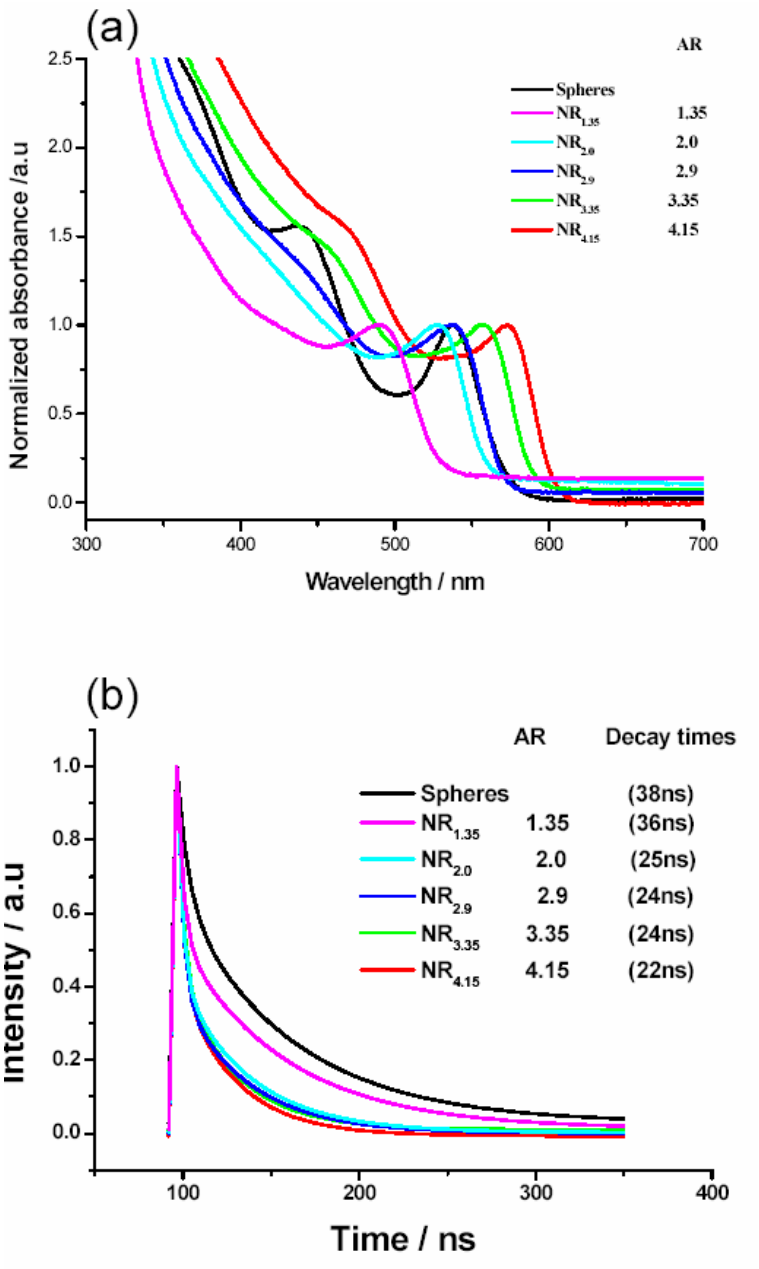

Figure 4-1: Absorption spectra of CdSe nanospheres (D0) and 5 nanorod samples ($NR_{A.R}$) (a), and the corresponding fluorescence decay lifetime spectra (b). The fluorescence lifetime is much slower for $NR_{1.35}$, similar to the dot sample, where as the fluorescence decay lifetime becomes faster for rods with an aspect ratio of 2.0 and larger.

b. Effect of passivation on the quantum yield and lifetimes of the band gap emission of 3.8 nm quantum dots:

Figure 4-2 shows the absorption and emission spectra of the uncapped dots (D0) and dots passivated with ZnS (the extent of the ZnS capping increases in the order D1→D3) with their band gap absorption at ~565 nm. The band gap absorption shifts slightly from 560 nm for the unpassivated sample to 568 nm for the most passivated sample. Figure 4-2b shows that the fluorescence quantum yield increases by 4 fold for the capped particles. Emission quantum yield increases with the extent of capping but with excessive capping (for D3), the quantum yield begins to decrease. The decrease in quantum yield is explained by Klimov in terms of lattice mismatch between the CdSe and ZnS layers. After excessive ZnS capping, the lattice mismatch between ZnS and CdSe results in an increase in the interfacial defects or dislocations that act as trapping sites for the excited charge carriers (7).

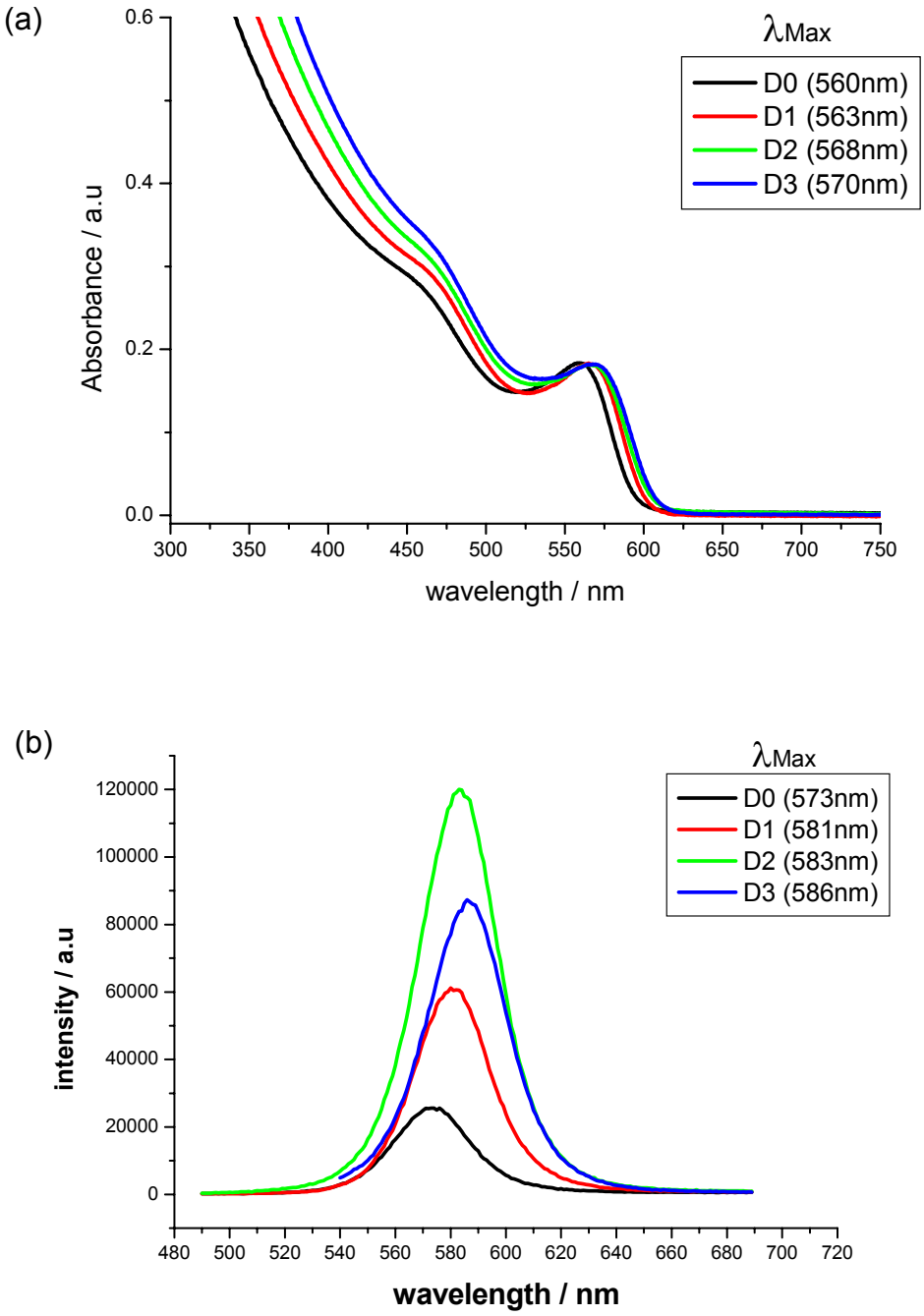

Figure 4-2: (a) Absorption spectra of uncapped CdSe nanodots (D0) and capped dot samples (D1→D3). D1 is not fully capped with ZnS and D2 and D3 are samples with increasing capping respectively. (b) Emission spectra of the samples in (a). Fluorescence intensity increases greatly with increasing capping for D1 and D2 but starts to decrease again for D3, which has the largest amount of capping.

Fluorescence lifetimes of capped and uncapped quantum dots are shown in figure 4-3 with the decay times of ~27 ± 0.5 ns for the capped dots and ~25 ± 0.5 ns for the uncapped dots. Although passivating the surface increases the quantum yield by 400%, it only increases the fluorescence lifetimes by ~10%.

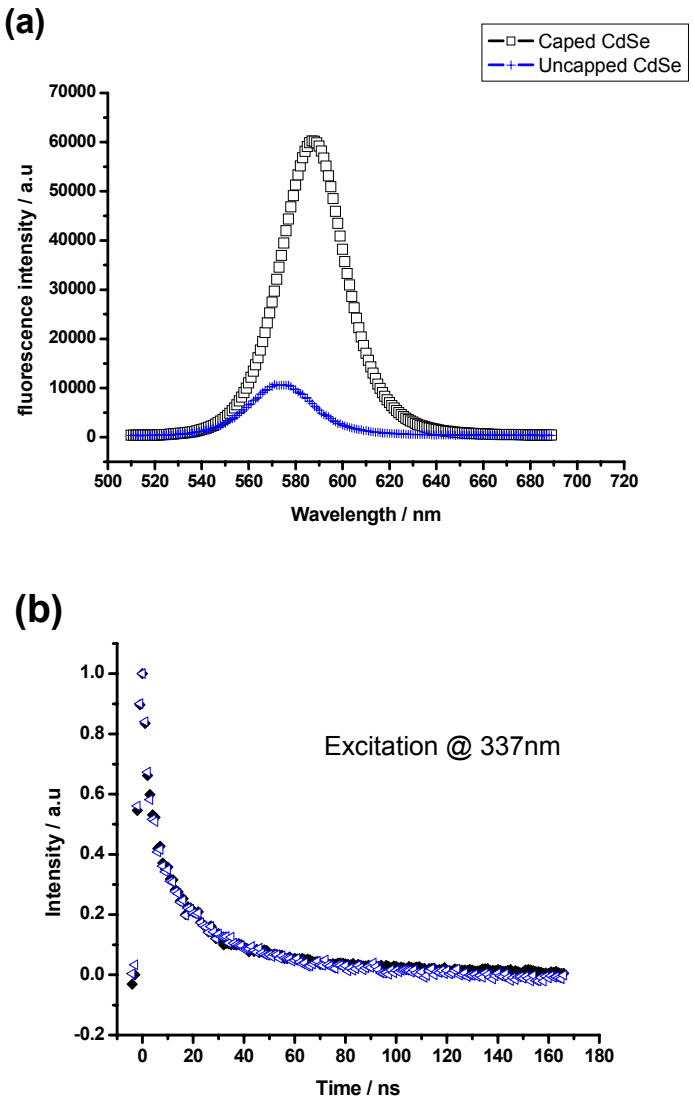

Figure 4-3: (a) Emission spectra of passivated (black) and unpassivated (blue) CdSe nanodots (3.8nm). (b)Corresponding normalized fluorescence lifetime decay spectra for passivated (black) and unpassivated (blue) dots. The fluorescence decay times are similar for these samples though the emission intensities of passivated samples are greatly enhanced.

c. Effect of excitation Wavelength on the fluorescence and lifetime of CdSe nanoparticles:

The effect of excitation wavelength on the band gap emission and lifetime of CdSe nanodots of 3.0 nm in diameter was studied and is shown in figure 4-4. The optical density of the sample was maintained at ~ 0.1 for each excitation wavelength used. The emission intensity is higher when the sample is excited close to the band gap state and decreases as the sample is excited at higher energies. Fluorescence lifetime spectra of CdSe nanodots excited at wavelengths close to the band gap (520 nm) and at higher energies (337 nm) are shown in figure 4-4b. The decay times are measured to be about 30 ns for both excitations.

The effect of excitation wavelength on the emission intensity of a passivated and an unpassivated sample is shown in figure 4-5. For both samples, the optical density at the excitation wavelength is kept constant at 0.1. The relative decrease in the emission intensity is greater for the unpassivated sample than for the passivated sample at the two excitation wavelengths studied. For the unpassivated sample, the emission decreases by a factor of 2.85 whereas it only decreases by a factor of 1.15 for the passivated sample (for excitations at 490 nm and 350 nm).

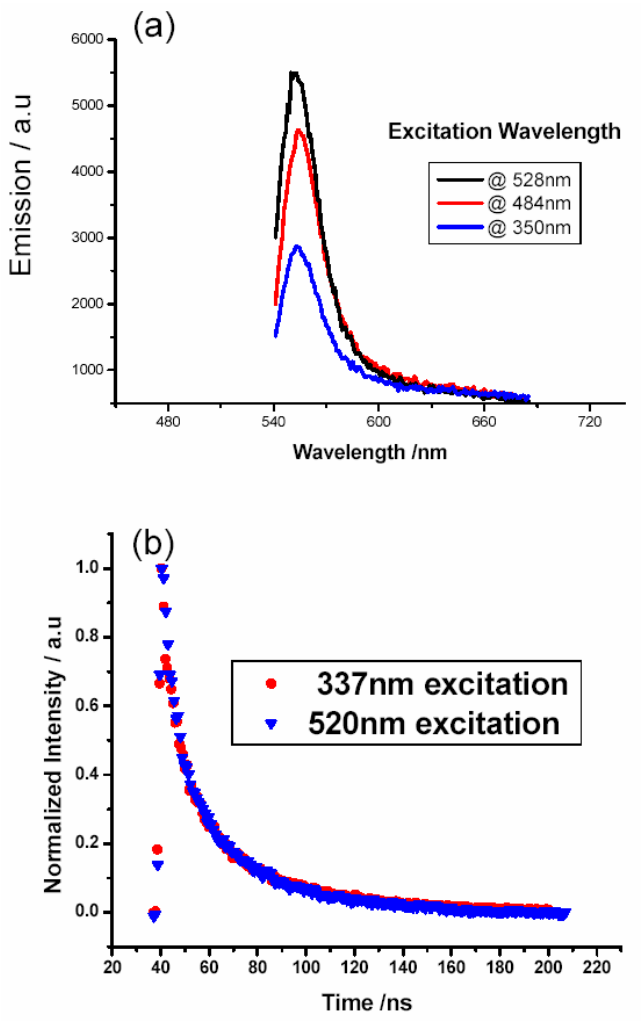

Figure 4-4(a): Effect of excitation wavelength on the band gap emission of uncapped CdSe nanodots of 3.5 nm in diameter. Optical density was adjusted to 0.1 where the sample was excited**.** (b): Normalized fluorescence lifetime spectra of CdSe nanodots excited at 337nm and 520nm wavelength of light. For both wavelengths, the decay rates are the same (~30ns), indicating that the fluorescence mechanism is not affected, but only the quantum yield decreases when excited at higher energies.

Similarly, for passivated samples, the fluorescence emission is higher when the sample is excited close to the band gap and decreases with decreasing excitation wavelength. Figure 4-5 shows the emission spectra at two excitation wavelength for passivated and unpassivated samples.

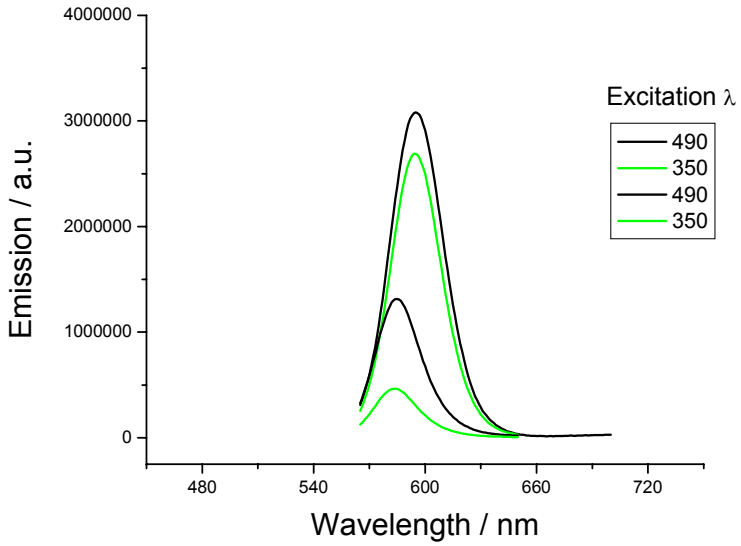

Figure 4-5: Emission spectra of passivated (strong emission) and unpassivated CdSe nanoparticles (4.0 nm) excited at 490 nm (black) and 350 nm (green).

Discussion

A number of CdSe rods are studied to understand the effect of the aspect ratio on their radiative lifetimes. In the samples studied, CdSe spheres and the rod sample with an aspect ratio of 1.35 have fluorescence lifetimes of about 37 ns. As the aspect ratio of the nanorods increases above 1.35, the fluorescence lifetime becomes shorter, around 23 ns, and becomes insensitive to the aspect ratio. There is a slight change in the fluorescence lifetimes once the aspect ratio is greater than the critical value of 1.35. These dramatic changes in the fluorescence lifetimes of CdSe nanoparticles can be explained in terms of changes in the electronic states as the particles change shape from spheres to rods (figure 4-6). Semi-empirical pseudopotential calculations show that the energy levels cross as the aspect ratio increases and it is this crossover between the highest occupied levels ($4p_{x.y}$ and $4p_z$) that leads to a sharp change in the linear polarization of the emission along the long axis (z direction) at an aspect ratio of about 1.3 (1). For similar reasons, some of the electronic transitions that are not allowed in spheres and rods with aspect ratios less than ~1.3 become allowed for longer rod, which leads to faster decay rates.

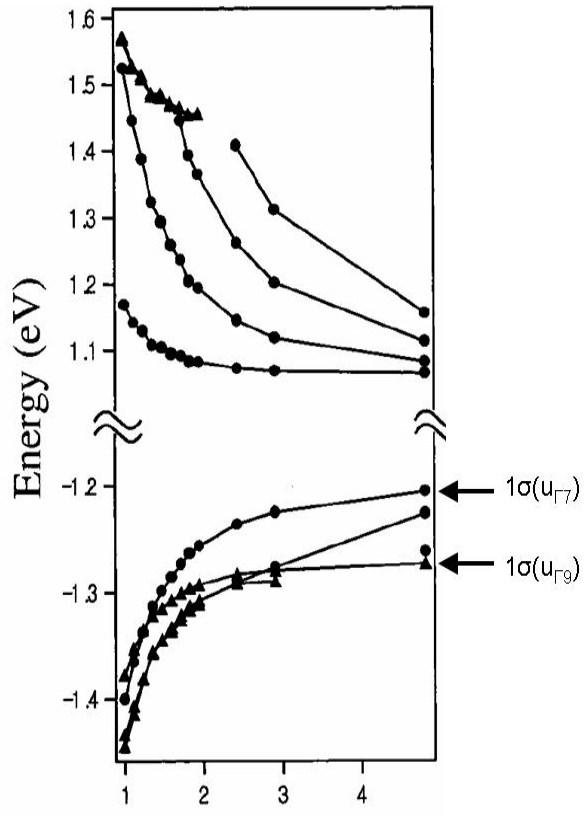

Figure 4-6: The energy change of the band edge levels versus aspect ratio for 3.0 nm. Notice the crossing of $P_{x,y}$ ($1\sigma(u_{\Gamma 9})$) and P_z ($1\sigma(u_{\Gamma 7})$) at aspect ratio of 1.35, from ref 1.

The effect of surface passivation on the fluorescence quantum yield can be understood in terms of surface defects or free cadmium or selenium ions on the surface that can act as trapping sites for the charge carriers en route to the band gap emitting state. Thus passivation of CdSe nanoparticles with materials of lager band gaps, such as ZnS, prevents trapping of the charge carriers by the surface during their relaxation from upper excited states en route to the lowest excited state. This leads to an increase in the probability of the charge carrier recombination and hence the quantum yield increases.

Upon exciting the electrons to a high energy state (337 nm), passivation increases the fluorescence quantum yield by almost 300%, but the fluorescence lifetime is not greatly affected. This suggests that the surface traps are not effective in trapping the electrons in the lowest excited state that give rise to the fluorescence. Instead, it is more effective in trapping the charge carriers relaxing from the upper excited states on their way to the emitting state. This reduces the density of the electrons (or holes) reaching the band gap state. Thus the number of electrons and holes that combine (giving rise to fluorescence) decreases. For this reason the quantum yield decreases but not the fluorescence lifetime as those charge carriers relaxing to the band gap state decay with normal band gap emission lifetime. About an 8% change in fluorescence lifetime could be due to the change in the environment of the sample after being capped with ZnS and/or due to a change in the sample quality during capping since reheating is required. We can also conclude that the electrons are predominantly trapped from the higher excited state since the fluorescence lifetime is not affected after passivating the surface with ZnS as shown in figure 4-3.

To further show that electronic trapping occurs mostly from higher excited states, we measured the fluorescence quantum yield as a function of the excitation wavelength. Figure 4-4a shows the emission spectra of unpassivated CdSe nanoparticles excited at three different wavelengths.

For all three wavelengths, the absorption optical densities were adjusted to be the same (0.1) at the excitation wavelengths in order to excite the same number of electron-hole pairs. The emission increases by almost 300% when the sample was excited close to the band gap and decreases as the energy of the excitation energy of the light increases. This shows that some electrons are trapped and do not make it to the lowest excited state to give fluorescence if excited to higher electronic state. This is consistent with the study of the fluorescence lifetimes of CdSe nanoparticles when excited close to the band gap and at the higher excited state.

Figure 4-4b shows the fluorescence lifetimes of CdSe nanoparticles when the sample is excited at 337 nm and 520 nm light. The fluorescence lifetimes for both excitation wavelengths are calculated to be about 30 ns. This again shows that the band gap fluorescence mechanism does not change with excitation wavelength and therefore further validates the proposal that the electrons are trapped predominantly from higher excited states and not from the band gap state. That is why the emission quantum yield increases with decreasing excitation wavelength, but the band gap fluorescence lifetime is unaffected.

Figure 4-5 shows the effect of different excitation wavelengths on the emission yield of passivated and unpassivated CdSe nanodots. Emission yield for both the passivated and unpassivated CdSe nanoparticles decreases with increasing

excitation energy. One thing to note is that the fraction of emission loss for the two excitation wavelengths used is greater for the unpassivated sample (2.85) than for the passivated sample (1.15). This shows that the electron trapping probability is greater for unpassivated samples because of the presence of more trapping sites due to bad surface and organic capping molecules attached directly to the CdSe nanoparticles.

Figure 4-7(a) shows the emission spectra of passivated and unpassivated CdSe nanoparticles with excitation at 500nm. Figure 4-7b shows the absorption spectra of CdSe nanoparticles together with excitation spectra of the two samples in Figure 4-7 (a). The excitation spectra are normalized at the band gap state to show that the emission is weaker when excited at higher energy than when excited close to band gap state. This supports the proposal that trapping of the excited electrons in the unpassivated sample at higher excited state is higher than in the passivated sample. This shows that passivating the surface of CdSe nanoparticles with a larger band gap material is effective in reducing the amount of traps at the surface even though there is still a significant amount of energy loss due to nonradiative relaxations.

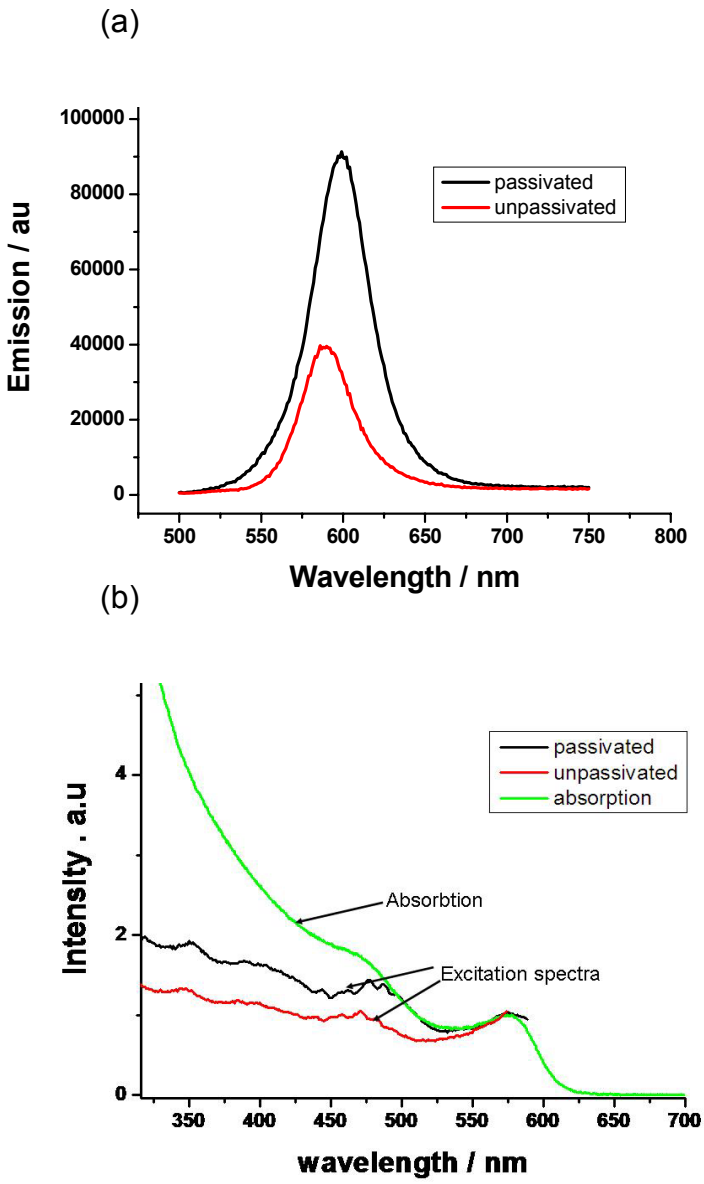

Figure 4-7 (a): Emission spectra of passivated (black) and unpassivated (red) CdSe nanoparticles. (b) In black and red are the excitation spectra of the corresponding samples of whose emission are given in 7a with the same color. The green spectrum is the absorption spectrum of 4.0 nm unpassivated sample.

The conclusion that electrons are getting trapped more efficiently from higher excited states is in agreement with the previous theoretical discussion (16) by our group that showed that the excited electrons at high energies have larger densities at the surface (where the traps are located) than the lower excited states.

Figure 4-8 shows a simple illustration of the mechanism of electron relaxation for a capped and uncapped sample and how it leads to a change in quantum yield.

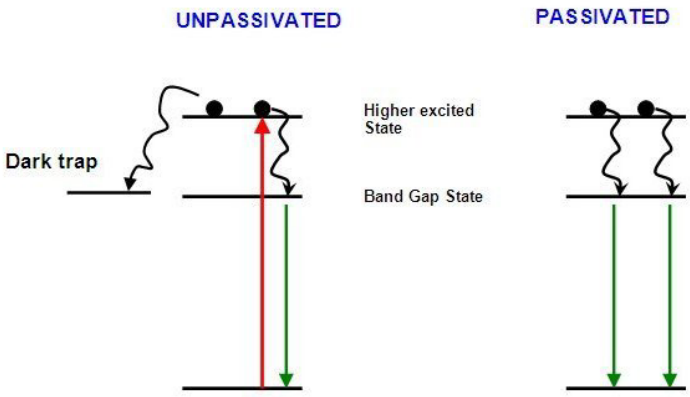

Figure 4-8 Schematic showing the mechanism of electron relaxation in passivated and unpassivated CdSe nanoparticles and upon high energy excitation. Electrons are more likely to be trapped in unpassivated samples or when excited to higher excited states resulting in poor fluorescence quantum yield.

Conclusion

We have presented the results of detailed studies on the optical and dynamic properties of CdSe nanoparticles of different shape, size and surface properties under varying experimental conditions. We have shown that the fluorescence lifetime changes dramatically for samples with aspect ratios larger than 1.3. According to the theoretical calculations (1) this is due to the interchange of two excited states at this aspect ratio which was observed previously in the changes in the polarization behavior (15). We have also showed that the fluorescence quantum yield of CdSe nanorods and nanodots is greatly increased when the sample is passivated with a ZnS layer. Though the emission quantum yield is enhanced for passivated particles, the fluorescence lifetime is unaffected. This suggests that quenching from higher excited energy levels is taking place. Furthermore, the fluorescence quantum yield decreases as the excitation wavelength decreases below that of the band gap state. These two results suggest that trapping of the charge carriers is more probable from the higher excited states than from the band gap state. This conclusion is in agreement with our previous theoretical study given on the rapid relaxation of the hot electrons (chapter III).

Table 4.1

Size of the nanorods.

$NR_{1.35}$ = 2.2+/- 0.5 X 3.0 +/- 0.8

$NR_{2.0}$ = 2.5+/- 0.5 X 5.0 +/- 1.4

$NR_{2.9}$ = 3.0+/- 0.6 X 8.0 +/- 1.7

$NR_{3.35}$ = 3.3+/- 0.8 X 11.0 +/- 1.8

$NR_{4.15}$ = 3.3+/- 0.5 X 14.5 +/- 1.5

References

(1) Hu, J.; Wang, L.; Li, L.; Yang, W.; Alivisatos, A. P. *J. Phys. Chem. B,* **2002**, 106*,* 2447-2452.

(2) Murray, C. B.; Norris, D. J.; Bawendi, M.G. *J. Am. Chem. Soc.,* **1993**, 115, 8706.

(3) Brus, L. *Appl. Phys. A*, **1991**, 53, 465.

(4) Alivisatos, A.P. *Science*, **1996**, 271, 933.

(5) Bruchez, M.; Moronne, M.; Gin, P.; Weiss, S.; Alivisatos, A. P. *Science*, **1998,** 281, 2013-2016.

(6) Chan, W. C. W.; Nie, S. *Science*, **1998,** 281, 2016-2018.

(7) Klimov, V. I.; Mikhailovsky, A. A.; Xu, S.; Malko, A.; Hollingsworth, J. A.; Leatherdale, C. A.; Eisler, H.-J.; Bawendi, M. G. *Science,* **2000,** 290, 314-317.

(8) Peng, Z. A.; Peng, X. *J. Am. Chem. Soc*. **2001**, 123, 183.

(9) Peng, Z. A.; Peng, X. *J. Am. Chem. Soc*. **2002**, 124, 3343.

(10) Hines, M.; Guyot-Sionnest, P. *J. Phys. Chem*. **1996**, 100, 468.

(11) Peng, X.; Manna, L.; Yang, W.; Wickham, J.; Scher, E.; Kadavanich, A.; Alivasatos, A. P. *Nature*, **2000,** 404, 59.

(12). Schlegel, G.; Bohnenberger, J.; Potava, I.; Mews, A. *Physical Review Letters*, **2002,** 88, No. 13, 13740-1.

(13) Dabbousi, B. O.; Rodriguez-Viejo, J.; Mikulec, F. V.; Heine, J. R.; Mattoussi, H.; Ober, R.; Jensen, K. F.; Bawendi, M. G. *J. Phys. Chem. B* **1997,** 101*,* 9463-9475.

(14) Wu, F.; Zhang, J. Z.; kho, R.; Mehra, R. K. *Chemical Physics letters*, **2000**, 330, 237-242.

(15) Hu, J.; Li, L.; Yang, W.; Manna, L.; Wang, L.; Alivisatos, A. P. *Science*, **2001,** 292, 5524, 2060-2063.

(16). Darugar, Q.; Landes, C.; Link, S.; Schill, A.; El-Sayed, M. A., *Chem. Phys. Lett.,* **2003**, 373, 284.

CHAPTER V

SIZE DEPENDENT ULTRAFAST ELECTRONIC ENERGY RELAXATION AND ENHANCED FLUORESCENCE OF COPPER NANOPARTICLES[†]

Abstract

The energy relaxation of the electrons in the conduction band of 12 and 30 nm diameter copper nanoparticles in colloidal solution was investigated using femtosecond time-resolved transient spectroscopy. Experimental results show that the hot electron energy relaxation is faster in 12 nm copper nanoparticles (0.37 ps) than in 30 nm copper nanoparticles (0.51 ps), which is explained by the size-dependent electron-surface phonon coupling. Additional mechanisms involving trapping or energy transfer processes to the denser surface states (imperfection) in the smaller nanoparticles are needed to explain the relaxation rate in the 12 nm nanoparticles. The observed fluorescence quantum yield from these nanoparticles is found to be enhanced by roughly five orders-of-magnitude for the 30 nm nanoparticles and four orders of magnitude for the 12 nm nanoparticles (relative to bulk copper metal). The increase in the fluorescence quantum yield is attributed to the electromagnetic enhancement of the radiative recombination of the electrons in the s-p conduction-band below the Fermi level with the holes in the d bands due to the strong surface plasmon oscillation in these nanoparticles.

Furthermore, effect of solvent on the long time phonon-phonon relaxation in 30 nm copper nanoparticles is also studied in solvents with different thermal conductivities. The optical density of the sample in each solvent was ~1.0 at the plasmon absorption. It is found that the phonon-phonon relaxation is faster in ethylene glycol, a more conductive solvent than in ethanol.

[†] Qusai Darugar, Wei Qian, Marie-Paule Pileni and Mostafa. A. El-Sayed; Journal of Physical Chemistry B, **2006,** 110 (1) 143-149.

Introduction

The study of electronic and optical properties of metallic nanoparticles is presently one of the most active areas of nanoscience and technology. The results have attracted more and more attention from experimentalists, theorists and technologist during the last decade (1-12). There are several motivations from both scientific and technological points of view which drive the intensive investigations of both static and dynamic electronic/optical properties of metallic nanoparticles. First, it is possible to discover new physical phenomena in metallic nanoparticles. Metallic nanoparticle has electronic structure which is in the transition between atomic-like and bulk-like structures. Many phenomena related to the properties of electronic wave function, such as electronic and thermal transport (13-15), the interaction processes of the elementary excitations (16,17), and the coupling between elementary excitations with the environment (18,19), will be different in metallic nanoparticle with respect to those present in the corresponding isolated atoms and bulk metal. Second, the metallic nanoparticles have numerous potential applications ranging from optical waveguides to biosensor (20-22). The basis for most of the potential applications of metallic nanoparticles is their unique localized surface plasmon resonance (LSPR) and scattering due to the excitation of collective oscillation of the electrons in the conduction band. For example, the LSPR oscillations can tremendously enhance the local electromagnetic field making it possible to use surface enhanced spectroscopy for single molecule detection (23,24).

Physical properties of nanoparticles could be tailored by simply controlling their size and/or shape (10,25,26). This fact lead an intense research to understand the dependence of the physical properties on the size and shape (10,25,27-33). For steady-state absorption spectra, it is well known that both the LSPR frequency and linewidth depend on the nanoparticle size and shape and this dependence could be explained using classical electrodynamics theory (25). According to this theory, if the metallic particle size is comparable to or smaller than the mean free path of the conduction electrons in the bulk, the electrons will be scattered by the surface (25), then both the dielectric function of particle which determine LSPR frequency and the phase-coherence time of the collective excitation which determines the LSPR linewidth become size and shape dependent.

With the advancement of ultrafast laser spectroscopy, it is possible to study the nonequilibrium relaxation dynamics of excited conduction electrons in metallic films and nanoparticles (13,34-40). The large difference in the heat capacity of the electrons and the lattice makes it possible to create a significant temperature rise of the electrons with respect to the ionic lattice in metallic nanoparticles by irradiating them with a sufficiently short laser pulse. Before irradiation, the electrons are located in the energy states below the Fermi level. Immediately upon irradiation, the energy is transferred to the electrons by absorption of photons via interband and intraband transitions. This quasi-instantaneous excitation of multi-electrons is a coherent collective excitation process, where the

phase memory is conserved between the electromagnetic field and the newly occupied electronic states. According to Fermi-Dirac statistics, the excited electrons are in a non-thermal distribution. The relaxation process of the non-thermally distributed electrons starts with the rapid thermalization of electrons via electron-electron (e-e) scattering on a time scale of tens of femtoseconds. At this point the electrons tend to have a Fermi-Dirac distribution with a well defined temperature that depends on the incident laser intensity. Following thermalization of electrons, electrons relax by transferring energy to the lattice via electron-phonon (e-ph) coupling on a timescale of subpicosecond to several picoseconds. This forms a new thermal equilibrium of the electron-lattice system. The energy is finally dissipated throughout the surrounding matrix by phonon-phonon coupling. This process corresponds to the heat transfer from the metal nanopaticles to the environment and therefore it is expected to be dependent on the thermal conductivity of the surrounding medium.

From the above, it is obvious that there has been considerable interest in obtaining a comprehensive understanding of the electron energy relaxation dynamics in metallic nanoparticles. This research enables us to gain insight into several elementary processes, such as e-e scattering and e-ph coupling in systems with sizes between those of isolated atoms and the bulk metal. These processes are the source of a wide range of phenomena in solid state physics. For example, e-e scattering plays an essential role in optical, electronic, and magnetic properties of disordered metallic systems. Electron-phonon coupling is

of major importance to laser-induced transformation of materials (41), selective heating in condensed phase and biological system (42), and governs the formation of the superconducting state in both conventional and high-transition-temperature superconductors (43,44). It has been predicted that due to the reduced dimensionality, the surface phonon modes (both acoustic and capillary) increase the energy transfer between the electrons and the lattice in metallic nanoparticles and the electron energy relaxation rate should increase with decreasing the size of the particles (45,46).

Extensive work has been carried out on several different noble metal nanoparticle systems by examining particle size effects on electron energy relaxation. Logunov (47,48) from our group studied thiol modified gold nanoparticles with diameters of 1.9, 2.6, and 3.2 nm in toluene. Link et al (49) in our group reported on 9 and 50 nm diameter gold nanoparticles in aqueous solutions. Hartland's group (5,30,39) obtained data on both 10 and 50 nm silver and 4.6 to 120 nm gold particles in aqueous solution. None of these papers reported any effect of particle size on the electron energy relaxation rates and all of the e-ph coupling constants were found to be similar to the corresponding bulk values. However, for very small silver nanoparticles in dielectric matrices with 3 to 10 nm diameters, Bigot and Del Fatti have observed an increase of the relaxation rate when the particle size is decreased (31,32). The results are interpreted as size-dependent coupling between the electrons and surface phonon modes and energy transfer to the dielectric matrix. As far as we know,

there has not been a report of size dependent electron energy relaxation in large noble metal nanoparticles with diameters larger than 10 nm. The reason for the few observations of size dependent electron energy relaxation is due to relative small contributions of surface phonon modes to the total e-ph coupling. For gold nanoparticles with a diameter as small as 2 nm, calculations (33) show that the contribution of the electron scattering from the surface phonon modes is less than 10% of the total e-ph processes. The contribution of the surface phonon modes to the total e-ph coupling is determined by the ratio of free electron density to the metal density (n/ρ), which is proportional to the valence of the metal divided by its atomic mass (29,33). The values of (n/ρ) for gold, silver, and copper are $3.06\times10^{21}g^{-1}$, $5.57\times10^{21}g^{-1}$, and $9.46\times10^{21}g^{-1}$, respectively. So electron-surface phonon coupling should be much stronger in copper nanoparticles than in gold and silver nanoparticles. Therefore, copper nanoparticles may offer a better test system to detect the effects of coupling to the surface phonons on the electron energy relaxation by studying the effect of the size on the e-ph relaxation time.

In this paper, we present time resolved transient absorption data for copper nanoparticles with diameters of 12 nm and 30 nm. Analysis of the data shows that conduction electron energy relaxation is faster in 12 nm copper nanoparticles than in 30 nm copper nanoparticles. Our result could be interpreted by including contribution of size-dependent electron-surface phonon modes coupling. Furthermore, additional coupling of the excited electron to surface

imperfections is necessary to account for the observed relaxation rate of the excited (hot) electrons in 12 nm nanoparticles. We have also observed strong fluorescence from the 30 nm particles and weak fluorescence from the 12 nm copper particles. Fluorescence quantum yield in the particles we studied is found to be enhanced by about 4-5 orders-of-magnitude compared to that of bulk copper metal.

Experimental

a. Photochemical synthesis of copper nanoparticles

Copper nanoparticles are more easily oxidized than gold and silver nanoparticles, which make the synthesis of stable copper nanoparitlces to be more difficult. Currently, only very few methods have been reported on the preparation of copper nanoparticles in solution (50,51). The copper nanoparticles in ethanol solution used in this paper are made by photochemically reducing a commercially available precursor bis(2,4-pentanedionato)copper(II), [$Cu(acac)_2$] with UV light as proposed by Giuffrida et al. (51). In a typical copper nanoparticle synthesis, $5\times10^{-4}M$ $Cu(acac)_2$ in deoxygenated ethanol is irradiated at 254 nm at an intensity of 5 mW/cm^{-2} under anaerobic conditions. Growth of copper nanoparticles is monitored by the appearance of an absorption peak around 570 nm, which is characteristic of the plasmon band of copper nanoparticles (27,50).

The irradiation is stopped when a maximum value of plasmon absorption is observed. Copper nanopaticles prepared this way are very unstable. In order to increase their stability, poly(N-vinylpyrrolidone) was added to the solution before irradiating with UV light. This allowed the formation of isolated copper nanoparticles that were stable for days when left in an inert atmosphere. Particle size variation was very critical for our research and was difficult to obtain by only controlling the parameters of one-step photochemical reduction (such as concentration of solution, irradiation light intensity, and irradiation time). By using previously synthesized nanoparitcles (about 10 nm) as seeds (seed-mediated growth method), copper nanoparicles in ethanol with an average diameter of 30 nm were successfully grown.

The size and morphology were examined by using a JEOL 100CX II transmission electron microscope (TEM) and the linear absorption spectrum of our samples was measured by using a Shimadzu UV-3101-PC spectrophotometer. The TEM images of two samples, Cu1 and Cu2, are shown in figure 5-1a and 5-1b, respectively. The average diameters of Cu1 and Cu2, determined by measuring the sizes of roughly 200 particles, were 12 nm and 30 nm, respectively. The linear optical absorption spectrum of Cu1 and Cu2 are shown in figure 5-2. A nice plasmon absorption band is clearly seen in both samples with a slight blue shift from 568.5 nm for Cu1 to 565.0 nm for Cu2. The blue shift of the surface plasmon absorption of copper nanoparticles as increasing their sizes is consistent with the theoretical prediction made by Pileni's group (52). By taking

into account the size effect of dielectric constant $\varepsilon_2(R)$, using the Mies' theory, they have demonstrated that there is a progressive blue shift of surface plasmon absorption upon increasing the size of copper nanoparticles. Besides the TEM images, the absorption spectrum also confirm that the size of Cu2 is larger than that of Cu1.

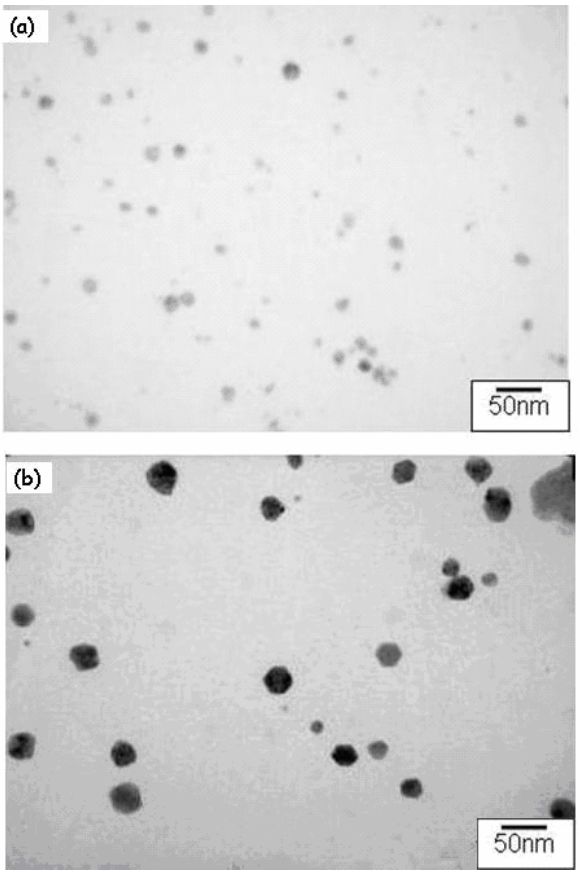

Figure 5-1. Transmission electron microscope images of (a) Copper 12nm and (b) Copper 30nm particles. The measured average diameter of these nanoparticles was determined by measuring sizes of roughly 200 particles. In (b), we also observed nonspherically shaped copper nanoparticles synthesized by the photochemical method.

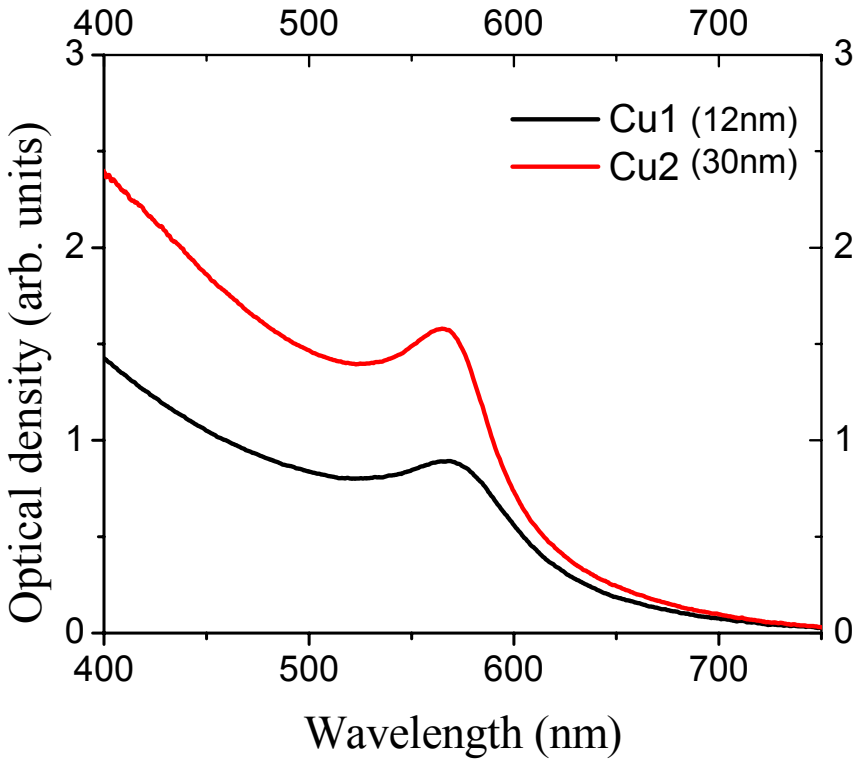

Figure 5-2. Absorption spectra of copper nanoparticles in ethanol solution synthesized by photochemical reduction of the precursor bis(2,4-pentanedionato)copper(II), [$Cu(acac)_2$] in ethanol in the presence of PVP with 254 nm UV radiation. The absorption around 570 nm is characteristic of the plasmon band of copper nanoparticles.

b. Steady-state fluorescence

The steady-state fluorescence spectra were obtained using a PTI Model C60 Steady-State Spectrofluorometer with an arc lamp source and a photomultiplier detection system. Copper nanoparticles were excited with a 337 nm emission from a xenon arc lamp and fluorescence spectra were taken from 540 nm to 660 nm with 1 nm spectral resolution and a 500 ms integration time. The fluorescence quantum yield of copper nanoparticles was determined by comparing their fluorescence intensities with the fluorescence of Rhodhamine 6G, assuming 100% quantum yield for Rhodhamine 6G.

c. Femtosecond transient time resolved absorption apparatus

Time resolved transient absorption experiments performed with a femtosecond laser system have been described elsewhere (53). Briefly, an amplified Ti-Sapphire laser system (Clark MXR CPA 1000) is pumped by a frequency-doubled Nd:Vanadate laser (Coherent Verdi). This generates laser pulses of 100 fs duration (fwhm) with energy 1 mJ at 800 nm and a repetition rate of 1 kHz. The femtosecond laser pulses of 800 nm are frequency doubled in a 1 mm BBO crystal to generate 400 nm pump pulses. A small portion of the fundamental pulse (about 40 μj) was used to generate a femtosecond white light continuum in a 1 mm sapphire plate, which was used as the probe. The range of the femtosecond continuum was from 400 nm to 1100 nm. The pump beam traveled

through a computer controlled variable optical delay line with a resolution of 3 um (20 fs) and was mechanically chopped at a frequency of 500 Hz by a synchronous light beam chopper (HMS 221). A master clock generated by Clark-MXR DT 505 was used to set the chopper frequency and phase. The pump and probe beams were focused and overlapped at the sample with a diameter of about 250 um. In order to minimize noise due to fluctuations in the intensity of the white light continuum, a reference beam was split-off from the probe beam before the sample. Both the reference beam and transmitted signal beam were focused into an optical fiber cable coupled to a monochromator (Acton Research). After passing the monochromator, the signal and reference beams were detected by two matched photodiode (Thorlabs)-boxcar integrator (Stanford Research System, SR 250) systems. The output from the signal boxcar was divided by the output from the reference boxcar with an analog divider. A lock-in amplifier (Stanford Research System SR 530), referenced to the synchronous chopper monitored the output of the divider. The induced changes of the sample absorption were probed at the peak of the LSPR absorption by measuring the differential transmission $\Delta T(t)/T = (T_{on}(t) - T_{off})/T_{off} = -\Delta\alpha(t)L$ as a function of the temporal delay between the pump and probe. Here, $T_{on}(T_{off})$ refers to the transmission with (without) the pump beam and L is the interaction length between the pump (probe) pulse and the sample. The high stability of our femtosecond laser system and phase lock technique permit high sensitivity measurements with a noise level for ($\Delta T/T$) in the 10^{-4} range. The cross-correlation between the pump beam and probe beam at the peak of the LSPR

absorption of our samples had a FWHM of 180 fs at the sample position. All the experiments reported below were completed at room temperature with pump pulse energy used within 0.01-0.1 uJ/pulse.

Results and discussion

The differential transmission $\Delta T / T$ measured for the 12 nm diameter copper nanoparticles in ethanol solution (Cu1) excited at 400 nm with the probe wavelength set to the plasmon band maximum (568 nm) is shown in figure 5-3. Each trace corresponds to different incident pump pulse energy. By looking carefully on the rise of transient bleach signal, we could find that the buildup time of the signal is clearly longer than the FWHM of our instrument response function (180 fs). This phenomenon has been previously observed and is ascribed to the internal thermalization of the hot electrons[4,10,38]. The relaxation process of electrons from the non-thermally distribution to Fermi-Dirac distribution via electron-electron (e-e) scattering varies from 5 to about 500 fs, depending on the intensity and the frequency of the pump laser pulse (39,54). For the processes of energy relaxation of Fermi-Dirac distributed electrons in metallic nanoparticles, it can be described as two-exponential decays (3).

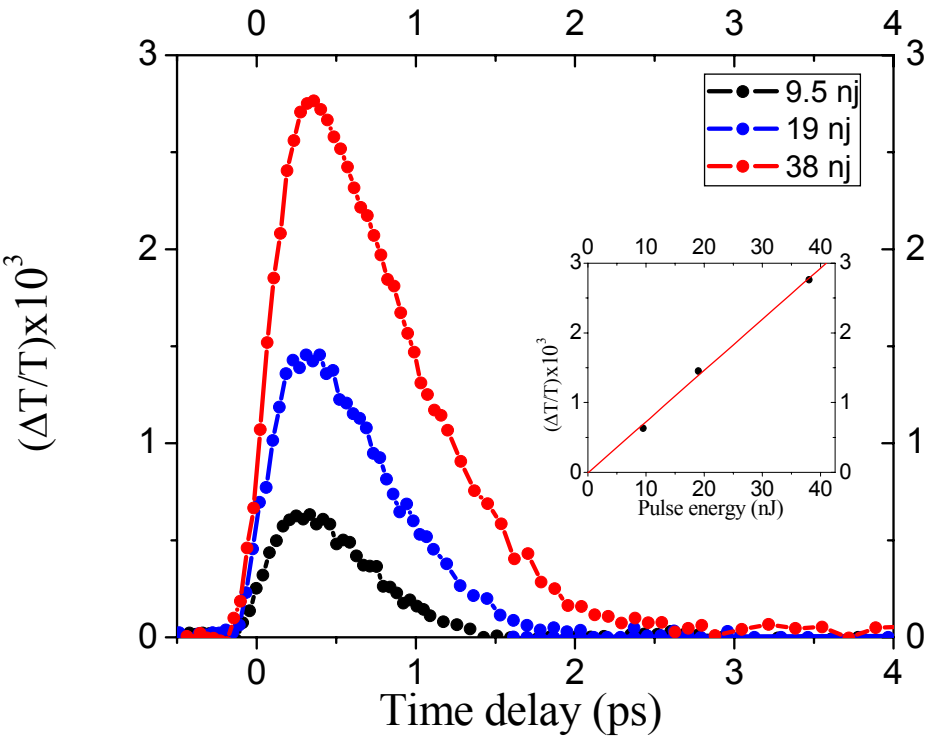

Figure 5-3. The differential transmission $\Delta T / T$ measured in 12 nm diameter copper nanoparticles (Cu1) with the probe wavelength set to the maximum of the plasmon band (568 nm). The different traces correspond to different pump pulse energies. The inset shows the dependence of the signal maximum on the pump pulse energy. The signal amplitude is linearly proportional to the pump pulse energy, confirming that the transient transmission is dominated by linear free electron absorption and that nonlinear absorption is negligible.

The fast contribution, in the picosecond time scale, is due to the relaxation of hot electrons through coupling with the phonons (lattice). The slow contribution that decays on a time scale of hundreds of picoseconds is due to relaxation involving the surroundings (phonon-phonon coupling). The ratio between slow contribution and fast contribution is increased as the pump pulse energy increases. In our

experiment, due to the low pump power (the maximum pump pulse energy is 38 nJ), it can be seen in figure 5-3 that the ph-ph coupling contribution to the total transient transmission is less than 1% and is negligible in the following data analysis. The inset of figure 5-3 shows the signal maximum under different pump pulse energies. The signal amplitude is found to be proportional to the pump pulse energy, suggesting that the transient transmission is dominated by the induced changes of the linear free electron absorption and that nonlinear absorption is negligible. The normalized traces of the transient transmission signals in figure 5-3 are shown in figure 5-4.

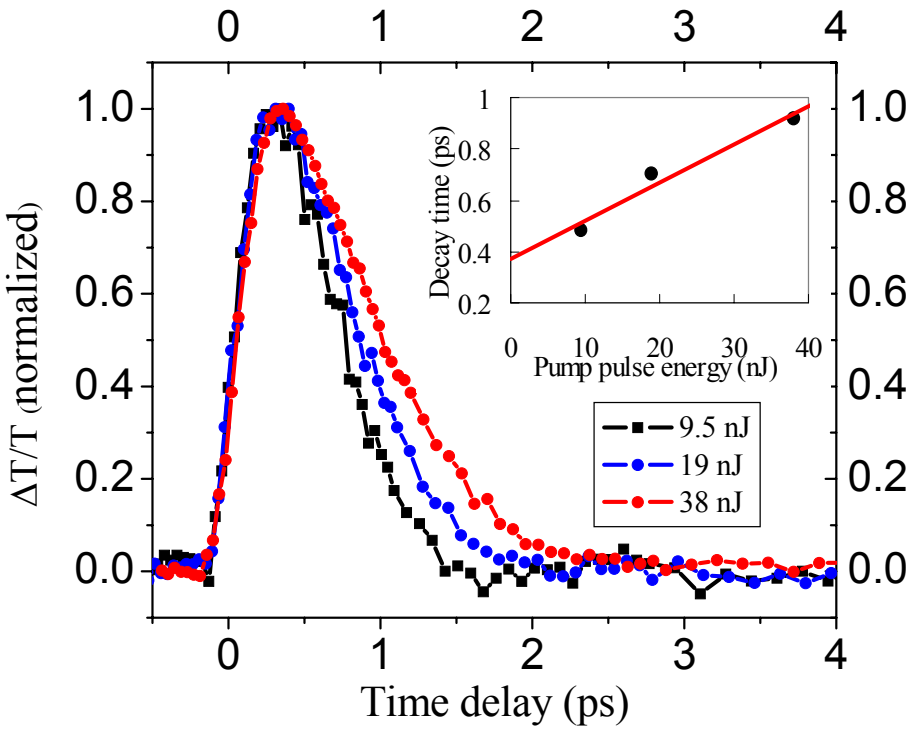

Figure 5-4. The normalized traces of the transient transmission signal shown in figure 5-3. It is clear that the e-ph coupling process depends on the pump pulse energy. A reliable value of electron phonon coupling constant g can be obtained by extrapolating the lifetimes measured at different pump powers to zero pump power. The intercept is given by $\gamma T_0 / g$. The inset shows an example of this extrapolation procedure.

It is clear that the e-ph coupling process depends on the pump pulse energy. This effect has been studied and is usually interpreted in terms of the two-temperature-model (TTM) (30,39). Essentially, it is the linear increase of the electronic heat capacity with the electron temperature that causes the hot electron energy transfer rate between the electrons and phonon baths to be dependent on the pump pulse energy. In TTM, the electrons and phonon baths form two sub-systems of the metal, each characterized by a different heat

capacity and temperature. The time evolution of the electron and lattice temperatures T_e and T_l can be described by the following pair of coupled nonlinear differential equations (34,35):

$$C_e(T_e)\frac{\partial T_e}{\partial t} = \kappa\nabla^2 T_e - g(T_e - T_l) + A(r,t), \qquad (5.1)$$

and

$$C_l\frac{\partial T_l}{\partial t} = g(T_e - T_l). \qquad (5.2)$$

Where C_e and C_l are the electronic and lattice heat capacities. $C_e(T_e) = \gamma T_e$ ($\gamma = 96.6$ $Jm^{-3}K^{-2}$ for copper) is proportional to the electron temperature as long as T_e is much smaller than the Fermi temperature, which is in the order of 10^4 K. The first term on the right-hand side of the Eq. (1) represents thermal-conductivity losses and κ is the thermal conductivity. Within the time scale used in the present work (few picoseconds after excitation), the thermal conductivity is thought to have negligible contribution and this term could be ignored. The second term in the Eq. (1) represents electron and lattice temperature coupling through the e-ph coupling constant g, which is independent of temperature. Heating due to the incident optical pulse is accounted for by the source term $A(r,t)$. When the pump intensity is low, as the situation was in our experiments, the temperature change in the electron gas is small, and the relaxation time is given by $\gamma(T_0 + \Delta T)/g$ according to equations (5-1) and (5-2), where T_0 is the ambient temperature and ΔT is the initial electronic temperature increase of electron subsystem induced by the pump laser pulse after internal

thermalizaiton of non-thermal electrons via electron-electron scattering. A reliable value of g can be obtained by extrapolating the lifetime measured at various pump powers to zero, where the intercept is given by $\gamma T_0 / g$ (30,39). The inset in figure 5-4 shows an example of this extrapolation procedure.

The primary aim of this paper is to understand how the electron energy relaxation depends on the copper nanoparticle size. Figures 5-5(a)-(c) compare the transient transmission signal of Cu1 and Cu2 under pump pulse energies of 9.5 nJ, 19 nJ, and 38 nJ.

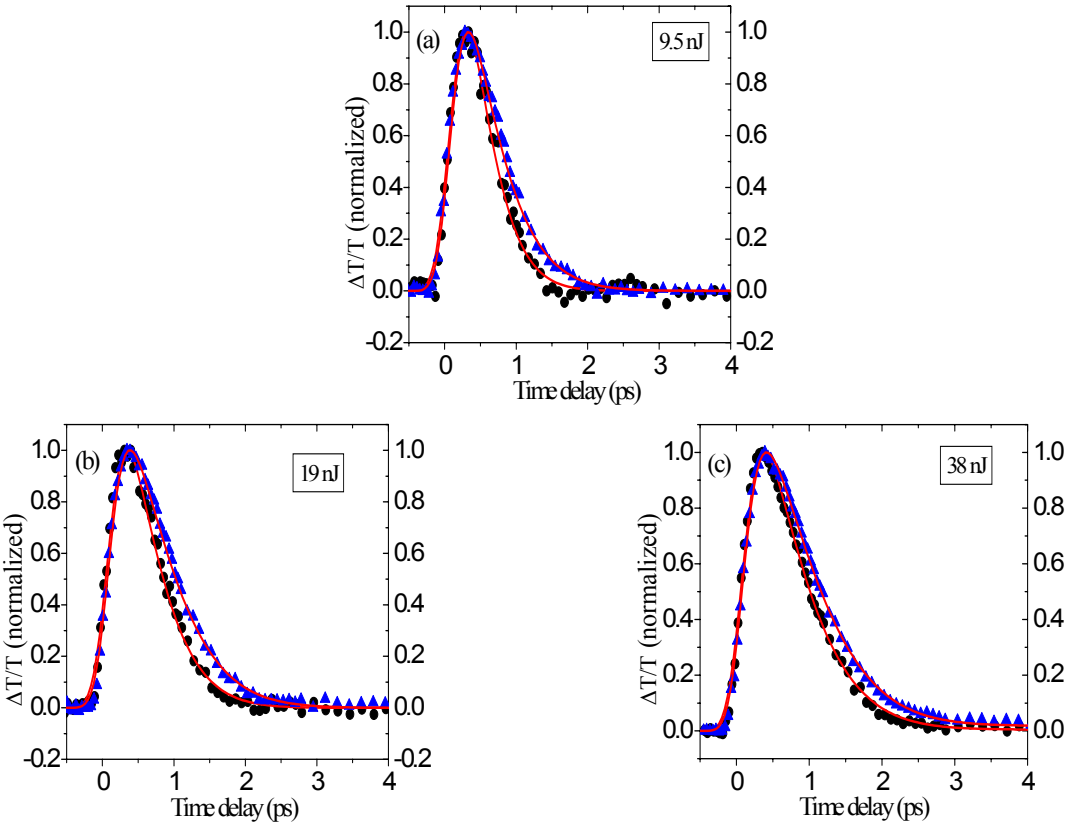

Figure 5-5. (a)-(c) comparison of the transient transmission signal of Cu1 (black circles) and Cu2 (blue triangles) under pump pulse energies of 9.5 nJ, 19 nJ, and 38 nJ. It is obvious that electron energy relaxation is size dependent and the lifetime is shorter for smaller nanoparticles. The experimental data $\Delta T(t)/T$ is simulated (red lines in (a)-(c)) by convoluting the theoretical response function $I(\tau)$ with the instrument response function $R(t-\tau)$.

It is clear that the dynamics of electron energy relaxation are size dependent, with the shorter lifetime for smaller nanoparticles. The experimental data of ($\Delta T(t)/T$) is simulated (red lines in figures 5-5(a)-(c)) by convoluting the theoretical response function $I(\tau)$ with the instrumental response function $R(t-\tau)$ (18,38):

$$\begin{aligned}\frac{\Delta T(t)}{T} &= I(\tau)\otimes R(t-\tau) \\ &= \int_{-\infty}^{\infty}\left(1-\exp(-\tau/\tau_{e-e})\right)\exp(-\tau/\tau_{e-ph})\exp(-(t-\tau)^2/\tau_0^2)d\tau\end{aligned} \quad . \qquad (5.3)$$

Where, τ_{e-e} and τ_{e-ph} are the thermalization times of the electrons due to e-e scattering and e-ph interactions, respectively. τ_0 is determined by measuring the cross correlation between the pump and probe at the sample position (180 fs in our experiments). For Cu1 (Cu2), the lifetimes of τ_{e-ph} obtained from simulation are 0.48 (0.64) ps, 0.70 (0.86) ps, and 0.93 (1.12) ps under pump pulse energies of 9.5 nJ, 19 nJ, and 38 nJ, respectively. Extrapolating the lifetimes measured at different pump powers, we obtained lifetimes of $\tau_{e-ph}(0)$ at zero pump power for both Cu1 and Cu2, which are 0.37 ps and 0.51 ps, respectively. Using the equation:

$$\tau_{e-ph}(0) = \frac{\gamma T_0}{g_{\exp}}, \qquad (5.4)$$

we find that the experimental e-ph coupling constants $g_{\exp}$ for Cu1 and Cu2 are 7.8×10^{16} $Wm^{-3}K^{-1}$ and 5.7×10^{16} $Wm^{-3}K^{-1}$, respectively. Equation 5.4 assumes that all the electron energy relaxation is due to phonon interactions. However in our case we believe that surface imperfections in colloidal copper nanoparticles may also contribute to the overall electron energy relaxation. Equation 5.4 is modified to not only account for the electron energy relaxation due to phonon interactions but also due to surface imperfections. We replaced τ_{e-ph} and $g_{\exp}$ with τ_{eR} and α_{eR}, where τ_{eR} and α_{eR} are the total electron energy relaxation time and total electron relaxation coupling constant, respectively.

If the radius of the nanoparticle is comparable or smaller than the bulk electron mean free path, surface scattering of the electrons becomes relevant (29,45,46). In this case, the hot electron energy relaxation occurs through two different channels: electron-bulk phonon coupling and electron-surface phonon coupling. There are two kinds of surface phonon modes (33,45,55), namely, acoustic and capillary surface modes. Since all these coupling processes occur simultaneously, the total electron-phonon coupling, g_{total}, is determined by summing of the three different contributions (33):

$$g_{total} = g_{bulk} + g_A + g_C, \qquad (5.5)$$

The last two terms, which are size dependent, stand for the acoustic and capillary surface modes coupling, respectively.

The value of electron-bulk phonon coupling g_{bulk} in copper has been reported by Brorson (36) and Tien (56) to be $g_{bulk} = (4.8 \pm 0.7) \times 10^{16}$ $Wm^{-3}K^{-1}$. The contribution of electron-surface phonon coupling to the electron energy relaxation in metallic nanopartilces can be derived with a quantum-kinetic treatment (45,46,55). By considering the Hamiltonian which describes the interaction of electrons in a spherical potential well of depth V_0, the expression for the coupling constant between the electrons and the surface capillary modes is (33,45,55):

$$g_C = \frac{3}{16\pi} \kappa_B \frac{v_F}{R} n \frac{m_e \omega_l^2}{\sigma} \left(\frac{V_0}{\varphi_0} \right)^2 , \qquad (5.6)$$

where κ_B is Boltzmann's constant, v_F is Fermi velocity, R is radius of particle, n is the free electron density, m_e is the electron mass, ω_l is the maximum frequency of the capillary modes, σ is the surface tension, V_0 is the Fermi energy, φ_0 is the work function of the metal. The limiting frequency ω_l is approximately given by (29,33):

$$\omega_l = \sqrt{\frac{\sigma}{\rho R^3} l(l-1)(l+2)} , \qquad (5.7)$$

where ρ is the density of the metal and l is the angular momentum number corresponding to the shortest possible surface wave, which is given by the

integer part of $\pi R/d$, where d is the lattice parameter. The electron energy relaxation associated with electron-surface acoustic modes coupling is given by (33,45,55):

$$g_A = \frac{1}{16\pi}\kappa_B \frac{\nu_F}{R^2} n \frac{m_e}{\rho}\left(\frac{\omega_D}{c_l}\right)^2\left(\frac{V_0}{\varphi_0}\right)^2, \qquad (5.8)$$

where c_l is the longitudinal speed of sound and ω_D is the Debye frequency. With the following parameter (57,58): $\nu_F = 1.57\times10^6$ m/s, $n = 8.45\times10^{28}$ m^{-3}, $\rho = 8.93\times10^3$ Kg/m^3, $d = 0.256$ nm, $V_0 = 7.0$ eV, and $\varphi_0 = 4.65$ eV. Using Eqs. (5-6) and (7) we calculated g_C for Cu1 and Cu2, which are summarized in Table 5.1.

Table 5.1. Comparison of the experimentally determined total electron relaxation coupling constant (α_{eR}) for two sizes of the copper nanoparticles with the calculated total e-ph coupling constant g_{total}, $g_{total} = g_{bulk} + g_C$, assuming that the electron-phonon coupling within the nanoparticle is the same as that for the bulk (56). The unit is $10^{16} Wm^{-3} K^{-1}$.

Particle diameter (nm)	Experimentally determined total electron relaxation coupling constant (α_{eR})	Calculated electron-Surface Phonon coupling constant (g_C)	Total Calculated electron-phonon coupling constant $g_{total} = g_{bulk} + g_C$
12	7.8	0.8	5.6 ± 0.7
30	5.7	0.3	5.1 ± 0.7
bulk	4.8 ± 0.7	0	4.8 ± 0.7

From our calculations, the contribution of g_A is about two orders-of-magnitude smaller than that of g_C, so the values of g_A are not reported in Table 5.1. The total e-ph coupling constant (Table 5.1) $g_{total} = g_{bulk} + g_C$ for 12nm and 30nm diameter copper nanoparticles were $(5.6 \pm 0.7) \times 10^{16}$ $Wm^{-3}K^{-1}$ and $(5.1 \pm 0.7) \times 10^{16}$ $Wm^{-3}K^{-1}$, respectively, with a reported value of $(4.8 \pm 0.7) \times 10^{16}$ $Wm^{-3}K^{-1}$ for g_{bulk} (36,56). The size distributions of the two samples are 15%. Using Eqs. (5)-(8), we estimate that the error bars for e-ph coupling constants because of

nonuniformity of nanoparticle size are less than 2% and are neglected in the Table 5.1. By comparing the total e-ph coupling constants g_{total} to the experimental values of total electron relaxation coupling constant α_{eR} obtained from the decay of the bleach spectrum, we see that for both 12 nm and 30 nm diameter copper nanoparticles, α_{eR} is larger than g_{total}. The difference between α_{eR} and g_{total} becomes bigger as the diameter of copper nanoparticles is decreased from 30 nm to 12 nm. This suggests that another size dependent dissipation channel is needed besides the electron-surface phonon modes coupling mechanism to account for the observed difference between α_{eR} and g_{total}. One possible mechanism is electron-defect scattering on surface imperfections (59). For chemically synthesized nanoparticles, there are always some imperfections on their surfaces. We believe that, for copper nanoparticles used here, the surface imperfections consist of several different kinds of defects, such as oxidized copper atoms, uncompensated surface charges, the capping material-surface atom complex, vacancies, dislocations, and dangling bonds. It is reasonable to believe that this phenomenon's contribution to the total electron energy relaxation in nanoparticles is size dependent because smaller metallic nanoparticles have more surface imperfections due to their higher surface energy, larger surface curvature, and larger surface-to-volume ratio. Also, the tendency for copper nanoparticles to be oxidized could produce surface imperfections which are formed easier in smaller nanoparticles. Surface imperfections could introduce several new mechanisms for the electronic relaxation process. First, surface imperfections could trap free electrons and

localize them at the defect sites (traps). Second, surface imperfections could cause stronger inelastic scattering than from passivated surfaces. Energy transfer processes to the defect surface states could also lead to an increase in the rate of the electron relaxation.

A more effective nonradiative electronic relaxation in smaller copper nanoparticles is observed from the study of the quantum yield of fluorescence of these nanocrystals. In 1969, Mooradian observed fluorescence from bulk copper metal with an emission maximum at 600 nm (60). The quantum yield of this fluorescence was found to be about 10^{-10}. We observe much stronger fluorescence from copper nanoparicles. Figure 5-6 shows the fluorescence spectrum of Cu1 and Cu2 with excitation at 337 nm. The fluorescence bands are observed at 610 nm, close to that of bulk copper, suggesting the same electronic origin.

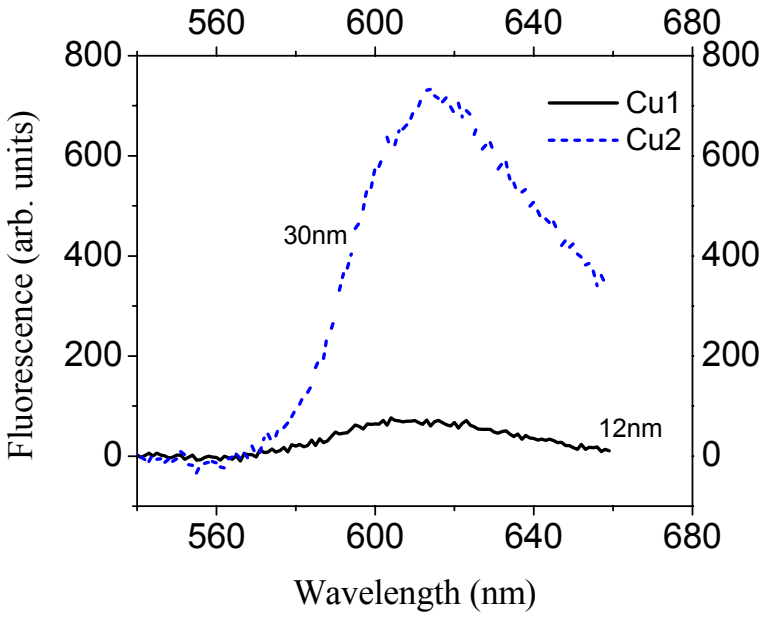

Figure 5-6. The fluorescence emission spectra of from copper nanoparticles in ethanol solution synthesized using photochemical reduction. The quantum yield of the 30nm nanoparticles was found to be as high as 10^{-5} and ~10^{-6} for 12 nm particles. The lower fluorescence quantum yield of the 12nm particles could be due to more surface imperfection in smaller nanoparticles.

This fluorescence is due to radiative recombination of the s-p conduction-band electrons below the Fermi level with the holes in the d bands. The fluorescence quantum yields of Cu1 and Cu2 are calculated to be 10^{-6} and 10^{-5}, respectively, which are greatly enhanced when compared to the value of 10^{-10} for the bulk copper metal. The mechanism for the enhancement of the fluorescence quantum yield is similar to the mechanism in gold nanorods (61), an LSPR induced enhancement of the electric fields of the incoming and the outgoing radiation. The lower fluorescence quantum yield of Cu1 compared to that of Cu2 suggests

more efficient fluorescence quenching for smaller nanoparticles which is probably due to the surface imperfections. This indicates that the contribution of surface imperfections to the electron energy relaxation is larger in Cu1 than that in Cu2, which is consistent with our experimental result. Furthermore, using the numbers in Table 5.1, we can estimated the ratios of contribution from bulk phonons, surface phonons, and surface imperfections to the total electron energy relaxation, which are 61.6% (84.2%), 10.2% (5.3%), and 28.2% (10.5%) for 12 nm (30 nm) copper nanoparticles in ethanol solution.

In their paper of silver nanoparticles embedded in dielectric matrices (32), Bigot et al. also included the effect of heat transfer to the dielectric matrix to interpret the size dependence of the electron energy relaxation. We think this mechanism does not effectively contribute to observed size dependence of electron energy relaxation observed in copper nanoparticles in ethanol solution. This is because the thermal conductivity of ethanol is about two orders-of-magnitude smaller than those of the dielectric matrix used by Bigot et al. This means that heat transfer in ethanol will occur on a time scale that is much longer than that in a dielectric matrix so its effects on the size dependent electron energy relaxation is negligible.

Effect of surrounding on the cooling dynamics was studied by El-Sayed and coworkers (40, 62). They found that the bleach dynamics was influenced by changing the surrounding medium. Changing the medium from an organic

solvent to $MgSO_4$ (62), or from aqueous medium to a series of polymer gels, the relaxation times where different. The bleach recovery becomes slower when the thermal conductivity of the medium was decreased.

We also explain the effect of solvent on the phonon-phonon relaxation in copper nanoparticles. Copper nanoparticles used for these studies were similar to the once used above (30 nm in diameter) whose absorption spectrum is shown in figure 5-2. For phonon-phonon relaxation in copper nanoparticles, 700 µL of 30 nm diameter copper nanoparticles prepared in Ethanol was added in two cuvettes. To one cuvette, 300 µL of ethanol and to the other 300 µL of ethylene glycol was added. The relaxation dynamics are shown in figure 5-7 below. The thermal conductivities of ethanol and ethylene glycol are 0.176 and 0.256 W/m K, respectively. The phonon-phonon relaxation times for copper in ethanol and ethylene glycol were determined to be 900 ps ± 10% and 583 ps ± 10%, respectively. It is found that under the same conditions, the phonon-phonon relaxation is faster in more conductive solvent (Ethylene glycol) than in ethanol. This is expected since the copper particles can dissipate heat more efficiently to the surrounding medium of higher thermal conductivities.

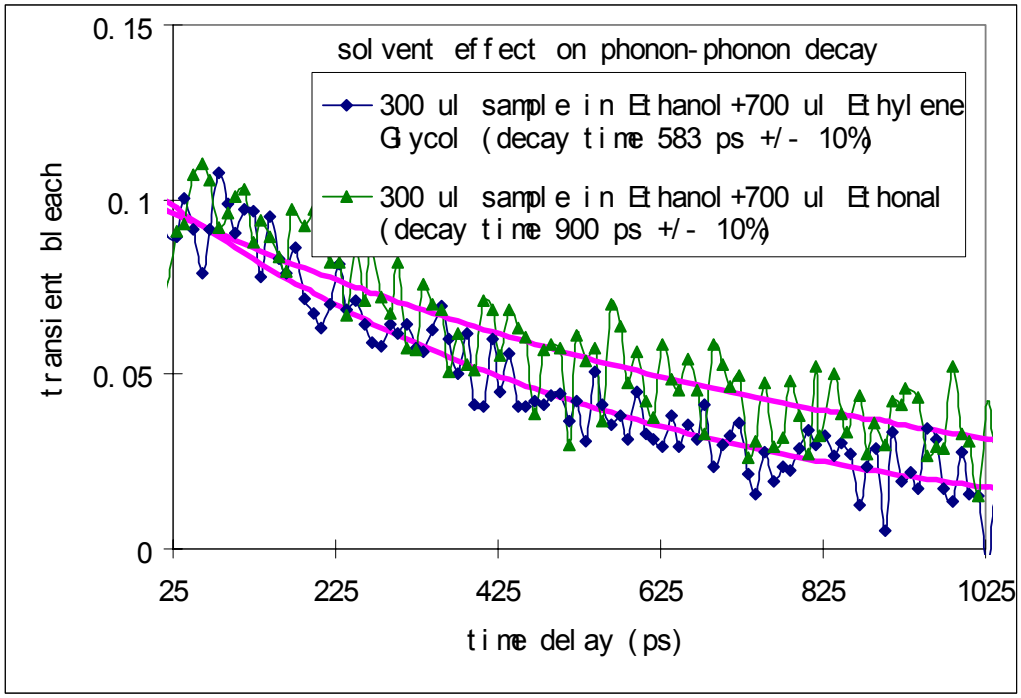

Figure 5-7: Phonon-phonon relaxation dynamic of copper nanoparticles pumped with 400 nm femtosecond pulse and probed at the plasmon maximum (565 nm). Decay times of 900 ps and 583 ps for particles in ethanol and ethylene glycol are determined, respectively.

Conclusions

We studied the ultrafast relaxation dynamics of hot electrons in copper nanoparticles in ethanol solution. The results show that the temporal behavior of the electron energy relaxation has clear size dependence. Both size-dependent electron-surface phonon coupling mechanism and the additional mechanisms involving electron trapping or electron energy transfer to surface imperfections are used to interpret the experimental results. We also observed an enhancement of the steady-state fluorescence by five orders of magnitude in copper nanoparticles compared with the bulk metal. The fluorescence is ascribed to radiative recombination between electrons in the s-p conduction-band below the Fermi level with the holes in the d bands. The observed enhancement is attributed to the localized surface plasmon resonance induced enhancement of the electric field of the incoming and outgoing radiation. Additionally, we show that phonon-phonon relaxation is faster in a more conductive medium such as ethylene glycol than in ethanol.

Acknowledgement

This work is supported by the Division of Material Research of the National Science Foundation (# 0138391) and the National Science Foundation-CNRS (# INT-0129263).

References

(1) El-Sayed, M. A. *Accounts of Chemical Research* **2001**, *34*, 257.

(2) Kreibig, U.; Vollmer, M. *Optical properties of metal clusters*; Springer: Berlin New York, 1995.

(3) Link, S.; El-Sayed, M. A. *Optical Properties and Ultrafast Dynamics of Metallic Nanocrystals* **2003**, *54*, 331.

(4) Bigot, J. Y.; Halte, V.; Merle, J. C.; Daunois, A. *Chemical Physics* **2000**, *251*, 181.

(5) Hodak, J. H.; Martini, I.; Hartland, G. V. *Journal of Physical Chemistry B* **1998**, *102*, 6958.

(6) Del Fatti, N.; Vallee, F.; Flytzanis, C.; Hamanaka, Y.; Nakamura, A. *Chemical Physics* **2000**, *251*, 215.

(7) Zhang, J. Z. *Accounts of Chemical Research* **1997**, *30*, 423.

(8) Qian, W.; Lin, L.; Deng, Y. J.; Xia, Z. J.; Zou, Y. H.; Wong, G. K. L. *Journal of Applied Physics* **2000**, *87*, 612.

(9) Huang, W. Y.; Qian, W.; El-Sayed, M. A. *Nano Letters* **2004**, *4*, 1741.

(10) Link, S.; El-Sayed, M. A. *Int. Reviews in Physical Chemistry* **2000**, *19*, 409.

(11) Qian, W.; Yan, H.; Wang, J. J.; Zou, Y. H.; Lin, L.; Wu, J. L. *Applied Physics Letters* **1999**, *74*, 1806.

(12) Qian, W.; Yan, H.; Wang, J. J.; Zou, Y. H.; Lin, L.; Wu, J. L. *Chinese Physics Letters* **1998**, *15*, 834.

(13) Bigot, J. Y.; Merle, J. C.; Cregut, O.; Daunois, A. *Physical Review Letters* **1995**, *75*, 4702.

(14) Tokizaki, T.; Nakamura, A.; Kaneko, S.; Uchida, K.; Omi, S.; Tanji, H.; Asahara, Y. *Applied Physics Letters* **1994**, *65*, 941.

(15) Roberti, T. W.; Smith, B. A.; Zhang, J. Z. *Journal of Chemical Physics* **1995**, *102*, 3860.

(16) Bosbach, J.; Hendrich, C.; Stietz, F.; Vartanyan, T.; Trager, F. *Physical Review Letters* **2002**, *89*.

(17) Voisin, C.; Christofilos, D.; Loukakos, P. A.; Del Fatti, N.; Vallee, F.; Lerme, J.; Gaudry, M.; Cottancin, E.; Pellarin, M.; Broyer, M. *Physical Review B* **2004**, *69*.

(18) Westcott, S. L.; Averitt, R. D.; Wolfgang, J. A.; Nordlander, P.; Halas, N. J. *Journal of Physical Chemistry B* **2001**, *105*, 9913.

(19) Bloemer, M. J.; Haus, J. W.; Ashley, P. R. *Journal of the Optical Society of America B-Optical Physics* **1990**, *7*, 790.

(20) Quinten, M.; Leitner, A.; Krenn, J. R.; Aussenegg, F. R. *Optics Letters* **1998**, *23*, 1331.

(21) Storhoff, J. J.; Elghanian, R.; Mucic, R. C.; Mirkin, C. A.; Letsinger, R. L. *Journal of the American Chemical Society* **1998**, *120*, 1959.

(22) Riboh, J. C.; Haes, A. J.; McFarland, A. D.; Yonzon, C. R.; Van Duyne, R. P. *Journal of Physical Chemistry B* **2003**, *107*, 1772.

(23) Schatz, G. C.; Van Duyne, R. P. Electromagnetic mechanism of surface enhanced spectroscopy. In *Handbook of Vibrational Spectroscopy*; Chalmers, J. M., Griffiths, P. R., Eds.; John Wiley & Sons Ltd: Chichester, 2002.

(24) Hao, E.; Schatz, G. C. *Journal of Chemical Physics* **2004**, *120*, 357.

(25) Coronado, E. A.; Schatz, G. C. *Journal of Chemical Physics* **2003**, *119*, 3926.

(26) Efros, A. L.; Rosen, M. *Annual Review of Materials Science* **2000**, *30*, 475.

(27) Salzemann, C.; Lisiecki, I.; Brioude, A.; Urban, J.; Pileni, M. P. *Journal of Physical Chemistry B* **2004**, *108*, 13242.

(28) Molina, R. A.; Weinmann, D.; Jalabert, R. A. *Physical Review B* **2002**, *65*.

(29) Nisoli, M.; Stagira, S.; DeSilvestri, S.; Stella, A.; Tognini, P.; Cheyssac, P.; Kofman, R. *Physical Review Letters* **1997**, *78*, 3575.

(30) Hodak, J. H.; Henglein, A.; Hartland, G. V. *Journal of Chemical Physics* **1999**, *111*, 8613.

(31) Del Fatti, N.; Flytzanis, C.; Vallee, F. *Applied Physics B-Lasers and Optics* **1999**, *68*, 433.

(32) Halte, V.; Bigot, J. Y.; Palpant, B.; Broyer, M.; Prevel, B.; Perez, A. *Applied Physics Letters* **1999**, *75*, 3799.

(33) Hodak, J. H.; Henglein, A.; Hartland, G. V. *Journal of Chemical Physics* **2000**, *112*, 5942.

(34) Elsayedali, H. E.; Norris, T. B.; Pessot, M. A.; Mourou, G. A. *Physical Review Letters* **1987**, *58*, 1212.

(35) Schoenlein, R. W.; Lin, W. Z.; Fujimoto, J. G.; Eesley, G. L. *Physical Review Letters* **1987**, *58*, 1680.

(36) Brorson, S. D.; Kazeroonian, A.; Moodera, J. S.; Face, D. W.; Cheng, T. K.; Ippen, E. P.; Dresselhaus, M. S.; Dresselhaus, G. *Physical Review Letters* **1990**, *64*, 2172.

(37) Groeneveld, R. H. M.; Sprik, R.; Lagendijk, A. *Physical Review B* **1995**, *51*, 11433.

(38) Sun, C. K.; Vallee, F.; Acioli, L. H.; Ippen, E. P.; Fujimoto, J. G. *Physical Review B* **1994**, *50*, 15337.

(39) Hodak, J.; Martini, I.; Hartland, G. V. *Chemical Physics Letters* **1998**, *284*, 135.

(40) Mohamed, M. B.; Ahmadi, T. S.; Link, S.; Braun, M.; El-Sayed, M. A. *Chemical Physics Letters* **2001**, *343*, 55.

(41) Link, S.; Burda, C.; Nikoobakht, B.; El-Sayed, M. A. *Journal of Physical Chemistry B* **2000**, *104*, 6152.

(42) Huttmann, G.; Birngruber, R. *Ieee Journal of Selected Topics in Quantum Electronics* **1999**, *5*, 954.

(43) Bardeen, J.; Cooper, L. N.; Schrieffer, J. R. *Physical Review* **1957**, *108*, 1175.

(44) Lanzara, A.; Bogdanov, P. V.; Zhou, X. J.; Kellar, S. A.; Feng, D. L.; Lu, E. D.; Yoshida, T.; Eisaki, H.; Fujimori, A.; Kishio, K.; Shimoyama, J. I.; Noda, T.; Uchida, S.; Hussain, Z.; Shen, Z. X. *Nature* **2001**, *412*, 510.

(45) Belotskii, E. D.; Tomchuk, P. M. *International Journal of Electronics* **1992**, *73*, 955.

(46) Belotskii, E. D.; Tomchuk, P. M. *Surface Science* **1990**, *239*, 143.

(47) Ahmadi, T. S.; Logunov, S. L.; ElSayed, M. A. *Journal of Physical Chemistry* **1996**, *100*, 8053.

(48) Logunov, S. L.; Ahmadi, T. S.; El-Sayed, M. A.; Khoury, J. T.; Whetten, R. L. *Journal of Physical Chemistry B* **1997**, *101*, 3713.

(49) Link, S.; Burda, C.; Wang, Z. L.; El-Sayed, M. A. *Journal of Chemical Physics* **1999**, *111*, 1255.

(50) Lisiecki, I.; Pileni, M. P. *Journal of the American Chemical Society* **1993**, *115*, 3887.

(51) Giuffrida, S.; Condorelli, G. G.; Costanzo, L. L.; Fragala, I. L.; Ventimiglia, G.; Vecchio, G. *Chemistry of Materials* **2004**, *16*, 1260.

(52) Lisiecki, I.; Billoudet, F.; Pileni, M. P. *Journal of Physical Chemistry* **1996**, *100*, 4160.

(53) Logunov, S. L.; Volkov, V. V.; Braun, M.; El-Sayed, M. A. *Proceedings of the National Academy of Sciences of the United States of America* **2001**, *98*, 8475.

(54) Schmuttenmaer, C. A.; Aeschlimann, M.; Elsayedali, H. E.; Miller, R. J. D.; Mantell, D. A.; Cao, J.; Gao, Y. *Physical Review B* **1994**, *50*, 8957.

(55) Tomchuk, P. M. *International Journal of Electronics* **1992**, *73*, 949.

(56) Qiu, T. Q.; Tien, C. L. *International Journal of Heat and Mass Transfer* **1992**, *35*, 719.

(57) *American Institute of Physics handbook*; 3rd ed. ed.; McGraw-Hill: New York, 1972.

(58) Kittel, C. *Introduction to solid state physics*, 6th ed. ed.; Wiley: New York, 1986.

(59) Theilmann, F.; Matzdorf, R.; Meister, G.; Goldmann, A. *Physical Review B* **1997**, *56*, 3632.

(60) Mooradian, A. *Physical Review Letters* **1969**, *22*, 185.

(61) Mohamed, M. B.; Volkov, V.; Link, S.; El-Sayed, M. A. *Chemical Physics Letters* **2000**, *317*, 517.

(62) Link, S.; Farube, A.; Mohamed, M.; Asahi, T.; Masuhara, H.; El-Sayed, M. J. Phys. Chem. B. **2000,** 106, 945.

CHAPTER VI

OBSERVATION OF OPTICAL GAIN IN SOLUTIONS OF CdS QUANTUM DOTS AT ROOM TEMPERATURE IN THE BLUE REGION †

Abstract

The optical gain dynamics has been studied for two CdS quantum dot samples dispersed in toluene at room temperature. This was carried out by using femtosecond transient absorption technique with an excitation at 400 nm and gain measurement was studied at the fluorescence maxima (440 nm and 460 nm). The optical gain lifetime was found to be as long as 20 picoseconds under pump fluence as low as 0.77 mJ/cm^2. The low threshold is the result of long lifetime of electrons and holes and narrow emission band width. These results suggest that CdS quantum dots in solution are excellent gain media for optically pumped high power blue lasers.

† Qusai Darugar, Wei Qian, Mostafa A. El-Sayed; Applied Physics Letters, **2006,** 88, 26 (26 Jun 2006)

Introduction

Semiconductor nanocrystal quantum dots (QDs) have attracted great attention due to their tunable electronic and optical properties arising from three-dimensional quantum confinement effects (1-3). The advantages of using semiconductor QDs in the strong confinement regime as gain media in lasing devices (due to their predicted reduced lasing threshold and improved temperature stability (4,5)) are the driving forces in the development of semiconductor QDs based lasers. A large amount of study has been devoted to optical gain and amplified spontaneous emission (ASE) in semiconductor nanocrystals (6-12). Most of them are in the visible range with wavelengths longer than 500 nm using CdSe (6-10) (540-680 nm) and in the near-infrared range using PbSe (1425-1625 nm)(12) or InAs (1570 nm)(11). Furthermore, all the observations of optical gain and ASE in quantum dots were from self-assembled close-packed QD films or QDs in solid matrices but none were in the solution. For high power lasers, liquids are advantageous for heat circulator and dissipation.

As a direct wide band gap semiconductor, CdS nanocrystal QD is an excellent candidate for realizing optical gain and ASE in blue range. Optical gain in sol-gel derived CdS nanocrystal QDs embedded in glass matrices pumped by intense nanosecond laser pulses was observed at low temperature (below 170 K) by Butty et al. in 1995 (13). With the advances in incorporating QDs into host

matrices, Bawendi et al. (14) have recently observed lasing in the blue region from core-shell CdS/ZnS nanocrystals stabilized in a sol-gel derived silica matrix pumped by 100 fs laser pulses at 400 nm. However, up to now, optical gain dynamics and measurement of optical gain lifetime have not been reported for CdS QDs and certainly not for the solution of CdS QDs at room temperature. In the present work, we present experimental results of optical gain dynamics in the strongly confined CdS QDs dissolved in toluene solution at room temperature using femtoseocnd transient absorption technique. Because of the long lifetime of electrons and holes and narrow fluorescence band width, one can observe gain with a low threshold in the solution of CdS QDs at room temperature.

Experimental

CdS nanocrystal QDs were prepared by using a method similar to the one used by Bawendi et al. (15) and modified by Peng et al. (16) Instead of using more common sulfur and tri-n-octylphosphine (TOP) complex, we used bis(trimethylsilyl)sulfide [$(TMS)_2S$]. In a typical synthesis, 0.2 g CdO (Sigma) was mixed with 3 g tri-n-octylphosphine oxide (TOPO), 1 g stearic acid and heated to 280 ˚C. Once the solution in the flask became optically clear, 0.5 ml of $(TMS)_2S$ was rapidly added. The solution turned yellow immediately and the growth of CdS nanocystal QDs was monitored by using a Shimadzu UV-3101-PC spectrophotometer. The size and morphology of the nanoparticles were examined using a JEOL 100CX II transmission electron microscope (TEM).

Nanosecond time-resolved photoluminescence decay was measured using PTI model C-72 fluorescence lifetime spectrometer. The CdS QDs solution was excited by laser pulses (0.8 ns, 10 Hz) at 337 nm generated from a PTI-GL-3300 nitrogen and the photoluminescence was detected using a switchable analog/photon counting photomultiplier tube and was fitted to biexponential decay.

The optical gain measurements at room temperature were performed using a femtosecond transient absorption technique, which has been described elsewhere (17). 100 fs laser pulses at 400 nm and femtosecond white light continuum ranging from 400 nm to 1100 nm with 1 kHz repetition rate were used as pump and probe light, respectively. The pump and probe beams were focused and overlapped at the sample with a diameter of about 250 μm. The time delays between them were controlled by optical delay line with a resolution of 3 um (20 fs).

Results and Discussion

In order to investigate the effects of sample quality on optical gain properties, two samples were prepared with different initial Cd:S ratio of the precursors. Using initial ratio of Cd:S to control the final quality of CdS QDs is motivated by the work of Peng et al. (18). In their work, (18) they demonstrated that with Se precursor initially in excess, which provides relatively stable environment during the surface optimization/reconstruction process, CdSe nanocrystals could be synthesized with high lattice quality. Using the same logic, we used biased amount of S precursor to make two samples for our studies. Sample 1 and 2 were prepared under excess Cd and S precursor, respectively. As shown in the following, these two samples have different quality, indicated by their photoluminescence (PL) quantum yields (QYs). The absorption and PL spectra of sample 1 (blue lines) and sample 2 (red lines) are presented in figure 6-1a. Due to the strong quantum confinement, the first absorption maxima is blue shifted from the bulk CdS absorption edge at 500 nm to 420 nm for sample 1 and to 440 nm for sample 2. The average sizes of CdS QDs estimated from the wavelengths of the first absorption maxima using empirical equation in Peng's paper (19) are about 4.0 nm and 4.8 nm for sample 1 and sample 2, respectively. The real size of sample 1 was also directly measured from its TEM image (inset to figure 6-1a) and gave an average diameter of 3.8 nm, close to the estimation. The PL spectra (figure 6-1a) show two emission bands. The peaks in the blue region at 440 nm for sample 1 and at 460 nm for sample 2 are from band edge

emission. The linewidth of band edge emission is pretty narrow, approximate 28 nm (FWHM). The narrow emission helps to decrease optical gain threshold in two ways. First the shape band edge emission indicates a narrow size-distribution so the percentage of the QDs in the subgroup of an ensemble of QDs, which contribute to optical gain measurement, is higher compared to sample with broad size-distribution. Second, the fluorescence resonance energy transfer within QDs serving as a channel for losing absorbed optical energy will be inhibited further due to narrow size distribution and emission band. Beside the sharp band edge emission, there are broad emission bands on the red side from 500 nm to 700 nm. These are assigned to deep trap emissions. The intensity of the deep trap emission is used to characterize the quality of sample because it results from the nonradiative electron and hole losses to the defects and impurities on the surface and/or within the QDs. The PL QYs of the band edge (deep trap) emission were 20% (30%) and 32% (12%) for sample 1 and sample 2, respectively by comparing the integrated PL intensities of the QDs to the well-characterized dye (Coumarin 460). It is obvious that sample 2 is of better quality than sample 1. As it is shown below, the bandedge emission has a long lifetime and suggests that the trap emission is populated from higher excited states. Figure 6-1b shows the photoluminescence decay of the two samples. The signal is fitted to a biexponential decay with time constants (amplitudes) of 2.7 ns (0.55) and 41 ns (0.45) for sample 1 and 2.5 ns (0.42) and 52 ns (0.58) for sample 2. The faster decay component of 2.7 (2.5) ns is due to the nonradiative loss of electrons and holes to the defects and/or impurities and the 41 (52) ns decay

component is the lifetime of e-h pairs at the band gap states (20). The lifetime is much longer than that observed for CdSe QDs of similar size (about 20 ns) (21).

Femotsecond transient absorption experiments have been used extensively to study the dynamical processes of optical gain in semiconductor QDs (6-8, 11, 13). In these experiments, one monitors the change of absorption of the sample before and after excitation. If the absorbance before and after the irradiation is α_0 and α, respectively, then optical gain is achieved when the pump-induced absorption bleach (negative absorption or transmission) $-\Delta\alpha = -(\alpha - \alpha_0)$ is greater than α_0 (or $-\Delta\alpha / \alpha_0$ is > 1) (6-8). Due to the overlap of the intense pump-induced absorption with the PL band, experiments with CdSe QDs solution (6) showed photoinduced absorption rather than bleach within the PL band. Numerous experiments have confirmed that the optical gain and ASE could only be observed in CdSe close-packed QD films and QD-polymer matrices due to the absence of pump-induced absorption and high QD loading fraction (6-9). However, as shown in the following figures, there is no pump-induced absorption (or the pump-induced absorption is very weak) within the PL band in the CdS QD solution. As a result, optical gain is directly observed at their PL peaks. It is worth to mention that one possible reason for the observable optical gain in CdS QDs solution is that the pump wavelength (400 nm) is close to the emission wavelength (440 nm or 460 nm), which can eliminate the loss of electron-hole pairs due to trapping of defects. As shown by Banin et al., (22) lasing has been achieved from the hexane solution of CdSe nanocrystals in the microcavity as

pump laser wavelength is set close to the band gap. In addition, Link et al. (8) from our group has also proved that by moving the excitation laser wavelength closer to band gap, the optical gain could be observed in CdSe nanorods solution.

Figure 6-2(a) and (b) present normalized transient absorption changes $-\Delta\alpha/\alpha_0$ as a function of time delay between the pump laser with different fluence and the probe laser. The probe laser wavelength was set at 440 nm and 460 nm for samples 1 and 2, respectively (the peak maxima of their PL spectra). Figure 6-2(c) shows the pump intensity dependence of the normalized absorption changes ($-\Delta\alpha/\alpha_0$) at a delay time of 6 ps. For both samples, we found that $-\Delta\alpha/\alpha_0$ could be greater than 1 (corresponding to optical gain). The thresholds of pump fluence ($-\Delta\alpha/\alpha_0 = 1$) for achieving optical gain are 2.24 mJ/cm^2 and 0.57 mJ/cm^2 for sample 1 and 2, respectively. Klimov et al. (6) have found that the gain threshold of QDs scales roughly as $1/R^3$ (R is the size of QDs). Based on their results, the threshold of sample 1 will be only 70 % higher than that of sample 2. However, here the gain threshold of sample 1 is nearly four times (or 300% higher) as high as that of sample 2. We believe this reflects the effects of sample quality on the optical gain threshold.

The band edge emission in II-VI semiconductor QDs is modeled as a two-level system with twofold spin-degenerate states (6-23). The complete bleach of the band gap absorption (corresponding to gain threshold) occurs at the minimum

carrier density of $N_{eh} = 1$ (N_{eh} is the number of e-h pairs per dot on average). The optical gain at the band edge emission is due to the transitions from the quantum-confined biexciton states to exciton states (6, 7, 10, 23). In the sample with poor quality, there are many defects and impurities on the surfaces of the QDs, such as the unpassivated Se or S lone pair sites in the case of CdSe and CdS. Experimental studies (7, 24, 25) showed that the holes could be trapped nonradiatively to these surface defects on the subpicosecond to picosecond time scale. This is faster than Auger recombination (several tens of picoseconds), (26) and sets the limit for optical gain threshold. In order to observe optical gain, the excited carrier density of e-h pairs N_{eh} needs to be well above 1 so that after saturating the surface defects, the biexciton-to-exciton transition can still occur. This explains that optical gain threshold depends on the sample quality.

The lifetime of optical gain under pump fluence higher than the threshold could be obtained from figure 6-2(a) and (b). The decay of optical gain is determined by two competitive processes, intrinsic multiparticle Auger recombination and nonintrinsic ultrafst hole trapping by surface defects (6,7) For sample 2, under moderate pump fluence (0.77 mJ/cm^2), it took 20 ps (corresponding to an effective amplification length about 6 mm) for ($-\Delta\alpha / \alpha_0$) to decay to 1 (optical gain threshold) at room temperature. The 20 ps optical gain lifetime observed for CdS QDs, which is related to the Auger recombination in CdS QDs, is longer as compared with close-packed CdSe QDs film which is less than 10 ps (7) even under higher pump fluence of 1.6 mJ/cm^2. The fact that CdS QDs show gain in

solution at relative lower pump fluence at room temperature, in spite of similar overlap between the emission maximum and the absorption bandedge spectrum as in CdSe, is due to the observed longer lifetimes of fluorescence and biexciton-to-exciton transitions and narrow fluorescence band width. This leads to the formation of the biexciton critical density (needed to achieve population inversion) at lower laser pump fluence.

Conclusion

We have observed optical gain in CdS nanocrystal QDs in strong confinement regime in toluene solution at room temperature using femtosecond transient absorption techniques. The optical gain dynamics of CdS QDs is sample quality dependent, due to the ultrafast hole trapping processes by the defects. The optical gain lifetime is measured to be 20 picoseconds under pump fluence of 0.77 mJ/cm^2. The relative lower gain threshold compared to that of CdSe QDs is attributed to the long lifetime of fluorescence and biexcitons and the relatively sharp PL linewidth. Our results indicate that CdS nanocrystals are excellent gain media for semiconductor QD based blue lasers.

Acknowledgments

This work was supported by DMR of the National Science Foundation (grant DMR-0527297) for financial support.

References

(1) Alivisatos, A. P. *Science* **1996**, 271, 933.

(2) Norris, D. J.; Bawendi, M. G. *Phys. Rev. B* **1996**, 53, 16338.

(3) Efros, A. L.; Rosen, M. *Annual Review of Materials Science* **2000**, 30, 475.

(4) Arakawa, Y.; Sakaki, H. *Appl. Phys. Lett.* **1982**, 40, 939.

(5) Asada, M.; Miyamoto, Y.; Suematsu, Y. Ieee *Journal of Quantum Electronics* **1986**, 22, 1915.

(6) Klimov, V. I.; Mikhailovsky, A. A.; Xu, S.; Malko, A.; Hollingsworth, J. A.; Leatherdale, C. A.; Eisler, H. J.; Bawendi, M. G. *Science* **2000**, 290, 314.

(7) Mikhailovsky, A. A.; Malko, A. V.; Hollingsworth, J. A.; Bawendi, M. G.; Klimov, V. I. *Appl. Phys. Lett.* **2002**, 80, 2380.

(8) Link, S.; El-Sayed, M. A. *J. Appl. Phys.* **2002**, 92, 6799.

(9) Sundar, V. C.; Eisler, H. J.; Bawendi, M. G. *Adv. Mater.* **2002**, 14, 739.

(10) Chan, Y.; Caruge, J. M.; Snee, P. T.; Bawendi, M. G. *Appl. Phy. Lett.* **2004**, 85, 2460.

(11) Chen, G.; Rapaport, R.; Fuchs, D. T.; Lucas, L.; Lovinger, A. J.; Vilan, S.; Aharoni, A.; Banin, U. *Appl. Phy. Lett.* **2005**, 87, 251108.

(12) Schaller, R. D.; Petruska, M. A.; Klimov, V. I. *J. Phys. Chem. B* **2003**, 107, 13765.

(13) Butty, J.; Hu, Y. Z.; Peyghambarian, N.; Kao, Y. H.; Mackenzie, J. D. *Appl. Phys. Lett.* **1995**, 67, 2672.

(14) Chan, Y.; Steckel, J. S.; Snee, P. T.; Caruge, J. M.; Hodgkiss, J. M.; Nocera, D. G.; Bawendi, M. G. *Appl. Phy. Lett.* **2005**, 86, 073102.

(15) Murray, C. B.; Norris, D. J.; Bawendi, M. G. *J. Am. Chem. Soc* **1993**, 115, 8706.

(16) Peng, Z. A.; Peng, X. G. *J. Am. Chem. Soc.* **2001**, 123, 183.

(17) Huang, W. Y.; Qian, W.; El-Sayed, M. A. *Nano Letters* **2004**, 4, 1741.

(18) Zhang, J. Y.; Wang, X. Y.; Xiao, M.; Qu, L.; Peng, X. *Appl. Phys. Lett.* **2002**, 81, 2076.

(19) Yu, W. W.; Qu, L. H.; Guo, W. Z.; Peng, X. G. *Chem. Mater.* **2003**, 15, 2854.

(20) Wu, F.; Zhang, J. Z.; Kho, R.; Mehra, R. K. *Chem. Phys. Lett.* **2000**, 330, 237.

(21) Crooker, S. A.; Hollingsworth, J. A.; Tretiak, S.; Klimov, V. I. *Phys. Rev. Lett.* **2002**, 89.

(22) Kazes, M.; Lewis, D. Y.; Ebenstein, Y.; Mokari, T.; Banin, U. *Adv. Mater.* **2002**, 14, 317.

(23) Hu, Y. Z.; Giessen, H.; Peyghambarian, N.; Koch, S. W. *Phys. Rev. B.* **1996**, 53, 4814.

(24) Klimov, V. I.; Schwarz, C. J.; McBranch, D. W.; Leatherdale, C. A.; Bawendi, M. G. **Physical Review B 1999**, 60, R2177.

(25) Underwood, D. F.; Kippeny, T.; Rosenthal, S. *J. Journal of Physical Chemistry B* **2001**, 105, 436.

(26) Klimov, V. I.; Mikhailovsky, A. A.; McBranch, D. W.; Leatherdale, C. A.; Bawendi, M. G. Science 2000, 287, 1011.

Figure captions;

Figure 6-1: (a) Absorption and photoluminescence (PL) spectra of sample 1 (blue lines) and sample 2 (red lines). Inset: TEM image of sample 1 shows an average diameters of about 3.8 nm, which is much smaller than the bulk exciton Bohr radius of CdS (2.8 nm). In addition to intense sharp band gap emission peaks, there are deep trap emission bands ranging from 500 nm to 700 nm caused by nonradiative electron and hole losses to the defects and impurities on the surface and/or within the QDs. (b) Photoluminescence decay of sample 1 (blue line) and sample 2 (red line). The signal is fitted by biexponential decay with time constants (amplitudes) of 2.7 ns (0.55) and 41 ns (0.45) for sample 1 and 2.5 ns (0.42) and 52 ns (0.58) for sample 2.

Figure6-2: (a) and (b) present normalized transient absorption changes $-\Delta\alpha/\alpha_0$ of samples 1 and 2 as function of time delay induced by 400 nm femtosecond laser at different pump fluence. The probe wavelength was set to their PL peaks, 440 nm and 460 nm for sample 1 and 2, respectively. Under moderate pump fluence (0.8 mJ/cm^2), the optical gain lifetime is determined to be as long as 20 ps at room temperature, corresponding to effective amplification length of about 6 mm. (c) Shows pump intensity dependence of the normalized absorption changes ($-\Delta\alpha/\alpha_0$) at a time delay of 6 ps. The pump fluence thresholds of optical gain are 2.24 mJ/cm^2 and 0.57 mJ/cm^2 for sample 1 and 2, respectively.

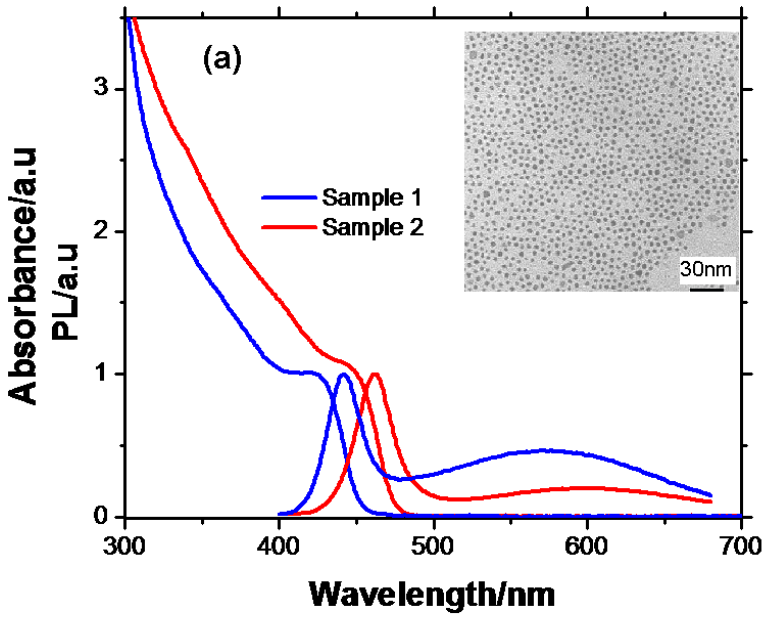
(a)
Sample 1
Sample 2
30nm
Absorbance/a.u
PL/a.u
Wavelength/nm
0
1
2
3
300
400
500
600
700

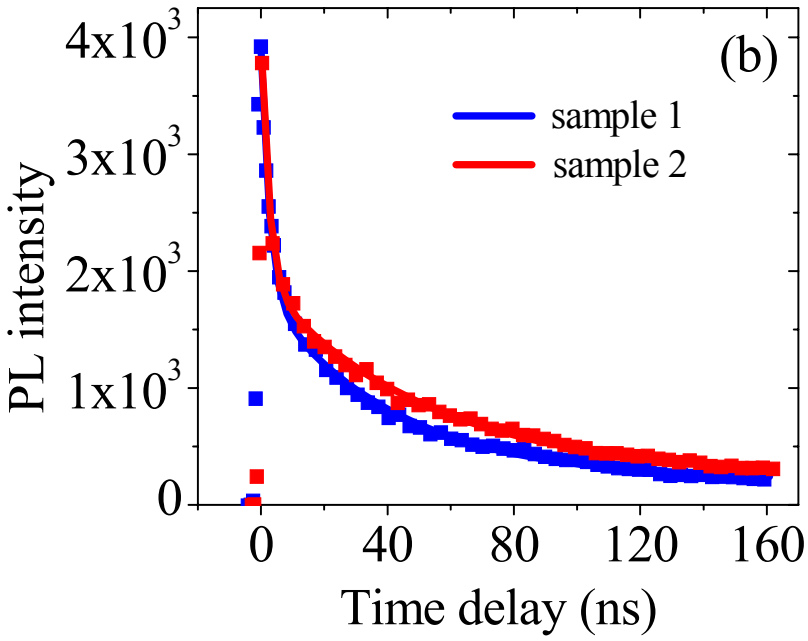
(b)
sample 1
sample 2
PL intensity
Time delay (ns)
0
1x10^3
2x10^3
3x10^3
4x10^3
0
40
80
120
160

Figure 6-1

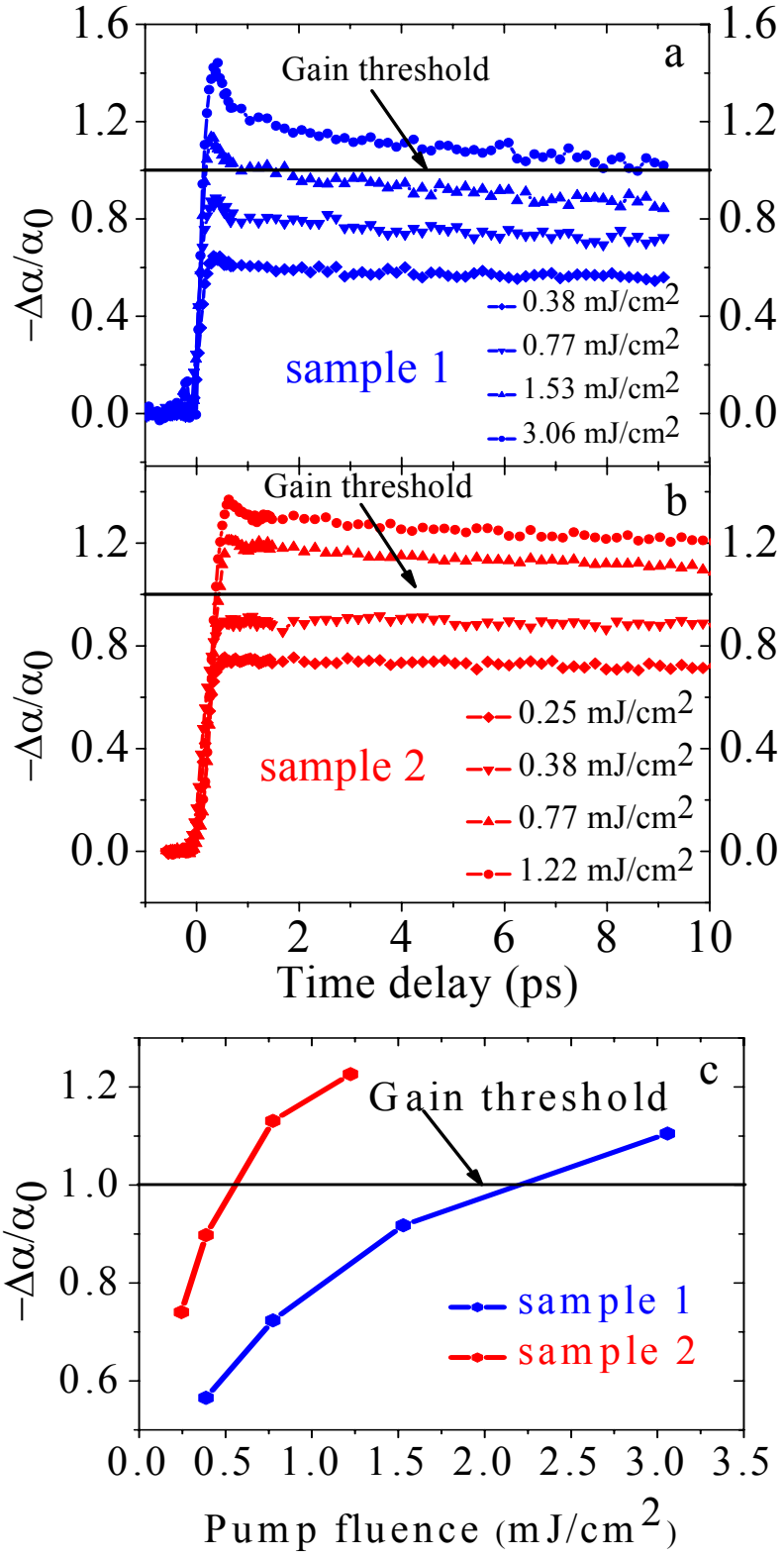
a
Gain threshold
sample 1
0.38 mJ/cm2
0.77 mJ/cm2
1.53 mJ/cm2
3.06 mJ/cm2
b
Gain threshold
sample 2
0.25 mJ/cm2
0.38 mJ/cm2
0.77 mJ/cm2
1.22 mJ/cm2
−Δα/α0
Time delay (ps)
c
Gain threshold
sample 1
sample 2
−Δα/α0
Pump fluence (mJ/cm2)

Figure 6-2

Chapter VII

Concentration Dependent Relaxation Dynamics of Hot Electrons in Colloidal CdSe Nanoparticles at room Temperature

Abstract

The concentration dependent relaxation of hot electrons in colloidal CdSe nanoparticles is followed by monitoring the 1S state rise time of the transient bleaching signal induced by excitation at 400 nm. It is found that the rise time of the 1S state (or the relaxation time of the hot electrons) depends on the concentration of the CdSe nanoparticles. A Förster resonance energy transfer mechanism was initially suggested, but the calculated interparticle distance of ~500 Å seemed very large for such process to occur. Therefore, the nature of the particles in solution (aggregates) could lead to the rise time dependence of rise time on concentration. An alternate mechanism of multiparticle (cluster) interaction is thus proposed such dependence. Additionally, Auger type ionization as a relaxation mechanism is also considered.

Introduction:

In the late 1940's, Förster proposed a theory (1) based on transition dipole-dipole interaction for describing long-range resonance energy transfer. He derived a transfer rate equation that relates the transfer rate to the sixth power of the donor–acceptor distance and the spectroscopic overlap integral between the normalized donor emission and the acceptor absorption line shape. Förster resonance energy transfer (FRET) has been studied for many years because of its essential role in various research fields, such as fluorescence quenching, radiation physics and chemistry, photosynthesis, and photobiology (2). In addition, FRET has become a standard spectroscopic technique for measuring distances in biological systems on the 10 to 100Å range. FRET between semiconductor nanoparticles within an inhomogeneous distribution. This results in fluorescence quenching of the smaller nanoparticles and enhancement of fluorescence of the larger nanoparticles have also been studied (3-5). The size-dependent optical and electrical properties as well as the strong and narrow emission of semiconductor nanoparticles are well known (6, 7). For this reason the direction and rate of the nonradiative FRET Förster resonance energy transfer between semiconductor nanoparticles is controllable via the control of extent of the separation of donor-acceptor and spectral overlap (8,9). Semiconductor nanoparticle-based artificial analogs of biological light-harvesting complexes have been designed to serve as a platform for studying complicated photosynthesis processes (10). Nanoscale biosensors have been developed

using energy transfer between semiconductor nanoparticle donors and functionalized acceptor biomolecules (11, 12). The spatial resolution of scanning probe microscopy has been improved using resonance energy transfer in its principle operation (13).

Recently, a very interesting idea has been theoretically proposed of using energy transfer between semiconductor nanoparticles to perform universal quantum logic steps and generate quantum entanglement (14). Due to the great significance for both fundamental studies and the practical applications given above, FRET between semiconductor nanoparticles received intense experimental and theoretical research in the past decade (3-5, 8-12).

The semiconductor samples that were used in our experiments for observing concentration dependent electron dynamics is colloidal CdSe nanoparticle. Numerous theoretical and experimental studies (6, 7, 15-20) have greatly improved our understanding of the electronic structure and optical properties of CdSe nanoparticles. A number of groups, including our own, have been interested in understanding the mechanisms (25, 29, 38, 39, 48) of cooling hot electrons (those that are excited to higher energy levels above the band gap excitations).

The exciton Bohr radius of bulk CdSe is 5.2 nm, thus CdSe nanoparticles of smaller sizes have discrete electron and hole energy levels. The three lowest

excited state electron energy levels (21) in the order of increasing energy are 1S, 1P, and 1D, and the three lowest hole energy levels in the order of increasing energy are $1S_{3/2}$, $1P_{3/2}$, and $2S_{3/2}$. The lowest state (band gap) in the linear absorption spectra of CdSe nanoparticles is assigned to the transition involving the lowest electron state (1S(e)) and the lowest hole state ($1S_{3/2}$(h)).

Because the spacing between the two lowest electron energy levels of semiconductors nanoparticle is around several hundred millielectronvolts and is much larger than the single longitudinal optical (LO) phonon energy of semiconductor (~ 300 cm^{-1}), the relaxation of hot electrons in semiconductor nanoparticles can not occur via a single LO phonon process and may require tens of LO phonons. Thus it is expected to be very slow and is known as a "phonon bottleneck" (22). Due to the "phonon bottleneck" effect, very slow thermalization process of hot electrons in semiconductor nanoparticles is predicted (23, 24). Contrary to this prediction, a large number of ultrafast spectroscopy experiments, including femtosecond transient absorption in the visible and infrared spectral ranges, (25-29.38) femtosecond fluorescence upconversion (30,31), and femtosecond photon-echo (32,33), demonstrated that in both III-V and II-VI semiconductor nanoparticles, the relaxation of hot electrons is extremely rapid (on the subpico-to-picosecond time scale), comparable to large molecules (34). This indicates the occurrence of other mechanisms that bypass the "phonon bottleneck". Several mechanisms have been proposed in the literature for the relaxation of hot electrons in semiconductor nanoparticles.

These include an interaction with defects (35), Coulomb scattering of the electron-hole plasma (36), coupling between electron and hole in an Auger-like relaxation process (37), and hot electrons trapped or relaxed by coupling with surface molecules or defects (38, 39).

In the present work, we examine the relaxation of hot electrons in CdSe nanoparticles from the excited states to the lowest electronic state (1S) as a function of particle concentration by monitoring the rise time of the transient absorption signal from the 1S state. It is found that such a relaxation occurs at a concentration as low as 10^{-5} M (with an average calculated particle distance of 500 Å). This efficient quenching is discussed in terms of Förster type energy transfer. However this distance is too long for such an energy transfer to occur and therefore an alternate mechanism is suggested and experimentally tested based on quenching within aggregates formed even at very low concentrations.

Experimental:

Colloidal CdSe nanoparticles passivated with molecules of tri-n-octylphrosphine oxide (TOPO) and dissolved in toluene were prepared using the method introduced by Murray et al. and modified by Peng et al. (40). In a typical synthesis, 5 g of TOPO is preheated to 300 $^{\circ}$C with about 0.2 g CdO. After the solution becomes optically clear, 0.15 g Se dissolved in 3 ml trioctylphosphine (TOP, Aldrich) is quickly injected in to the hot solution of TOPO/Cd. CdSe

nanoparticles are instantaneously formed and the reaction flask is heated until the desired particle size is obtained. Growth of the nanoparticles is monitored by measuring the absorption of the aliquot during the synthesis. A typical linear absorption spectrum of our sample is shown in Figure 7.1

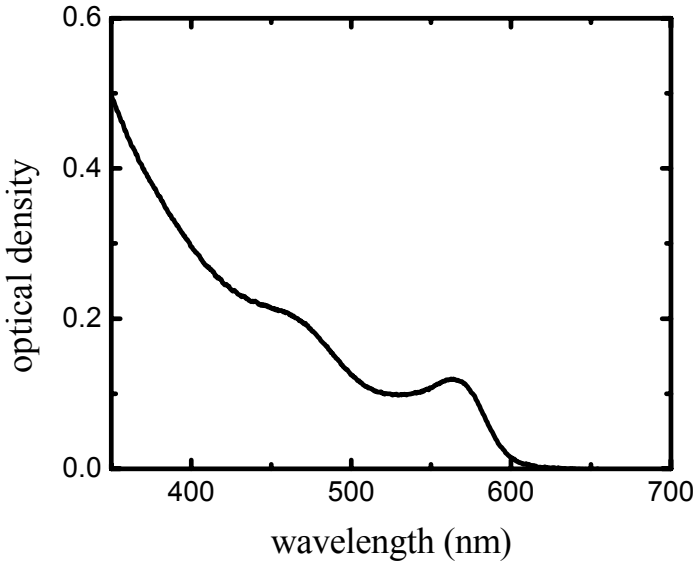

.

Figure 7.1: Typical linear absorption spectrum of TOPO-passivated CdSe nanoparticles. The two absorption peaks at 565 nm and 460 nm are due to the transitions to ($1S_{3/2}$(h); 1S(e)) and to ($1P_{3/2}$(h); 1P(e)) states, respectively.

Two absorption peaks at 565 nm and 460 nm are assigned to 1S ($1S_{3/2}$(h)-1S(e)) and 1P ($1P_{3/2}$(h)-1P(e)) transitions, respectively. The sizes were examined by using a JEOL 100CX II transmission electron microscope (TEM) operating at 100 kV in order to obtain information on the size. TEM images show that our CdSe nanoparticles have a mean diameter of 3.4 nm with 8% size dispersion. Empirical

functions (3) and (7) in reference 41 could be used for determination of the size dependent extinction coefficient of CdSe nanoparticles. For our 3.4 nm CdSe nanoparticles, the extinction coefficient is about 1.50×10^5 $cm^{-1}M^{-1}$ at 565 nm. A total of seven CdSe nanoparticle solutions (S1-S7) in order of increasing concentration were prepared and used in the experiments. The optical densities of S1-S7 at the first absorption peak (565 nm) are 0.0416, 0.118, 0.244, 0.305, 0.469, 0.581, and 0.738, respectively. Further, the concentration of these samples can be calculated using the extinction coefficient (1.50×10^5 $cm^{-1}M^{-1}$) of CdSe nanoparticles at 565 nm (41). The concentration of S1-S7 are 2.04×10^{-6} M, 5.80×10^{-6} M, 1.20×10^{-5} M, 1.50×10^{-5} M, 2.30×10^{-5} M, 2.85×10^{-5} M, and 3.63×10^{-5} M, respectively.

The femtosecond pump-probe experimental setup for monitoring carrier-induced absorption changes was described in previous paper (42). Briefly, an amplified Ti-sapphire laser system (Clark MXR CPA 1000) was pumped by a ND-YVO ring loss (Coherent Verdi 5 W) laser. This produced 1 kHz laser pulses of 100 fs duration (fwhm) and an energy of 1 mJ at 800 nm. A white light continuum used as probe light is generated by focusing a small part (4%) of the fundamental into a 1 mm sapphire plate. The pump (or excitation) light is produced by second harmonic generation (400 nm) and was modulated by an optical chopper (HMS 221), which is synchronized to the laser pulses and yields an excitation frequency of 500 Hz. The probe light is split into a signal and reference beam. After passing the monochromator (Acton Research), both beams are detected by

two matched photodiodes (Thorlab). The kinetic traces are obtained using a boxcar and lock-in-amplifier referenced to the 500 Hz frequency pump beam chopper.

After the carriers in CdSe nanoparticles are excited to states higher than the exciton ground state, it is apparent that the rise time of the exciton ground state is determined by the intraband relaxation rate from upper electronic states. Indeed, Klimov et al. (43, 44) have demonstrated experimentally that the growth of the 1S transition is complementary to the decay of the 1P transition. In our experiment, the relaxation processes of hot electrons in S1-S7 are tracked by monitoring the rise of transient bleaching signal probed at the 1S state (band gap) with excitation at 400 nm. The pump fluence is ~25 $\mu j/cm^2$, corresponding to the excitation of 0.1 exciton or less per CdSe nanoparticle (44). The use of low pump intensities allowed us to avoid intraparticle exciton-exciton interaction. The transient bleaching signal from the sample with the lowest concentration (S1) can let us extract the pure interparticle distance dependent hot electron relaxation rate. All the experiments are performed at room temperature.

Results and Discussion:

In figure 7.2 (a)-(g), we present the rise time curves of the transient bleaching signal (black squares) of the band gap absorption at 565 nm when the samples are excited at 400 nm as the nanoparticle concentration increases.

The experimental data can be simulated very well (solid lines in figure 7.2) by convoluting an exponential function with a cross correlation between excitation pulses and probe pulses. In order to clearly show the concentration dependence of the rise time of the 1S state, figure 7.3 shows a comparison of the rise curves of the transient bleaching signal. The rise times of transient bleaching signal of S1-S7, determined from theoretical simulation, are 498 fs, 487 fs, 437 fs, 420 fs, 360 fs, 316 fs, and 266 fs, respectively.

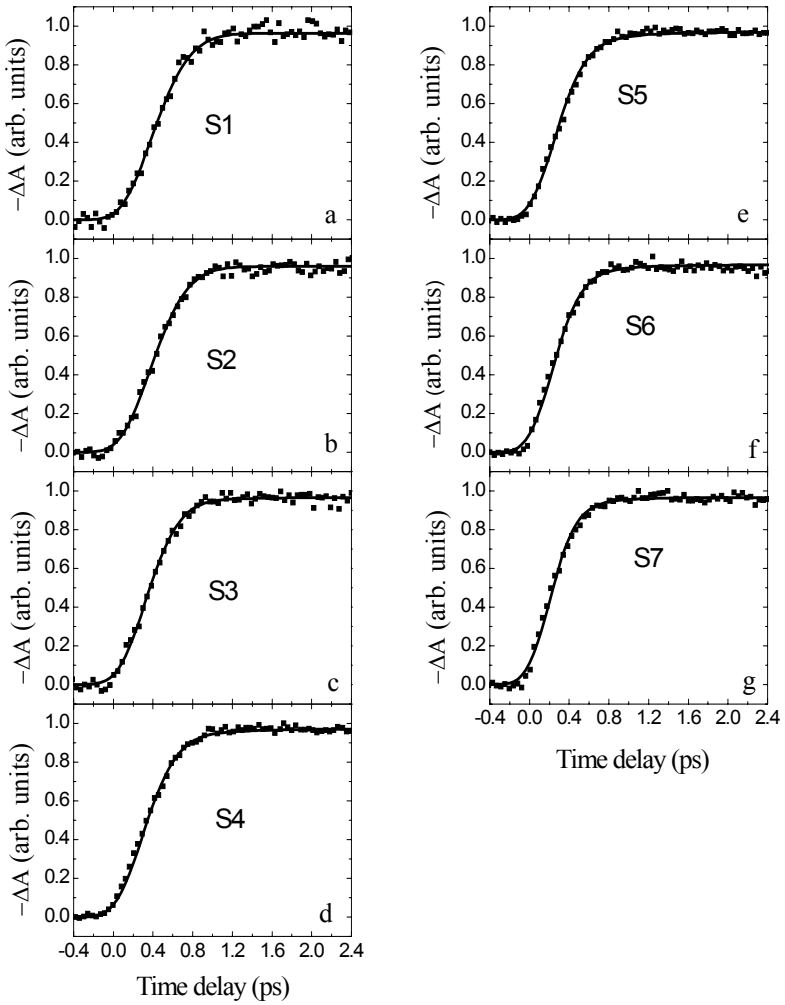

Figure 7.2 (a)-(g): The rise time curves of transient bleaching signal (black squares) at the band gap absorption at 565 nm, with excitation at 400 nm and as a function of concentration. The experimental data can be fitted (solid lines) by convoluting exponential function with a cross correlation between excitation pulses and probe pulses.

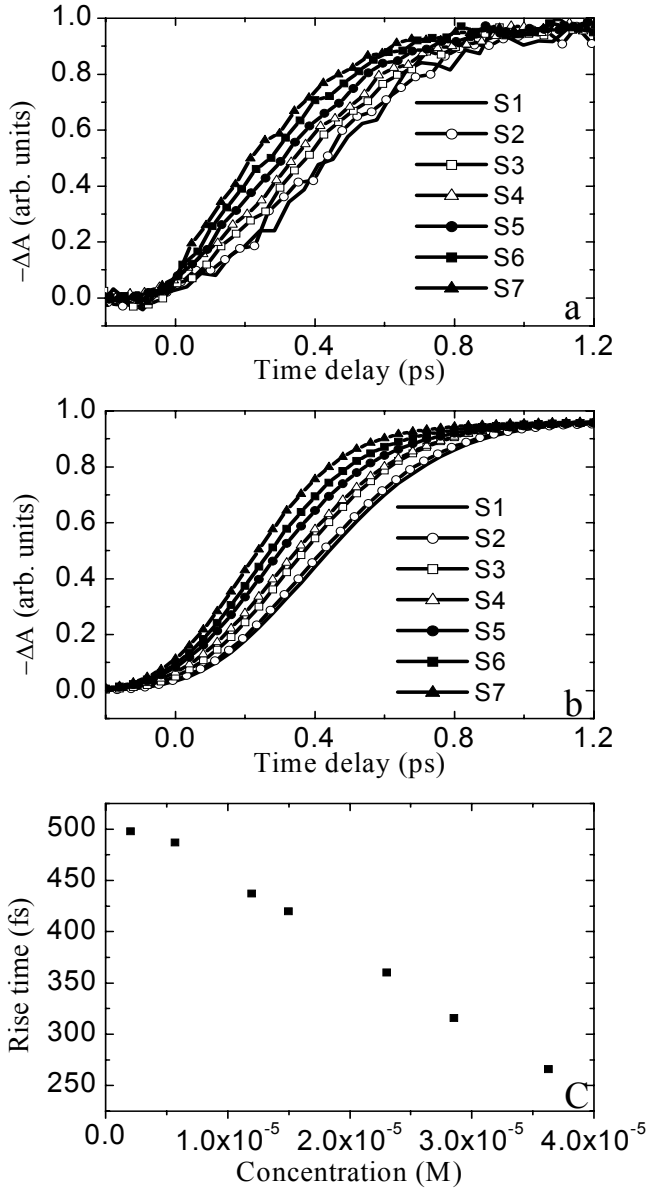

Figure 7.3 (a)-(c): Comparison of the observed concentration dependence of the rise curves of transient bleaching signal of S1 (solid line), S2 (line+open circles), S3 (line+open squares), S4 (line+open triangles), S5 (line+solid circles), S6 (line+solid squares), and S7 (line+solid triangles). (a) Comparison of actual experimental signal. (b) Comparison of simulation. (c) Concentration dependent rise time of 1S state. We find that as the concentration increases, the relaxation of hot electrons to the 1S state becomes faster. This indicates that the presence of interparticle coupling results in the relaxation of the hot electrons. Figure (c)

also shows that the experimental curve of concentration dependent rise time starts to saturate with nanoparticles concentration below 1.0×10^{-5} M. This indicates that with nanoparticles concentration below 1.0×10^{-5} M the relaxation of hot electrons mainly occurs via intrinsic intraparticle nonradiative relaxation processes and the contribution from energy transfer between nanoparticles is very little.

Possible aggregation effect on the relaxation of hot electrons:

It has been shown that Förster resonance energy transfer can occur in close-packed CdSe nanoparticle films (8-10) where the interparticle average distance is about 50 Å. However, we find it very surprising to see an inverse dependence of relaxation of hot electrons on nanoparticle concentration in CdSe nanoparticle solution, where the interparticle average distance is about 500 Å. Distances of 500 Å seem too long for energy transfer between the CdSe nanoparticles and suggest that CdSe nanoparticles in solutions may not be isolated as assumed and clusters may exist that influences the rise time. For this reason, other possible mechanisms for concentration dependent rise time of the 1S state should be realized.

As the CdSe nanoparticle concentration is increased (keeping the volume same) the number of clusters will also increase per volume of the sample used. To study the effect of clusters on the rise time of the 1S bleach signal, we added a drop of ethanol to the CdSe nanoparticle solution. Alcohol is used to aggregate CdSe nanoparticles from excess TOPO during the washing process (40). Also,

CdSe were incorporated into a polymer film since this would also form a high concentration of close packed particles on the substrates.

The rise time of the transient absorption spectra for the CdSe film and of the sample with a drop of alcohol are shown in figures 7.4. It can be seen that for both samples, the rise times are faster than the rise times for CdSe nanoparticles in toluene solution.

In the aggregates, the interparticle distance is very small and thus the coupling between them is very strong. This leads to rapid energy transfer between the excited nanoparticles with the hot electron and the nearby CdSe nanoparticles whose excited electrons are in the 1S state.

This type of excitation transfer is similar to that present in single molecular crystals and known as a Frenkel type exciton. As the distance increases, and becomes larger than the size of the excited dipole, an approximate form of the rate of the energy transfer is derived by Förster.

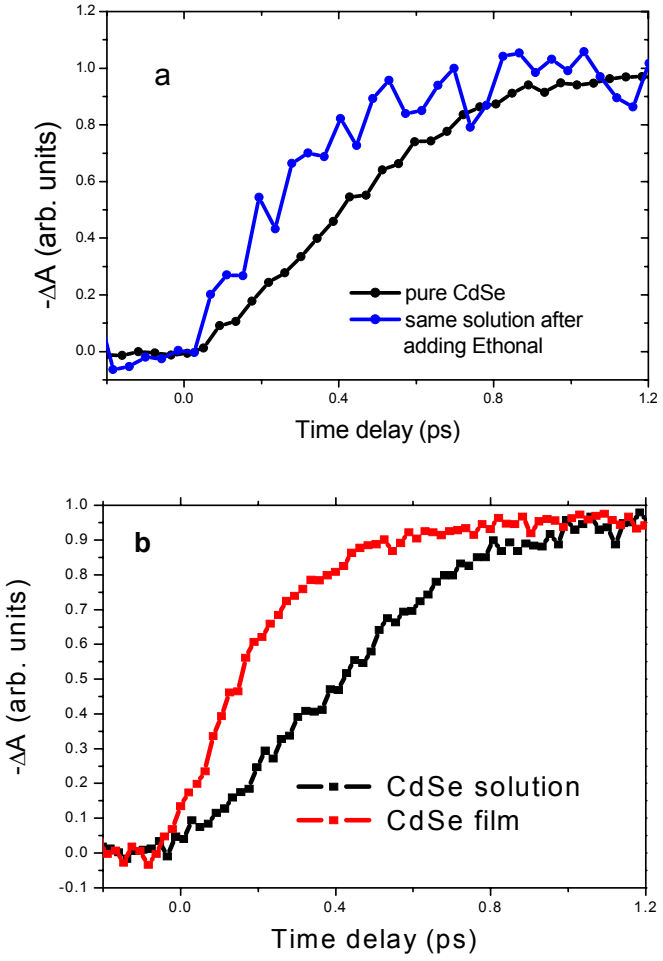

Figure 7.4: (a) Transient absorption spectra showing the 1S rise time in CdSe nanoparticles in pure toluene solution (black) and in a solution with a drop of alcohol (blue). This clearly shows that the rise time is much faster for solution after aggregation formation than the particles in toluene alone. (b) Transient absorption spectra showing the 1S rise time in CdSe nanoparticles in solution (Black) and in a film (red). This clearly shows that the rise time is much faster for the film sample than the particles in solution.

As the concentration of the CdSe particles increases, the size of the aggregates increases. This increases the electron energy transfer rate between the particles with hot electrons and those with the electrons in a 1S band gap state. Figure 7.5 shows a cartoon of the electron relaxation mechanism in aggregates.

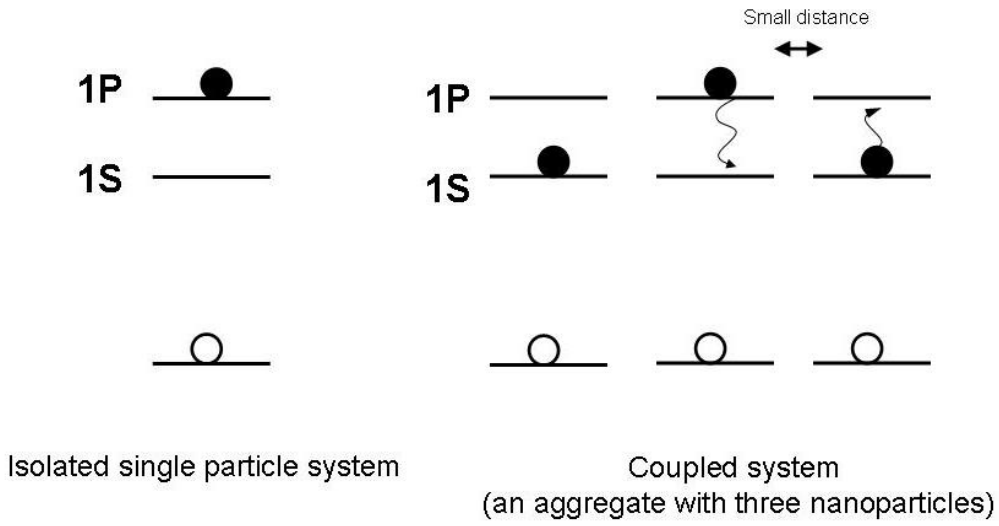

Figure 7.5: Three Excited CdSe nanoparticles in an aggregate. The middle has the hot electron (the donor) and the other two have their electron in the 1S state (acceptors).

Due to the small interparticle distance, the transfer rate should be high. As the size of the aggregate increases, the number density of the acceptors increases and therefore the transfer rate increases.

Auger type Ionization as a Relaxation Mechanism:

An interesting question might arise as to whether laser excited nanoparticles could lead to ionization of the neighboring particle and the relaxation of the donor. This mechanism corresponds to an interparticle nonlinear Auger type process. It could efficiently contribute to the relaxation of the hot electrons and an observed decrease of the rise time of the 1S state. This is expected to be both concentration and laser power dependent. In order to examine the contribution of this mechanism, we studied the pump fluence dependence on S7 whose concentration is highest. The experimental data is shown in figure 7.6. Upon changing the laser pump fluence from 25 uj/cm^2 up to 200 uj/cm^2 it seems that in the concentration and laser intensity range used, we did not observe nonlinear Auger type mechanism because there is no pump fluence effect on the rise dynamics of the 1S state transient bleaching signal. (At these pump fluences one can calculate (44) that there is less then one electron hole pair excited per nanoparticle thus eliminating intraparticle Auger processes.) At high laser powers, one expects that the intraparticle Auger processes would dominate the overall relaxation of hot electrons (47).

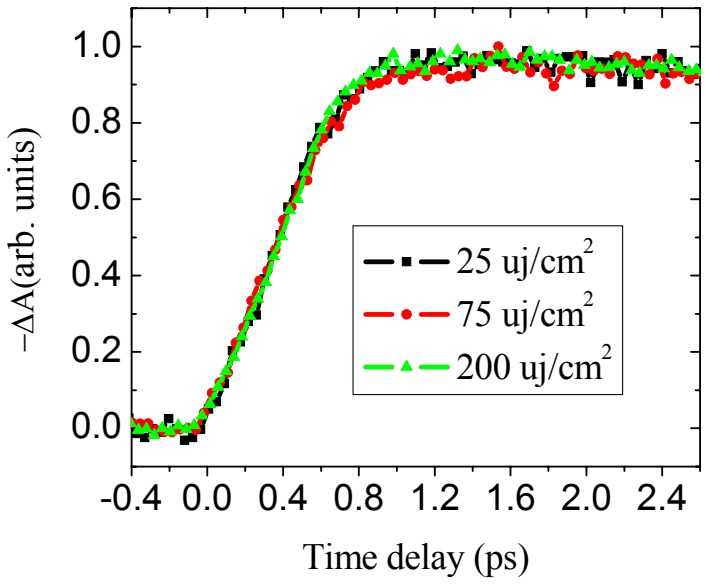

Figure 7.6: Transient bleaching signal of the sample with the highest CdSe nanoparticle concentration. The rise time curves of the transient bleaching signal do not show any pump fluence dependence with pump fluence up to 200 ųJ/cm2. This suggests that FRET induced ionization (due to interparticle Auger type process) of CdSe nanoparticles does not occur under our experimental conditions. The coupling between two excited CdSe nanoparticles is not observed.

Cause of aggregation in solution:

It is clear from the experiments that the rise time of the 1S state is influenced by the amount of aggregates in solution. Forming a CdSe film and the addition of alcohol to the solution show a faster rise time of the 1S state.

The cause of aggregation in solution is an interesting problem to investigate. Knowing that alcohol can cause CdSe nanoparticles to aggregate in solution, the effect of the number of times the sample is washed with ethanol on the rise time of 1S is studied.

Figure 7.7 clearly shows that the time gets faster when the sample is washed 3 times. This indicates that when the sample is washed with alcohol too many times, the capping ligands (TOPO) can be affected, leading some particles to aggregate.

It becomes necessary to be very careful in the number of times the sample is washed and the amount of alcohol used. Washing the sample once should be sufficient and one needs to make sure the sample is dried from any trace of alcohol before redissolving in toluene.

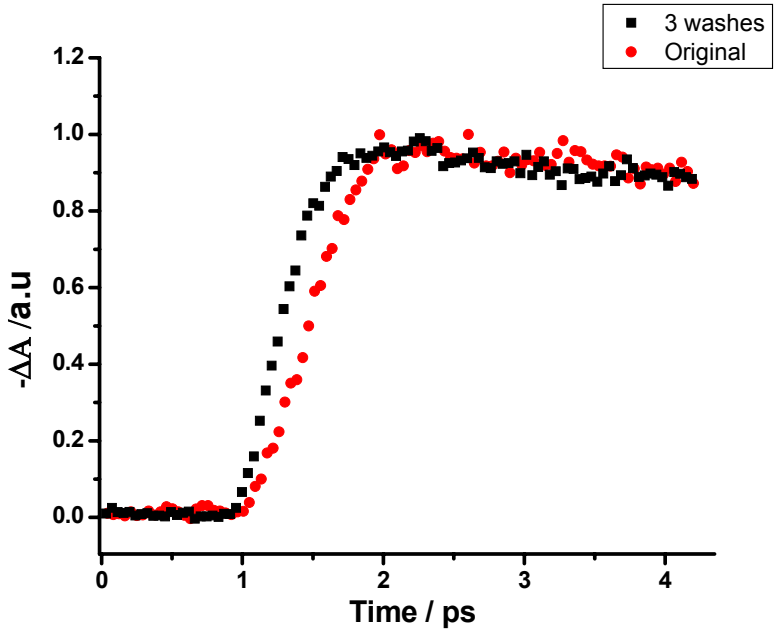

Figure 7.7: Transient bleaching signal of the original CdSe nanoparticle sample (red) and the sample washed 3 times and re-dissolved in toluene (black). It is clear that the rise time of the sample washed 3 times is faster than the original sample.

Concentration dependent rise time of 1S state was also measured for CdSe nanoparticles sample prepared using cadmium acetate precursor. This sample did not show any difference in rise time as a function of particles concentration unlike CdO prepared sample. It is likely that in addition to TOPO, the acetate ions also help passivate the particles, hence preventing the particles to aggregate. For this reason, the choice of precursors used becomes very important to the quality of the sample sysnthesized than initially realized.

Conclusion

Electron energy relaxation in CdSe nanoparticles as a function of concentration is observed. The relaxation mechanism is explained in terms of Förster type energy transfer as well as an effect from particles aggregation. The average distance of 500 Å between CdSe nanoparticles seems unusually large for such a process to occur, and therefore the effect of particle aggregation in solution is considered to promote fast relaxation dynamics. The presence of small amounts of aggregates in solution will result in particles to be much closer to each other than calculation show (500Å). In such cases, an excited electron in one particle can relax by giving off its energy to an electron in 1S state of the neighboring particle. With increasing concentration, by making a CdSe film and also by adding ethanol to CdSe nanoparticles in solution, the number of aggregates increase and the relaxation rate becomes faster. Additionally, washing the particles too much can result in aggregation, hence changing the ultrafast dynamics in these samples.

References

(1) Förster, T. *Naturwissenschaften* **1946**, 33, 166. Förster, T. *Ann. d. Physik.* **1948,** 2, 55.

(2) Andrews, D. L.; Demidov, A. A. *Resonance Energy Transfer*; Wiley: Chichester, U.K., 1999. Agranovich, V. M.; Galanin, M. D., *Electronic Excitation Energy Transfer in Condensed Matter*; North-Holland; New York, 1982.

(3) Kagan, C. R.; Murray, C. B.; Nirmal, M.; Bawendi, M. G., *Phys. Rev. Lett.* **1996**, 76, 1517.

(4) Murray, C. B.; Kagan, C. R.; Bawendi, M. G., *Science* **1995,** 270, 1335.

(5) Vossmeyer, T.; Reck, G.; Katsikas, L.; Haupt, E. T. K.; Schulz, B.; Weller, H., *Science* **1995**, 267, 1476.

(6) Efros, Al. L., Rosen, M.; *Annu. Rev. Mater. Sci.* **2000**, 30, 475

(7) Norris, D. J., Bawendi, M. G.; *Phys. Rev. B* **1996**, 53, 16338

(8) Kagan, C. R.; Murray, C. B.; Bawendi, M. G., *Phys. Rev. B* **1996**, 54, 8633.

(9) Achermann, M.; Petruska, M. A.; Crooker, S. A.; Klimov, V. I., *J. Phys. Chem.* **2003**, 107, 13782.

(10) Crooker, S. A.; Hollingsworth, J. A.; Tretiak, S.; Klimov, V. I., *Phys. Rev. Lett.* **2002**, 89, 186802.

(11) Clapp, A. R.; Medintz, I. L.; Mauro, J. M.; Fisher, B. R.; Bawendi, M. G.; Mattoussi, H., *J. Am. Chem. Soc.* **2003**, 126, 301.

(12) Wargnier, R.; Baranov, A. V.; Maslov, V. G.; Stsiapura, V.; Artemyev, M.; Pluot, M.; Sukhanova, A.; Nabiev, I., *Nano Lett.* **2004**, 4, 451.

(13) Shubeita, G. T.; Sekatskii, S. K.; Chergui, M.; Dietler, G.; Letokhov, V. S., *Appl. Phys. Lett.* **1999,** 74, 3453

(14) Lovett, B. W.; Reina, J. H.; Nazir, A.; Briggs, G. A. D., *Phys. Rev. B* **2003**, 68, 205319.

(15) Brus, L., *J. Phys. Chem.* **1986**, 90, 2555. Brus, L. E., *J. Chem. Phys.* **1984**, 80, 4403.

(16) Nirmal, M.; Norris, D. J.; Kuno, M.; Bawendi, M. G.; Efros, Al. L.; Rosen, M., *Phys. Rev. Lett.* **1995**, 75, 3728.

(17) Efros, Al. L.; Rosen, M.; Kuno, M.; Nirmal, M.; Norris, D. J.; Bawendi, M., *Phys. Rev. B* **1996**, 54, 4843.

(18) Norris, D. J.; Sacra, A.; Murray, C. B.; Bawendi, M. G., *Phys. Rev. Lett.* **1994**, 72, 2612.

(19) Bawendi, M. G.; Wilson, W. L.; Rothberg, L.; Carrll, P. J.; Jedju, T. M.; Steigerwald, M. L.; Brus, L. E., *Phys. Rev. Lett.* **1990**, 65, 1623.

(20) Li, J. B.; Xia, J. B., *Phys. Rev. B* **2000**, 61, 15880. Li, X. Z.; Xia, J. B., *Phys. Rev. B* **2002**, 66, 115316.

(21) Ekimov, A. I.; Hache, F.; Schanne-Klein, M. C.; Ricard, D.; Flytzanis, C.; Kudryavtsev, I. A.; Yazeva, T. V.; Rodina, A. V.; Efros, A. L., *J. Opt. Soc. Am. B* **1993**, 10, 100.

(22) Landberg, P. T., *Recombination in Semiconductor*; Cambridge University Press, Cambridge, 1991.

(23) Bockelmann, U.; Bastard, G., *Phys. Rev. B* **1990**, 42, 8947.

(24) Benisty, H.; Sotomayor-Torres, C. M.; Weibuch, C., *Phys. Rev. B* **1991**, 44, 10945

(25) Klimov, V. I.; McBranch, D.W., *Phys. Rev. Lett.* **1998**, 80, 4028.

(26) Burda, C.; Link, S.; Green, T. C.; El-Sayed, M. A., *J. Phys. Chem. B* **1999**, 103**,** 1783.

(27) Guyot-Sionnest, P.; Shim, M.; Matranga, C.; Hines, M.; *Phys. Rev. B* **1999,** 60, R2181.

(28) Klimov, V. I.; Schwarz, Ch. J.; McBranch, D. W.; Leatherdale, C. A.; Bawendi, M. G., *Phys. Rev. B* **1999**, 60, R2177.

(29) Blackburn, J. L.; Ellingson, R. J.; Mićić, O. I.; Nozik, A. J., *J. Phys. Chem. B* **2003**, 107, 102.

(30) Klimov, V.; Bolivar, P. H.; Kurz, H., *Phys. Rev. B* **1996**, 53, 1463.

(31) Underwood, D. F.; Kipp**e**ny**,** T.; Rosenthal, S. J., *J. Phys. Chem. B* **2001,** 105, 436.

(32) Schoenlein, R. W.; Mittleman, D. M.; Shiang, J. J.; Alivisatos, A. P.; Shank, C.V., *Phy*s. *Rev. Lett.* **1993**, 70, 1041.

(33) Mittleman, D. M.; Schoenlein, R. W.; Shiang, J. J.; Colvin, V. L.; Alivisatos, A. P.; Shank, C. V., *Phys. Rev. B* **1994**, 49, 14435.

(34) Avouris, P.; Gelbart, W. M.; El-Sayed, M. A., *Chem. Rev.* **1977**, 77, 793

(35) Sercel, P. C., *Phys. Rev. B* **1995**, 51, 14532.

(36) Bockelmann, U.; Egeler, T., *Phys. Rev. B* **1992**, 46, 15574.

(37) Efros, A. L.; Kharchenko, V. A.; Rosen, M., *Solid State Commun.* **1995**, 93, 281.

(38) Darugar, Q.; Landes, C.; Link, S.; Schill, A.; El-Sayed, M. A., *Chem. Phys. Lett.* **2003**, 373, 284.

(39) Blackburn, J. L.; Elllingson, R. J.; Mićić, O. I.; Nozik, A. J., *J. Phys. Chem. B*, **2003**, 107, 102

(40) (a) Murray, C.; Norris, D.; Bawendi, M., *J. Am. Chem. Soc.* **1993**, 115, 8706.

(b)Peng, Z. A.; Peng, X., *J. Am. Chem. Soc.* **2001**, 123, 183.

(c)Peng, Z. A.; Peng, X., *J. Am. Chem. Soc.* **2002**, 124, 3343.

(41) Yu, W. W.; Qu, L. H.; Guo, W. Z.; Peng, X. G., *Chem. Mater.* **2003**, 15, 2854.

(42) Logunov, S. L.; Volkov, V. V.; Braun, M.; El-Sayed, M. A., *PNAS* **2001**, 98, 8475.

(43) Klimov, V. I.; McBranch, D. W., *Phys. Rev. Lett.* **1998**, 80, 4028.

(44) Klimov, V. I., *J. Phys. Chem. B* **2000**, 104, 6112.

(45) Klimov, V. I.; McBranch, D. W.; Leatherdale, C. A.; Bawendi, M. G., *Phys. Rev. B* **1999**, 60, 13740.

(46) Wu, P. G.; Brand, L., *Anal. Biochem.* **1994**, 218, 1

(47) Klimov, V. I.; Mikhailovsky, A. A.; McBranch, D. W.; Leatherdale, C. A.; Bawendi, M. G., *Science,* **2000**, 287, 1011.

(48) El-Sayed, M. A., *Accounts of Chemical Research*, **2004**, 37 (5), 326.

CHAPTER VIII

EFFECT OF SAMPLE QUALITY AND SURFACE OXIDATION ON THE OPTICAL PROPERTIES OF CDSE NANOPARTICLES

Nature of the electron quenching sites:

Abstract

A detailed study on the effect of changing the cadmium to selenium ratio during the synthesis of CdSe nanoparticles on the optical properties is discussed. We also discuss the effect of surface photo-oxidation on the steady state fluorescence and lifetimes. The fluorescence lifetimes is found to be almost always bi-exponential decay with a fast decay of a few nanoseconds and a longer lifetime decay of tens of nanosecond. The fluorescence decay rates do not change under these perturbations but the contribution of each lifetime component and the overall fluorescence quantum yield do change. The fast decay component becomes dominant when the fluorescence quantum yield is poor which results when the sample is initially of poor quality from using excess cadmium or after photo-oxidation. The slower decay component is more prominent for a good quality CdSe nanoparticles sample with higher quantum yield. After photo-oxidation, the slow decay contribution decreases from 80% to about 50%. A mechanism for electron quenching that affects the quantum yield and lifetime as observed is proposed.

Introduction

Semiconductor nanoparticles have been studied for many years in order to understand their optical and electronic properties arising from quantum confinement (1-7). Though a lot of work has been carried out in order to understand the fluorescence mechanisms, there still remain many questions and conflicting theories about these processes (8-12). It is well documented that the surfaces of these nanoparticles play a very important role in the overall fluorescence mechanism and hence the quantum yield (6-12). The fast decay component is thought to be between the electronic bands (13) while the longer decay component is thought to be the fluorescence decay lifetime from the band gap state (9-10).

CdSe nanoparticles with narrow size distributions are prepared by the colloidal synthesis method in a hot surfactant solution of TOPO (14). This method allows us to make a narrow size distribution of particles with good control of the sizes and shapes. However, the quality of these particles can vary from one synthesis to another. Due to this variation, the fluorescence quantum yield can be different and hence the dynamics can vary from sample to sample. It becomes necessary to investigate the effect of different quality samples under different perturbations on the fluorescence quantum yield and fluorescence lifetimes. The presence of a capping material, such as TOPO and/or metal dangling bonds, on the surface can introduce states that can trap charge carriers and quench the fluorescence quantum yield.

It is shown that by capping CdSe nanoparticles with a material of a larger band gap, such as ZnS, one can reduce the surface trap states and greatly enhance the fluorescence quantum yield (15). Studies showed that by adding a hole acceptor, such as n-butylamine, quenches the fluorescence even though the fluorescence lifetimes was not affected (16). It is also shown that using a biased ratio of Cd:Se during the synthesis can greatly affect the quality of the sample (17). When using excess selenium, the fluorescence quantum yield is greatly enhanced, where as using less selenium shows very weak fluorescence quantum yield.

In order to understand the origin of fluorescence and the role that surface states play in the steady state fluorescence and the electronic dynamics, we have carried out a detailed study on the effect of capping, oxidizing the surface and changing the Cd:Se ratio during the synthesis on both the yield and the relative decay components of the same CdSe nanoparticles.

Experimental

Synthesis of CdSe nanoparticles

CdSe nanospheres were prepared using the method of Murray and Bawendi (14) as modified by Peng et al (18, 19). In this modified method, dimethylcadmium is replaced by less toxic CdO as the precursor. In a typical synthesis, 0.5g CdO (Strem) is loaded into a 3-neck flask with 4g trioctylphosphine oxide (TOPO, Aldrich) and 2g stearic acid (Aldrich) and heated to 320°C. At this temperature, the reddish brown solution turns optically clear. 0.2g selenium dissolved in 4mL of trioctylphosphine (TOP, Aldrich) is then quickly injected into the reaction flask and CdSe nanocrystals are instantaneously formed. The reaction flask is heated until the desired particle size is obtained. CdSe nanocrystals are washed from excess TOPO with methanol and then redesolved in Toluene.

Varying amounts of CdO and selenium are used depending on the quality of the sample required. For samples with excess selenium, 1:2 ration of Cd:Se was used and for less selenium, 2:1 ratio of Cd:Se was used. When noted, surface treatment or oxidation is achieved by bubbling air into CdSe nanoparticles and irradiating the sample with UV light (Photo-oxidation).

CdSe nanoparticles were passivated with a ZnS layer using the method of Hines and Guyot-Sionnest (15). In this method, dimethylzinc ($ZnMe_2$, Aldrich) and

hexamethyldisilathiane ($(TMS)_2S$, Fluka) were used as zinc and sulfur precursors, respectively. To the previously prepared CdSe nanoparticles, $ZnMe_2$ and $(TMS)_2S$ dissolved in TOP is added drop wise at ~130º C. The capped particles are once again washed using the method described above.

Freshly prepared CdSe particles were analyzed by a JEOL 100CX II field emission transmission electron microscope operating at 100 kV. Optical characterization was carried out using a Shimadzu UV-3101PC UV-VIS-NIR scanning spectrophotometer and a PTI Model C60 steady-state spectrofluorometer with a xenon arc lamp source and photomultiplier detection system. Fluorescence lifetime measurements were obtained on a PTI Model C-72 fluorescence lifetime spectrometer with a PTI GL-3300 nitrogen laser.

Results

Three samples studied are labeled S1, S2 and S3. S1 and S2 are samples prepared with excess cadmium cations (i.e. excess holes or deficient in electrons) with S1 having a diameter of about 3.5nm and S2 a diameter of about 4nm. Sample S3 was prepared with excess selenium anions and has a size of about 3.5nm in diameter. It is suggested that using biased ratios of Cd:Se affects the quality of the sample (17). Peng et al have shown that using excess selenium during the nanoparticles synthesis promotes surface optimization with fewer defect sites. They show that there exists lattice construction in the free-standing CdSe nanocrystals. The lattice construction indicates the occurrence of surface optimization during the growth resulting in a high quantum yield. When using excess cadmium, there exist more defects on the surface of the nanoparticles. We will refer to these defects due to excess cadmium within the CdSe crystal lattice and surface as electron deficient (ED) defects. Figure 8-1a shows the normalized absorption spectra of two CdSe samples, S1 and S2, and figure 8-1b shows the corresponding normalized steady state fluorescence.

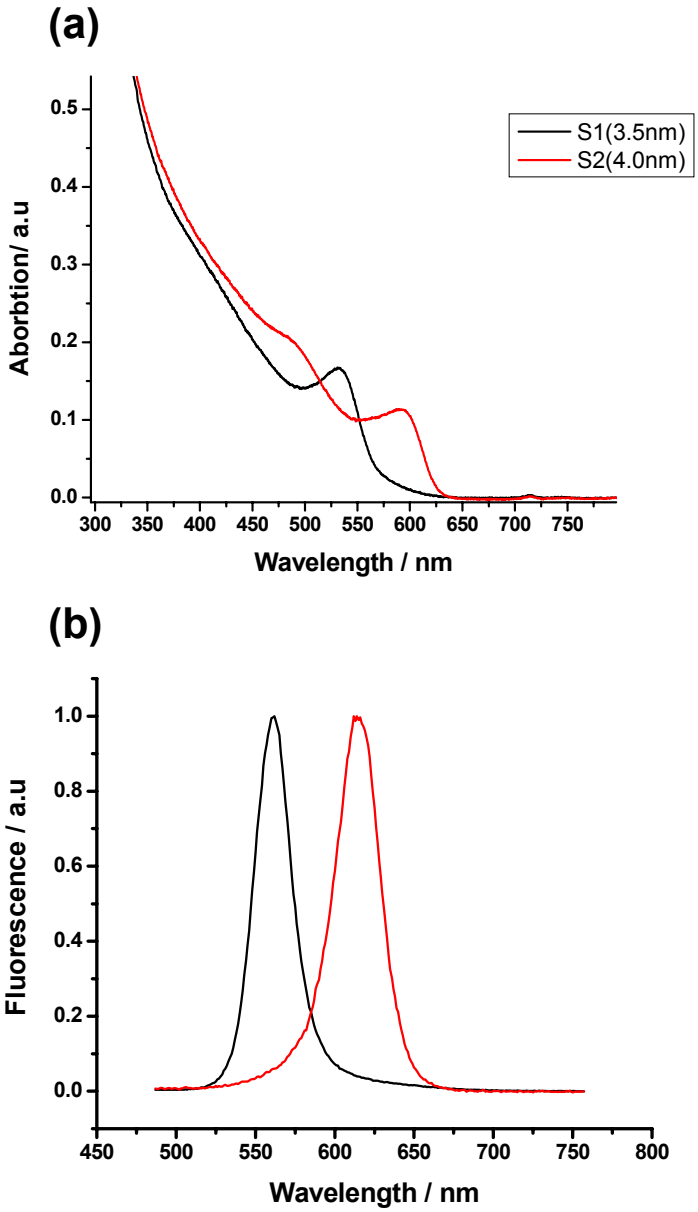

Figure 8-1: (a) Absorption spectra of two CdSe nanoparticle samples (red line is 4.0nm and black line is 3.5nm in diameter) prepared with excess cadmium cations and (b) corresponding steady state fluorescence spectra.

The quantum yields were found to be 4% and 3% for S1 and S2, respectively, with rhodamine B used as a reference. Figure 8-2 is the normalized absorption and fluorescence spectra of sample S3 (excess selenium) that was synthesized using excess selenium. The quantum yield for this sample was calculated to be 10% ± 5%.

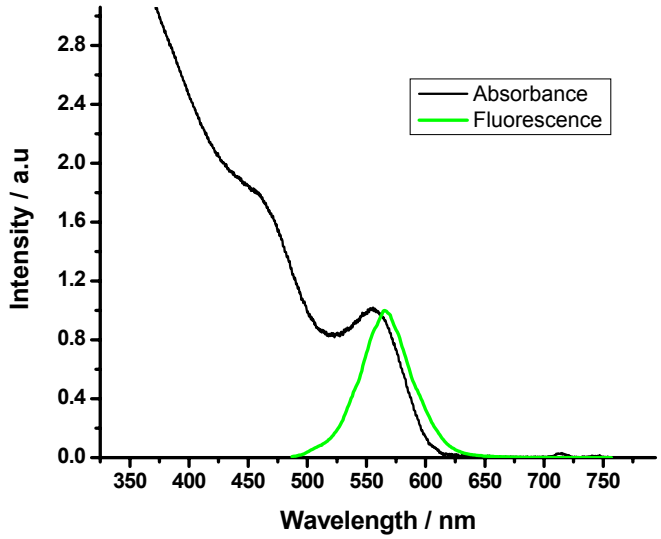

Figure 8-2: Normalized absorption (black) and fluorescence (green) spectra of CdSe sample (S3) prepared using excess selenium. Fluorescence quantum yield is more than 2 times stronger than samples S1 and S2.

Fluorescence spectra in figure 8-3 are for sample S1, and the decreasing emission yield is due to the effect of surface oxidation with increasing UV irradiation. Similarly, figures 8-4 and 8-5 are the fluorescence spectra for samples S2 and S3, respectively. As can be seen, the fluorescence for S1 decreases by a factor of 5 as the sample is photo-oxidized. Similarly,

fluorescence quantum yield for samples S2 and S3 decreases by factors of 6 and 5, respectively, after bubbling oxygen and irradiating with UV light. (Samples that are photo-oxidized will be called S1', S2' and S3'.)

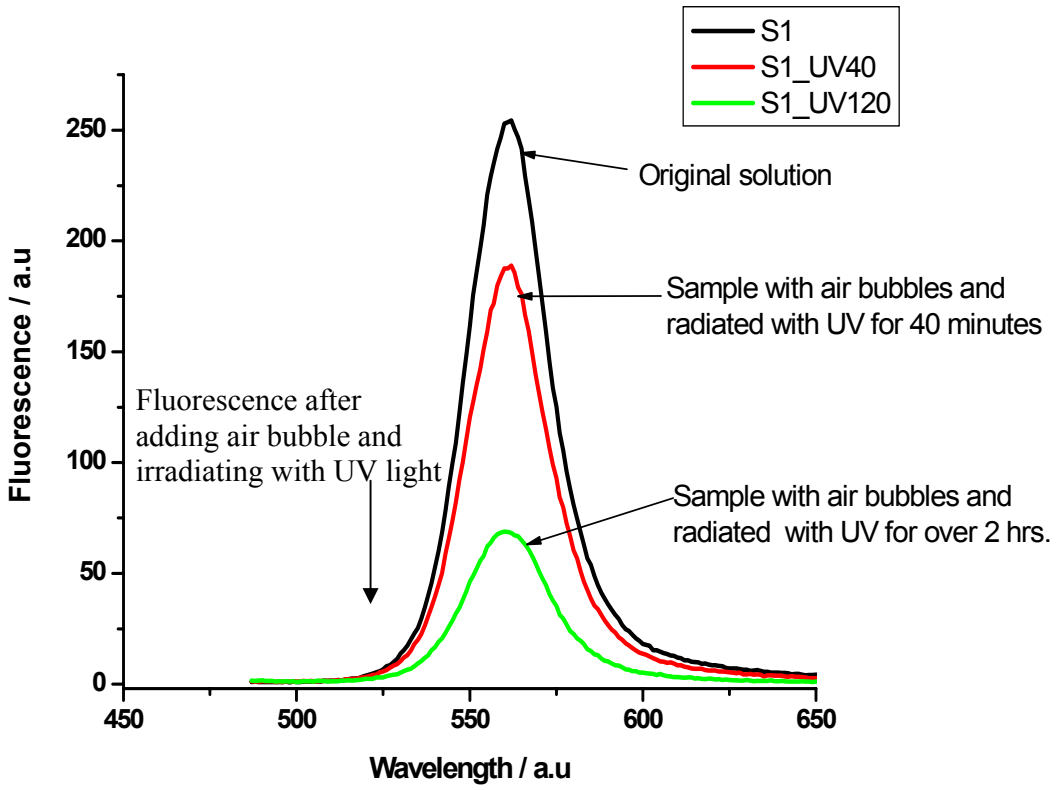

Figure 8-3: Decrease in fluorescence intensity with increasing UV irradiation time on sample S1. The fluorescence quantum yield decreases by a factor of 5 after UV irradiation in the presence of oxygen.

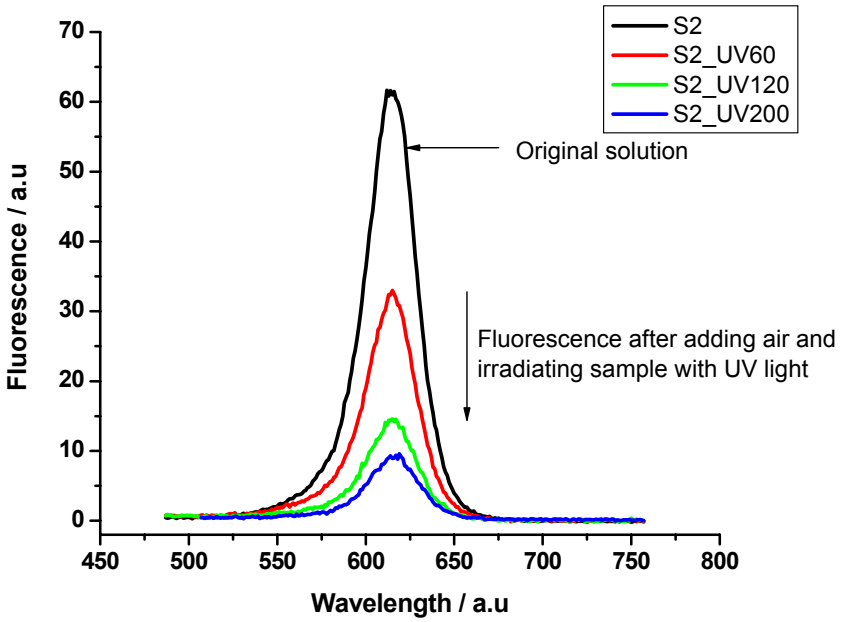

Figure 8-4: Decrease in fluorescence intensity with increasing UV irradiation time on sample S2. The black spectrum is the original sample, the red spectrum is measured after irradiating for 60 minutes, the green spectrum is measured after irradiating for 120 minutes and the blue spectrum is measured after irradiating for 200 minutes. The fluorescence quantum yield decreases by a factor of 6 after UV irradiation in the presence of oxygen.

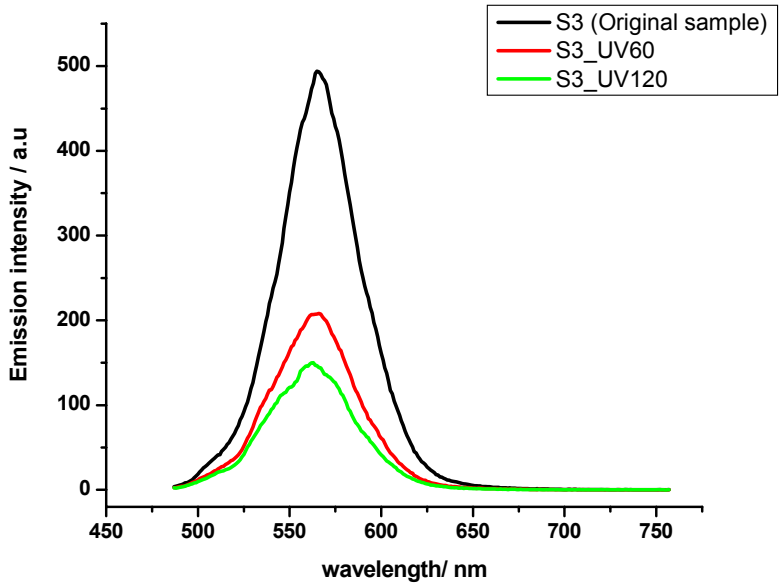

Figure 8-5: Decrease in fluorescence intensity with increasing UV irradiation time on sample S3. The black spectrum is the original sample, the red spectrum is measured after irradiating for 60 minutes, and the green spectrum is after irradiating for 120 minutes. The fluorescence quantum yield decreases by a factor of 6 after UV irradiation in the presence of oxygen.

The absorption spectrum of each sample remained unchanged after surface treatment. Figure 8-6 shows the fluorescence decay dynamics for each sample before and after surface treatment. The corresponding fluorescence lifetimes for samples S1 and S2 are tabulated in table 8.1. Samples S1 and S2 both show bi-exponential decay with over 50% contribution from the A1 component. After surface treatment, A1 contribution increases to about 80% for both S1 and S2 samples, while the decay times (τ) for both samples remain basically unchanged within the experimental error.

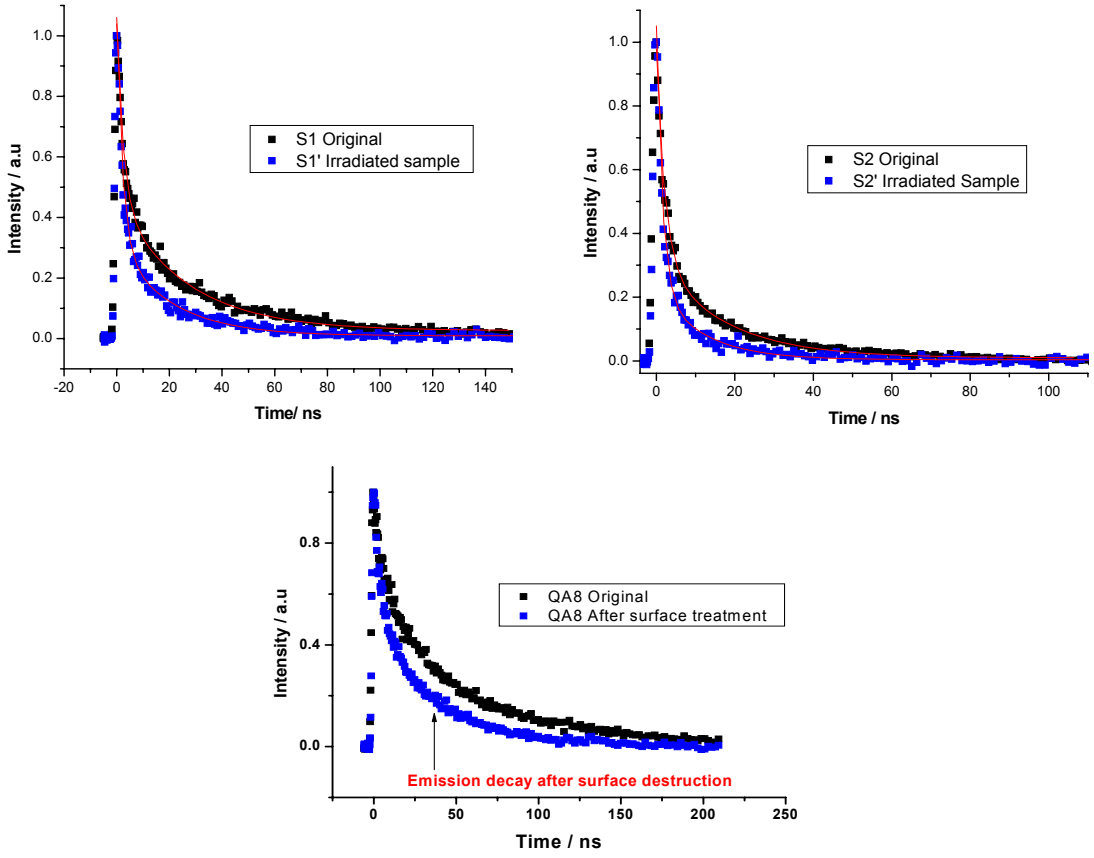

Figure 8-6: Fluorescence lifetime spectra for the three samples before and after UV radiation that shows an increase in the fast decay component after the sample undergoes photo-oxidation. The fast decay component becomes dominant (~80%) after UV irradiation for samples S1 and S2 prepared with excess cadmium. Similarly, sample S3, prepared with excess selenium, shows a dominantly bi-exponential decay after UV irradiation.

For sample S3 (excess selenium), the fluorescence decay was fit to a single exponential decay, and when fit to a bi-exponential equation, the contribution from A1 was minimal (less than 20%). After irradiating the sample with UV light, the fluorescence decay became dominantly bi-exponential with a contribution from A1 component of almost 50%. The time constants and each decay component are shown in table 8.1.

Table 8.1: Fast and slow emission decay times with their respective amplitudes for sample S1 and S3 before and after surface oxidation.

	S1 (excess Cd)	S1' (UV+O2)	S3 (excess Se)	S3' (UV+O2)
A1	0.57	0.77	0.2	0.46
τ1 (ns)	2.5	2.22	3.7	3.4
A2	0.43	0.33	0.8	0.54
τ2 (ns)	26.2	20.3	31.2	35.2

We also studied the effect of passivation on the fluorescence quantum yields and on the lifetime and their respective amplitudes. Figure 8-7a compares the emission spectra of capped and uncapped nanodots and figure 8-7b represents the corresponding fluorescence lifetime decay plots. These results were discussed in chapter IV and may help explain the electron relaxation mechanism

from upper excited states and their effect on the quantum yield in CdSe nanoparticles. Therefore, they are briefly discussed here. Quantum yield for the capped sample was calculated to be 30% where as for the uncapped sample was 6%. Although the fluorescence quantum yield for capped CdSe nanoparticles was greatly enhanced compared to the uncapped sample, the fluorescence lifetimes practically remain unchanged. We should note that the quality and size of CdSe nanoparticle samples may change slightly since capping with ZnS requires reheating the sample. As shown in figure 8-7b, the decay is bi-exponential with a fast component of ~3.5ns and a slow component of ~30ns. For both fast and slow decays, the amplitudes do not change before and after ZnS passivation.

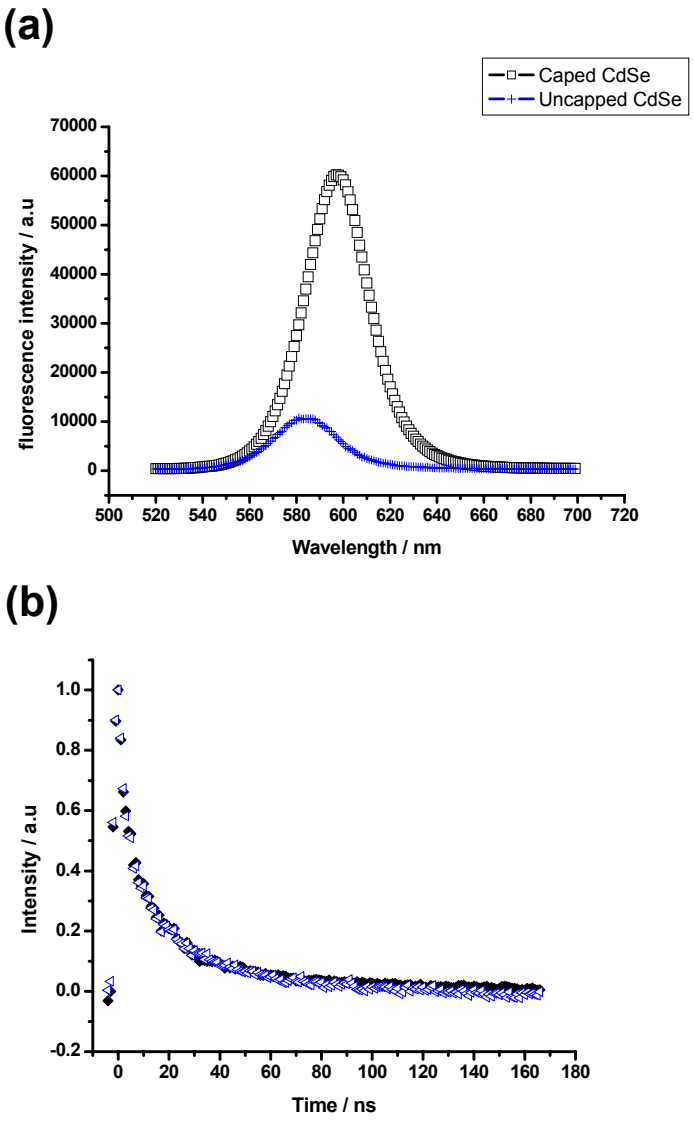

Figure 8-7: (a) Fluorescence spectra of capped and uncapped CdSe nanodots showing a significant increase in the quantum yield for the sample capped with a ZnS layer. (b) Corresponding fluorescence decay spectra for the capped and uncapped sample show no significant change in the decay lifetimes.

Discussion

Measuring optical properties of CdSe nanoparticles with different surface properties allows us to understand the role the particle surface has on the fluorescence mechanisms and the origin of the electron quencher. Using a biased ratio of Cd:Se creates defects within or on the surface of the CdSe lattice that can affect the optical and electronic properties. Samples S1 and S2 (less selenium) show weak fluorescence quantum yields and it is understood that this is due to poor surface construction when using biased ratio of cadmium to selenium during the synthesis (17). The fluorescence quantum yield further deceases when air is bubbled into the samples and irradiated with UV light. When the surface is oxidized, it tends to induce states that trap charge carriers and hence quenches the fluorescence. In the process of particles oxidation, the absorption spectra remained unchanged and the particles did not aggregate.

Different perturbations would dictate the optical and electronic properties of CdSe nanoparticles, such as experimental conditions and most importantly the quality of the sample. Traps states in semiconductor nanoparticles normally arise from surface defects and/or metal dangling bonds on the surface. Furthermore, impurities and defects within the CdSe lattice itself can create states that can trap electrons (or holes) and quench the fluorescence. When the electrons are excited to higher energy states, the probability for them to become trapped is high in samples that have a high density of trap states, as discussed in chapter IV. Electrons trapped from the upper excited states (higher than the band gap

state) do not affect the fluorescence lifetimes. Passivation of CdSe nanoparticles with ZnS does not change the lifetimes, indicating that trapping from higher excited states is mainly due to organic capping molecules and free cadmium or selenium dangling bonds. When CdSe nanoparticles are passivated with a material of a larger band gap, such as ZnS, the surface trap states are minimized because the free metal dangling bonds and organic capping molecules are no longer attached directly to the CdSe surface. Capping CdSe nanoparticles with ZnS greatly enhances the emission quantum yield (15) while the fluorescence lifetime remains the same, as discussed in chapter IV. This indicates that the trapping to surface states is very rapid and cannot be detected within the instrument's nanosecond response time. Although capping CdSe nanoparticles increases the steady state fluorescence quantum yield, the amplitude ratio of fast to slow decay rates does not change greatly. This indicates that fewer electrons are trapped from the excited states to the extrinsic trap sites (minimized due to capping) and therefore the number of electron that relax to the band gap state increases. From the lowest excited state, the mechanism for electron relaxation, either to the intrinsic trap sites or giving off fluorescence, remain the same since these trap states are not greatly affected by passivation. For this reason, the contribution of the fast and slow decay components remain the same for capped and uncapped particles (A1/A2=constant). This shows that the electron trapping to the extrinsic trap sites does not affect the lifetimes or the amplitudes.

One interesting observation is the fluorescence lifetime of the sample prepared with excess selenium is almost a single exponential. When the sample that shows fast and slow decay lifetimes is capped, the fluorescence quantum yield is greatly enhanced, though the fluorescence lifetime still shows bi-exponential decay. This would indicate that the trapping of electrons to surface states due to organic capping or other surface species does not play a major role in the observed fluorescence decay rates. Changing the ratio of cadmium to selenium during the synthesis of CdSe nanoparticles affects both the fluorescence quantum yield and the contribution from fast and slow decay lifetimes. Using excess selenium during the synthesis is shown to form better quality samples (17) and the quantum yield is much higher than compared to samples prepared with excess cadmium. Since the amount of cadmium and selenium determines the lattice quality of the CdSe particles formed, using excess cadmium will most likely create vacancies/defects within the CdSe nanoparticles (intrinsic trap states). When the electrons relax to band gap state, the probability for the electrons to become trapped will be higher in the sample that has a high density of intrinsic trap sites. The fast decay component is a result of electrons getting trapped by intrinsic trap states, i.e. more channels for the electrons to relax and hence faster decay. In a sample with a high density of intrinsic trap states, the fast decay component is more than 50%, as seen for sample S1. Irradiating the sample with UV light in the presence of oxygen further increases the trapping states; therefore, the contribution from the fast component is as high as 80%.

Sample S3 is prepared using excess selenium and shows almost single exponential decay with the lifetime comparable to the longer lifetime of the S1 sample. The fast decay component contribution is less than 20% in the S3 sample. This indicates that a good quality sample has less lattice defects and hence a smaller density of intrinsic trap states. The low density of intrinsic trap states would rapidly be saturated and would show a smaller fast decay component (20%). The electrons would then dominantly relax to the ground state giving bang gap florescence with a longer lifetime (~30 ns). Though the nature of the exact trapping sites is difficult to determine, and there exists many different types of trap sites, the above experiments suggest a trend of two dominant quenching sites. One is quenching due to surface capping molecules and the other is due to defects in the CdSe nanoparticles either on the surface of the nanoparticles or within the CdSe crystal. What sites are affected when the CdSe nanoparticles are oxidized is still unclear and needs further work. Figure 8-8 shows a cartoon of possible mechanisms to explain the presence of two lifetimes in CdSe nanoparticles. Electrons become trapped from the higher excited states or the from band gap state depending on the trap states present. The two fluorescence lifetime components are attributed to electron quenching (fast component) and band gap relaxation (slow component). Trapping from higher excited states affects the quantum yield but not the lifetime, where as trapping from the lowest excited states affects both the quantum yield and lifetime.

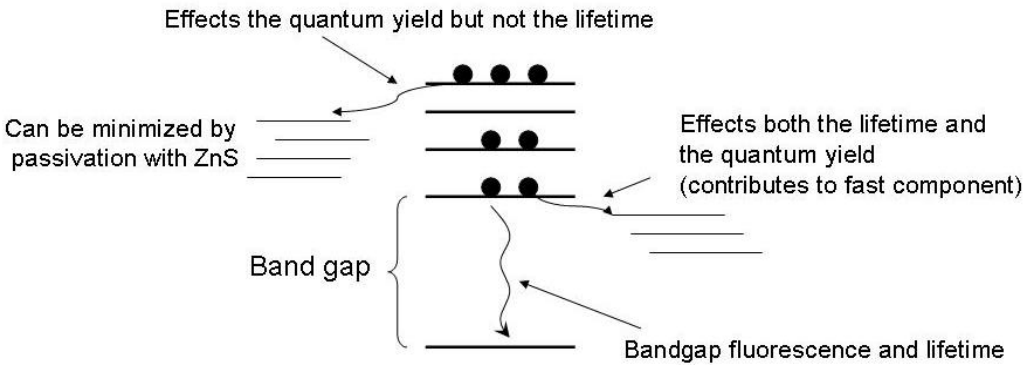

Figure 8-8: Different electron quenching sites that affect fluorescence quantum yield and lifetimes.

One thing to note is that, even for the best sample ever prepared, the quantum yield is at best 50% after surface passivation. Therefore there are other nonradiative processes involved in quenching the charge carriers that leads to lower quantum yields.

Conclusion

From the experimental results discussed above, we believe there are two major types of trap states that influence the steady state fluorescence intensity and florescence lifetimes. First is the trap sites caused by organic surface molecules and/or other surface impurities (extrinsic trap states). The second type of traps are due to intrinsic trap sites and these are caused by defects within the CdSe crystal due to poor lattice construction or the presence of impurities. By capping the particles with ZnS, we minimize the efficiency of the surface (due to surface capping molecules) trap sites by confining the charge carriers in CdSe nanoparticles within the larger band gap of the ZnS layer. This greatly enhances the fluorescence quantum yield while the fluorescence lifetime is not affected. This demonstrates that capping increases the probability of the charge carrier to relax to the lowest excited state rather than getting trapped; therefore, the quantum yield increases. The intrinsic trap states are most likely created during the particle synthesis when a biased Cd:Se ratio is used or the crystals have defects due to vacancies or impurities. These intrinsic trap sites vary from sample to sample and result in different relaxation contributions of the fast and slow lifetime components. Capping the CdSe nanoparticle surface does not change the contribution from the fast and slow decay components indicating that the fast component contribution of the fluorescence lifetime is the result of electrons being trapped to the intrinsic trap states.

References

(1). Bawendi, M. G.; Steigerwald, M. L.; Brus, L. E*. Annu. Rev. Phys. Chem*. **1990,** 41, 477.

(2). Alivisatos, A. P*. J. Phys. Chem*. **1996,** 100, 13226.

(3). Zhang, J. Z. *Acc. Chem. Res*. **1997,** 30, 423.

(4). Lugunov, S.; Green, T.; Marguet, S.; El-Sayed, M. A. *J. Phys. Chem. A*, **1998,** 102, 5652

(5). Burda, C.; Link, S.; Green, T.; El-Sayed, M. A. *J. Phys. Chem. B*, **1999,** 103, 10775

(6). Alivisatos, A.P. *Science*, **1996**, 271, 933.

(7). Eichkorn, K.; Ahlrichs. R. *Chem. Phys. Lett.* **1998,** 288, 235.

(8). Kuno, M.; Lee, J. K.; Dabbousi, B. O.; Mikulec, F. V.; Bawendi, M. G. *J. Chem. Phys*. **1997**, 106, 9869.

(9). Wu, F.; Zhang, J. Z.; kho, R.; Mehra, R. K. *Chem. Phys. Lett.*, **2000**, 330, 237-242.

(10). Schlegel, G.; Bohnenberger, J.; Potava, I.; Mews, A. *Physical Review Letters*, **2002,** 88, No. 13, 13740-1.

(11). Javier, A.; Magana, D.; Jennings, T.; Strouse, G. *Applied Physics Letters*, **2003**, 83, N0. 7,1423.

(12). Chamarro, M.; Gourdon, C.; Lavallard, P.; Lublinskaya, O.; Ekimov, A. I. *Physical Review B*, **1996,** 53, No. 3, 1336.

(13). Wang, X.; Zhang, J.; Nazzal, A.; Darragh, M.; Xiao, M. *Appl. Phys. Lett.*, **2002**, 81, 4829-4831.

(14). Murray, C. B.; Norris, D. J.; Bawendi, M.G. *J. Am. Chem. Soc.,* **1993**, 115, 8706.

(15). Hines, M.; Guyot-Sionnest, P. *J. Phys. Chem*. **1996**, 100, 468.

(16). Landes, C.; Burda, C.; Braun, M.; El-Sayed, M. A. *Nano Lett.* 1, **2001**, 667.

(17). a. Zhang, J-Y.; Wang, X-Y.; Xiao, M.; Qu, L.; Peng; P. *Applied Physics Letter*, **2002**, 81, 11, 2076-2078

b. Qu, L.; Peng, X. *J. Am. Chem. Soc.* **2003,** 124, No. 9, 2049.

(18) Peng, Z. A.; Peng, X. *J. Am. Chem. Soc*. **2002**, 124, 3343.

(19) Peng, Z. A.; Peng, X. *J. Am. Chem. Soc*. **2001**, 123, 183.

Qusai A Darugar

qdarugar@hotmail.com

Laser Dynamics Laboratory
770 States Street.
Atlanta, GA 30332-0400
Work: 4048944009

Education

June 2006 Georgia Tech, Atlanta, GA, 30332

Ph.D, Physical Chemistry, Minor: Analytical Chemistry

-Thesis topic:- Synthesis, Characterization and Ultrafast electronic relaxation of some Metallic and Semiconductor Nanoparticles
-Thesis research under the guidance of Professor Mostafa El-Sayed, Professor of Chemistry, GATech.
-Study-abroad program in Paris, France at the Université Pierre et Marie CURIE with Professor Marie-Paule Pileni on the project of copper nanoparticles preparation using reverse micelles.
- Major course of study and concentration in the field of Nanoscience, synthesizing, characterizing and functionalizing metallic (Copper, Cobalt, Gold, Platinum, Palladium) and semiconductor nanomaterials (Cadmium selenide, Cadmium Sulfide, and Cadmium Telluride).
-Study potential use of nanomaterials for light amplification (Optical Gain and Stimulated emission) for their potential use in making new generation Lasers and LEDs.
- Completing course work in Physical Chemistry has significantly contributed to my expertise in designing, synthesizing, characterizing and application of different nanomaterials.
-Potential use of these nanomaterials in catalysis, microprocessors, sensors, medical diagnostics, labeling reagents and in nanoelectronic devices and new generation Lasers.

May 2000 Erskine College, Due West, SC 29639

BS, Physics and Chemistry double major **with Departmental Honors,** ***Minor: Mathematics***

- Graduated Magna Cum Laude with Departmental Honors.
- Research with Dr. Kimberly A. O. Pacheco (currently at University of Northern Colorado) on the synthesis of metallophthalocyanine complexes for use in bio-sensors.
- Dean's List (1998, 1999, 2000)
- American Chemical Society, Division of Analytical Chemistry Award (1999).

Skills

• Reliable, focused, able to collaborate in a team.
• Work well in groups, Published scientific work in collaboration with others.
• Knowledge and expertise in making and characterizing nanostructures of different materials.
• Expertise in using Transmission Electron Microscope for imaging nanomaterials.
• Knowledge of wet chemistry and synthesis of complex organic molecules.
• Trained at the state of the art Laser Dynamics Laboratory (http://www.ldl.gatech.edu).
• Use of variety of instruments such as UV-Vis, Spectrofluorometer, and Lasers for optical and electronic characterization of materials.
• Fluent in speaking four languages (English, Kiswahili, Gujarati, Hindi)

Work Experience

August 2001 to Present — Georgia Tech, Atlanta, Georgia
Graduate Research Assistant

2003-2004 — Georgia Tech, Atlanta, Georgia
Research mentor

Undergraduate students assigned to work with me in the area of materials synthesis and characterization.

August 2000 to May 2001 — Georgia Tech, Atlanta, Georgia
Teaching Assistant
-Instructed freshman chemistry courses and of analytical chemistry for Chemical Engineer majors.

Activities and Honors

- Member- The American Chemical Society
- Inducted to Who's Who Among Students in American Universities and Colleges (2000)
- Received numerous awards through out the four years as an undergraduate for Technical support in sound and lights in theatrical plays performed by Erskine College English department and was inducted into Alpha Psi Omega, an honorary drama fraternity.
- Member of the Omicron Delta Kappa, the National Leadership Honor Society.
- President of Sigma Pi Sigma, National Physics Honor Society, Erskine College Circle - 1999-2000.
- Inducted to the Sigma Pi Sigma, National Physics Honor Society.
- Member of the Kappa Mu Epsilon, National Mathematics Honor Society.

Publications

(1) Qusai Darugar, Wei Qian, Mostafa El-Sayed, "Effect of surface passivation, excitation wavelength, and aspect ratio on the electron dynamics in CdSe nanoparticles" Manuscript in preparation.

(2) Wei Qian., Wenyu Huang, Qusai Darugar, Mostafa A. El-Sayed, "Ultrafast electronic and lattice process of plasmonic nanoparticles of different shape," Proceedings of the Femtochemistry VII (Elsevier), W. Castelman Ed., in press (2006).

(3) Qusai Darugar, Wei Qian, Mostafa A. El-Sayed, "Observation of optical gain in solutions of CdS quantum dots at room temperature in the blue region" Applied Physics Letters, 88, 26 (2006).

(4).Qusai Darugar, Wei Qian, Marie-Paule Pileni and Mostafa. A. El-Sayed, 'Size Dependent Ultrafast Electronic Energy Relaxation and Enhanced Fluorescence of Copper Nanoparticles' Journal of Physical Chemistry B, 110 (1) 143-149 (2006).

(5). Qusai Darugar, Christy Landes, Stephan Link, Alexander Schill, Mostafa A. El-Sayed, "Why is the thermalization of excited electrons in semiconductor nanoparticles so rapid? Studies on CdSe nanoparticles", Chem. Phys. Letters, 373, 284-291 (2003).